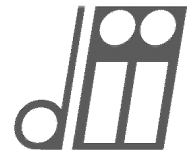


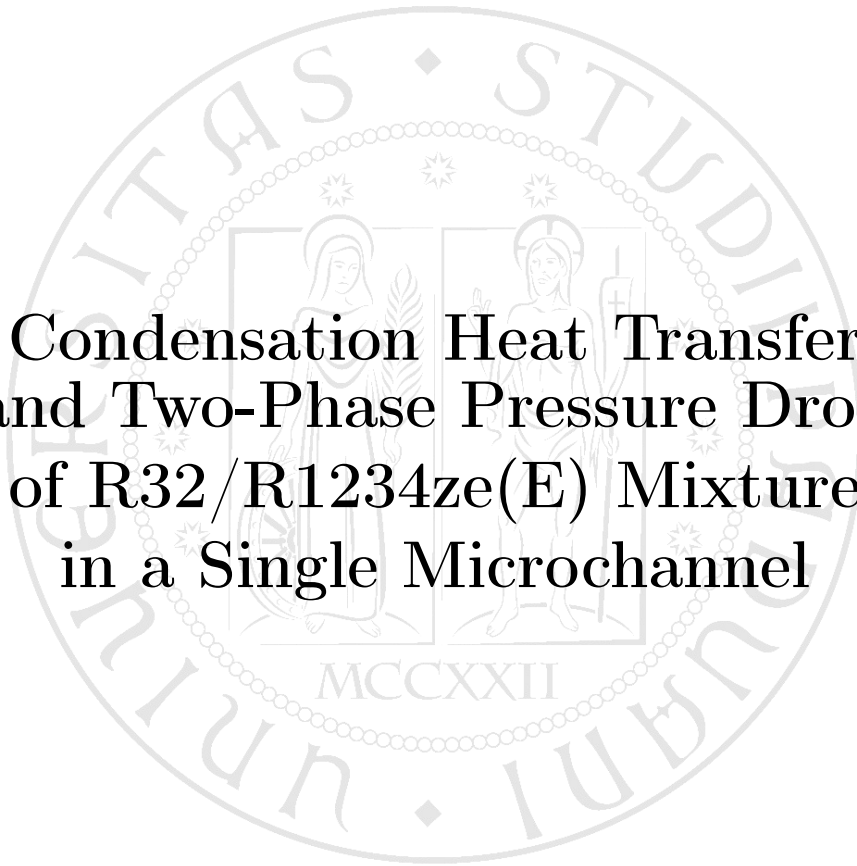


UNIVERSITAS STUDII PADUANI

DIPARTIMENTO DI INGEGNERIA INDUSTRIALE



CORSO DI LAUREA IN INGEGNERIA MECCANICA



**Condensation Heat Transfer
and Two-Phase Pressure Drop
of R32/R1234ze(E) Mixture
in a Single Microchannel**

Relatore:
Ch.mo Prof. **Davide Del Col**

Laureando:
Luca Mattiello

Correlatore:
Ing. **Marco Azzolin**

Anno Accademico
2013-2014

*To my Father and my Mother,
to my family,
to my closest friends.*

Abstract

The purpose of this work is to investigate the Heat Transfer Coefficient during condensation and two-phase adiabatic pressure drop inside a single circular microchannel of R32 and R1234ze(E) mixture at different compositions. In the literature, studies on condensation inside mini and microchannels are recent but few deal with zeotropic mixtures as working fluids. These mixtures differ from pure fluids during condensation because the temperature is not constant but varies between the dew point and the bubble point; this change in temperature is called glide and occurs with a variation in composition of both liquid and vapor phases during condensation.

The tests have been carried out for three different concentrations by mass of the two components R32 - R1234ze(E): 23% - 77%, 46% - 54% and 76% - 24%. Heat Transfer Coefficients during condensation have been measured at different mass velocities ranging from 150 to 800 kg m⁻²s⁻¹ with a mean refrigerant temperature of 40 °C at a constant pressure. The Heat Transfer measuring section is a counter current heat exchanger with an internal copper circular microchannel with a 0.96 mm inner diameter; the condensation process is controlled by water flowing in the external annulus. The Heat Transfer Coefficients are obtained by the specific heat flux, derived from the water temperature profile and from the saturation to wall temperature difference. Additional measures and analysis of the pressure drop have been also conducted in adiabatic conditions at different vapor qualities. The pressure drop measuring section is a copper microchannel with an inner diameter of 0.96 mm.

Experimental results are reported together with their uncertainty analyses and compared with previous developed theoretical correlations available in literature. A further analysis with a proper Performance Evaluation Criterion, dubbed Penalty Factor, have been made in order to compare the investigated mixtures, in terms of energy losses and Heat Transfer performances, with the two pure fluids at different operative conditions.

Sommario

Lo scopo di questa tesi é quello di indagare il Coefficiente di Scambio Termico in condensazione e la caduta di pressione bifase in condizioni adiabatiche all'interno di un singolo microcanale circolare di una miscela di R32 ed R1234ze(E) a differenti composizioni. In letteratura, gli studi riguardo la condensazione all'interno di mini e microcanali sono recenti ma solo alcuni trattano le miscele zeotropiche come fluidi operativi. Queste miscele differiscono dai fluidi puri durante la condensazione in quanto la temperatura non é costante ma varia tra il punto di rugiada e il punto di bolla; questa variazione di temperatura é detta scorrimento e avviene con una variazione di composizione in entrambe le fasi liquida e vapore durante la condensazione.

Le prove sperimentali sono state effettuate per tre differenti concentrazioni massive dei due componenti R32 - R1234ze(E): 23% - 77%, 46% - 54% e 76% - 24%. I Coefficienti di Scambio Termico in condensazione sono stati misurati per diverse portate specifiche da 150 fino a 800 kg m⁻²s⁻¹ con una temperatura media del refrigerante di 40 °C a pressione costante. La sezione di prova di scambio termico é costituita internamente da un microcanale di rame avente diametro interno pari a 0.96 mm e nell'anello esterno un flusso di acqua in controcorrente controlla il processo di condensazione. I Coefficienti di Scambio Termico sono ricavati dal flusso specifico di calore, ottenuto dal profilo di temperatura dell'acqua e dalla differenza di temperatura tra il refrigerante in saturazione e la parete interna del microcanale. Ulteriori misure e analisi della caduta di pressione sono state effettuate in condizioni di deflusso adiabatico per diversi titoli di vapore. La sezione di misura delle perdite di carico é costituita da un microcanale di rame con diametro interno di 0.96 mm.

I risultati sperimentali sono riportati insieme alle rispettive analisi delle incertezze e comparati con correlazioni teoriche precedentemente sviluppate e disponibili in letteratura. Un'ulteriore analisi é stata effettuata con un adeguato criterio di valutazione delle prestazioni, nominato Penalty Factor, in modo da confrontare le miscele indagate, in termini di prestazioni di scambio termico e perdite energetiche, con i due fluidi puri a differenti condizioni operative.

Contents

Abstract	v
Sommario	vii
List of Figures	xiv
List of Tables	xv
1 Introduction	1
2 Refrigerants	7
2.1 Refrigerants properties	7
2.2 A short historical review	8
2.3 Environmental characteristics	9
3 R32, R1234ze(E) and their mixtures	11
3.1 R32 (Difluoromethane)	11
3.2 R1234ze(E) (trans-1,3,3,3-Tetrafluoroprop-1-ene)	11
3.3 R32 and R1234ze(E) mixtures	13
Nomenclature	19
4 Experimental apparatus	21
4.1 Test rig	21
4.2 Heat Transfer test section	25
4.3 Pressure Drop test section	28
4.4 Measuring instruments	29
5 Experimental tests	33
5.1 Mixture preparation	33
5.2 Data acquisition	35
5.2.1 Condensation tests	35
5.2.2 Pressure drop tests	36
5.3 Preliminary tests	36
5.3.1 Heat transfer measuring section	36
5.3.2 Pressure drop measuring section	37
5.4 Data reduction for the heat transfer test section	38
5.4.1 First method [22]	39
5.4.2 Pre-section	40

5.4.3	Measuring section	41
5.4.4	Second method [23]	42
5.4.5	Experimental methods corrections [24]	43
5.5	Data reduction for the pressure drop test section	44
	Nomenclature	45
6	Experimental uncertainty	47
6.1	Uncertainty expression	47
6.2	Heat Transfer Coefficient uncertainty $u_c(HTC)$	48
6.2.1	Water flow rate uncertainty $u_c(\dot{m}_w)$	49
6.2.2	Water temperature gradient uncertainty $u_c(g)$	49
6.2.3	Saturation temperature uncertainty $u_c(T_{sat})$	51
6.2.4	Wall temperature uncertainty $u_c(T_{wall})$	52
6.2.5	Inner perimeter uncertainty $u_c(P)$	52
6.2.6	Overall uncertainty	52
6.3	Vapor quality uncertainty	52
6.4	Pressure drop uncertainty	54
6.5	Experimental uncertainties analysis	55
	Nomenclature	59
7	Experimental results	61
7.1	Heat Transfer Coefficients	61
7.2	Pressure Drops	68
	Nomenclature	71
8	Theoretical models	73
8.1	HTC theoretical models	73
8.1.1	Cavallini et al. model [5]	73
8.1.2	Moser et al. model [11]	76
8.1.3	Shah model [16]	78
8.2	Correction for zeotropic mixtures	79
8.3	Pressure Drop theoretical model	80
8.3.1	Del Col et al. model [8]	80
	Nomenclature	83
9	Data comparisons	85
9.1	Comparison against theoretical models	85
9.1.1	Heat Transfer Coefficients comparison	85
9.1.2	Pressure Drops comparison	92
	Nomenclature	95
10	Penalty Factor	97
10.1	Comparison against pure fluids	98
	Nomenclature	103
11	Conclusions	105
	References	109

Thanks	113
A Reduction codes	115
A.1 Program for HTC data reduction	116
A.2 Program for PD data reduction	129
A.3 Subroutines for HTC prediction	137
A.3.1 Cavallini et al. model Code	137
A.3.2 Moser et al. model Code	139
A.3.3 Shah model Code	141
A.4 Subroutine for PD prediction	143
A.4.1 Del Col et al. model Code	143
A.5 Subroutine for uncertainty calculation	145
A.5.1 HTC Uncertainty Function Code	145
Acronyms	149
Index	151

List of Figures

1.1	Scheme of ideal reversible cycles in an T-s diagram. Carnot cycle with constant temperatures (left) and Lorentz cycle with “gliding” temperatures (right) [2].	3
3.1	Scheme of temperature profiles during condensation of a pure refrigerant (left) and a zeotropic mixture (right).	13
3.2	Condensation process of a zeotropic mixture.	14
3.3	Equation of State manually inserted in Refprop [19] to evaluate mixture properties according to the Akasaka et al. [20] database.	16
3.4	Molar and massive phase diagrams of the investigated mixtures of R32 and R1234ze(E).	17
4.1	Experimental test rig scheme.	22
4.2	Experimental apparatus. Refrigerant loop auxiliary elements.	24
4.3	Heat transfer test section [4].	25
4.4	Measuring sector cross-section: thermocouple position.	26
4.5	Heat transfer test section pictures.	27
4.6	Pressure drop test section picture.	28
4.7	Instruments for thermocouples calibration.	29
4.8	Picture of the refrigerant Coriolis-effect mass flow meter and relative transducer installed in the test rig.	30
4.9	Pressure transducers picture.	31
5.1	Picture of the mixture reservoir and the vacuum pump used for the mixture charge.	34
5.2	Refrigerant, wall and water temperature profiles at $G = 400 \text{ kg m}^{-2}\text{s}^{-1}$ for a R32/R1234ze(E) mixture with a 46/54% mass fraction.	35
5.3	Experimental and predicted friction factor for the investigated mixtures.	37
6.1	Total experimental percentage uncertainties of the Heat Transfer Coefficient and its components.	57
7.1	Experimental HTC vs vapor quality diagrams at mass velocities ranging from $150 \text{ to } 800 \text{ kg m}^{-2}\text{s}^{-1}$ with HTC and vapor quality uncertainty bands.	64
7.2	Experimental HTC vs vapor quality for the investigated R32/R1234ze(E) zeotropic mixtures. The mass velocity ranges from $150 \text{ to } 800 \text{ kg m}^{-2}\text{s}^{-1}$	65

7.3	Experimental HTC vs vapor quality at mass velocities of 800, 400 and 200 kg m ⁻² s ⁻¹ for pure R32 and R1234ze(E) fluids and the investigated mixtures.	66
7.4	Experimental HTC vs R32 mass fraction in the mixture at constant vapor qualities for different values of mass velocities: 200, 400 and 800 kg m ⁻² s ⁻¹	67
7.5	Experimental pressure gradient vs vapor quality of pure R1234ze(E) and the investigated mixtures for a mass velocity equal to 400 kg m ⁻² s ⁻¹	68
7.6	Experimental pressure gradient vs vapor quality for mixture 50/50% at mass velocities equal to 200, 400 and 600 kg m ⁻² s ⁻¹	69
8.1	Transition between ΔT -dependent and ΔT -independent flow regime, Equation (8.3)	75
9.1	Experimental vs calculated HTC predicted by the Cavallini et al. model [5] at mass velocities ranging from 150 to 800 kg m ⁻² s ⁻¹ . The model implements the Silver, Bell and Ghaly correction [26] to account for the zeotropic characteristics of the mixture.	88
9.2	Experimental vs calculated HTC predicted by the Moser et al. model [11] at mass velocities ranging from 150 to 800 kg m ⁻² s ⁻¹ . The model implements the Silver, Bell and Ghaly correction [26] to account for the zeotropic characteristics of the mixture and the correction by Zhang and Webb [28] for minichannel flow.	89
9.3	Experimental vs calculated HTC predicted by the Shah model [16] at mass velocities ranging from 150 to 800 kg m ⁻² s ⁻¹ . The model implements the Silver, Bell and Ghaly correction [26] to account for the zeotropic characteristics of the mixture.	90
9.4	Experimental vs calculated HTC predicted by the Cavallini et al. model [5] without the Silver, Bell and Ghaly correction [26] at mass velocities ranging from 150 to 800 kg m ⁻² s ⁻¹	91
9.5	Experimental vs calculated pressure drop predicted by the model developed by Del Col et al. [8].	92
10.1	Penalty Factor vs vapor quality at $G = 400$ kg m ⁻² s ⁻¹ for pure fluids and mixtures.	99
10.2	Penalty Factor vs vapor quality for pure fluids and mixtures with $PF = 5$ K ² at $x = 0.5$ at specific mass velocities.	100
10.3	Predicted HTC vs vapor quality for pure fluids and mixtures with $PF = 5$ K ² at $x = 0.5$ at specific mass velocities.	101

List of Tables

3.1	Significant properties of R32 and R1234ze(E) [2],[19].	12
3.2	Mixtures significant properties [19].	16
6.1	Type B experimental uncertainties of measured parameters.	48
6.2	Experimental extended HTC uncertainty and vapor quality ranges of the investigated mixtures for the whole mass velocity span during condensation tests.	56
6.3	Experimental extended vapor quality uncertainty ranges of the investigated mixtures for the whole mass velocity span during condensation tests.	56
6.4	Experimental extended vapor quality and pressure drop uncertainties for the investigated mixtures at mass velocity of 200, 400 and 600 kg m ⁻² s ⁻¹ during pressure drop tests.	56
8.1	Cavallini et al. model [5] experimental ranges.	74
8.2	Moser et al. model [11] experimental ranges.	76
8.3	Zhang and Webb two-phase multiplier experimental ranges.	77
8.4	Shah model [16] experimental ranges.	78
8.5	Del Col et al. model [8] experimental ranges for microchannels.	80
9.1	Absolute Mean Deviations and Standard Deviations of the three theoretical models used for the comparison against experimental data.	86
9.2	Absolute Mean Deviations and Standard Deviations of the model developed by Cavallini et al. [5] with and without the Silver, Bell and Ghaly correction [26] for zeotropic mixtures.	87

Chapter 1

Introduction

The interest in the construction of more compact and efficient heat exchangers has led over the years to a downsizing and refinement process. In order to obtain high Heat Transfer Coefficients with reduced dimensions, solutions characterized by a high exchange surface versus refrigerant charge ratio was found to be a viable route. To obtain this relationship between surface area and refrigerant charge, heat exchangers formed by micro and minichannels had been introduced in the market and this technology is nowadays one of the most promising. They realize a high Heat Transfer Coefficient (HTC) while maintaining a compact design. Micro and minichannels technology is therefore suitable for all applications that require to remove high heat duties and to reduce implant dimensions. The compactness of microchannel heat exchangers brings the significant advantage of the drastic reduction of the refrigerant charge; micro and minichannels are in fact viewed as appropriate options for reducing inventories of hazardous fluids and also reducing greenhouse gas emissions by improving component and system energy efficiency. The reduction of the refrigerant charge, for example, in Heating, Ventilation and Air Conditioning (HVAC) systems, compact heat exchangers for condensation and vaporization processes in electronic equipment, spacecraft thermal control, heat pipes and automotive condensers is a first step towards the reduction of greenhouse gas emissions. Microchannels offer the possibility to realize compact systems that minimize the problems related to loss of hazardous fluids. The small amount of refrigerant in microchannels is also a favorable condition for the use of natural refrigerants, which are usually toxic and flammable and they would be unusable for most applications. Furthermore, small diameter tube channels can withstand high pressure fluids such as carbon dioxide in transcritical cycle equipment, since these elements are able to withstand high system pressures.

Coupled with reduced refrigerant charge, there is also considerable research that relates to synthetic fluids with a low Global Warming Potential (GWP) as the global warming problem has been considered by different authorities. The Montreal Protocol on Substances that Deplete the Ozone Layer imposed a ban on the use of Chloro-Fluoro-Carbons (CFCs) refrigerants and the progressive phase-out of the Hydro-Chloro-Fluoro-Carbons (HCFCs) refrigerants. These restrictions led to the choice of Hydro-Fluoro-Carbons (HFCs) as refrigerants in most applications. The Kyoto Protocol of the United Nations Framework Convention on Climate Change (1997) placed HCFCs among the six categories of greenhouse gases because of their

large values of GWP and called for their phase-out. Afterwards, in 2012, the European Commission proposed to cut F-gas emissions by two-thirds by 2030. The research is focused on the use of both natural refrigerants (hydrocarbons, ammonia, carbon dioxide) but mostly on new low-GWP refrigerants, as natural refrigerants are often flammable or toxic. In particular Hydro-Fluoro-Olefins (HFOs) fluids have been investigated, but unfortunately, only few single-component low-GWP refrigerants are well developed so far; one of them is the R1234ze(E) which has a 100 years-horizon GWP of about 6. Hence, for most applications an alternative to high GWP synthetic refrigerants would rely on refrigerant mixtures, the idea is to couple the low GWP of new refrigerants with the high performances of previous refrigerants. Koyama et al [1] tested a mixture of R32 and R1234ze(E) inside a heat pump to improve its Coefficient of Performance (COP). They found that at some operative conditions, the tested mixture with a 50/50% mass composition, achieves superior COP and they conclude that it is a suitable candidate to replace R410A in many refrigerating applications. The R32 - R1234ze(E) mixture is defined as zeotropic (or non-azeotropic), as it presents a change in temperature (glide) during the phase change as well as a change in composition for both the vapor and liquid phases.

For a cycle evolving between two temperatures T_1 and T_2 , the COP is defined referring to the Carnot Cycle as reported in Equation (1.1). If a zeotropic mixture is adopted as operative fluid, the glide temperature in the evaporator and condenser occurs and the Lorentz cycle must be taken as a reference. As reported by Granryd et al. [2], the COP defined by the Carnot cycle is still valid for reversible cycles with gliding temperatures, provided that T_1 and T_2 are properly evaluated. The two temperatures can be calculated as the logarithmic average of the absolute temperatures entering and exiting the hot side and the cold side, respectively, as shown in Equation (1.1).

$$\text{COP} = \frac{T_1}{T_1 - T_2} \quad ; \quad T_1 = \frac{T_{1,in} - T_{1,out}}{\ln\left(\frac{T_{1,in}}{T_{1,out}}\right)} \quad \text{and} \quad T_2 = \frac{T_{2,out} - T_{2,in}}{\ln\left(\frac{T_{2,out}}{T_{2,in}}\right)} \quad (1.1)$$

Figure 1.1 reports a scheme of the abovementioned thermodynamic cycles in a T-s diagram.

For ordinary practical application, the glide is quite small and for such cases the difference between the simple arithmetic mean value of the temperatures and logarithmic mean value is quite small. This is not the case for the mixture studied in this work. In fact the glide reaches values up to 11 K and varies its magnitude according to composition and pressure.

While evaporation and boiling processes inside minichannels were analyzed in detail, due to the high interest in the realization of heat fluxes achievable with this geometry, this is not true for the condensation process. In fact limited databases are available in the literature with regard to the forced convective condensation. This is due to the fact that contrary to the case of evaporation or boiling, where the heat flow is directly imposed and easily measurable as electrical input power, in the case of condensation the removed heat flux must be determined indirectly through measurements of temperatures, mass flow rates, pressures and operating fluid properties. These measurements present some difficulties as the small flow rate in a single minichannel results in small heat flux. This coupled with a high

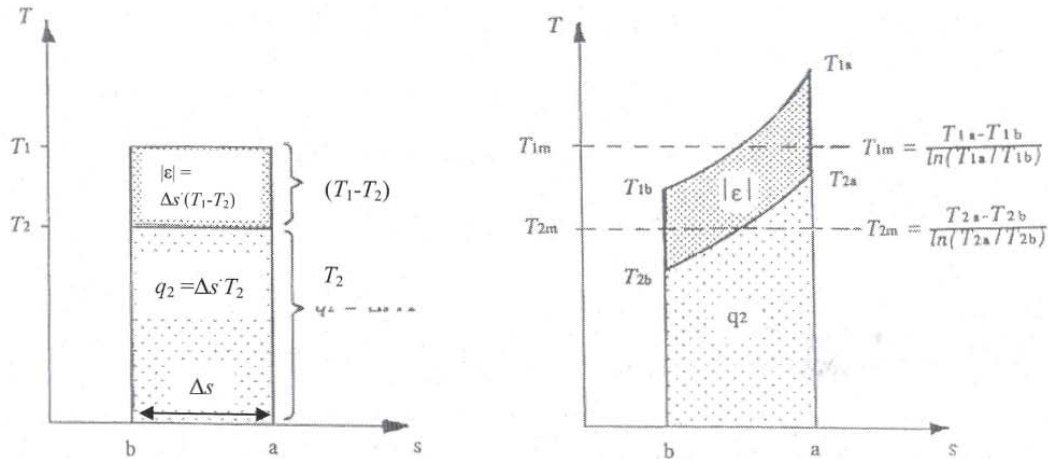


Figure 1.1: Scheme of ideal reversible cycles in an T-s diagram. Carnot cycle with constant temperatures (left) and Lorentz cycle with “gliding” temperatures (right) [2].

heat transfer coefficient led to its determination based on a small saturation to wall temperature differences hard to detect with good accuracy. The most used technique to evaluate condensation Heat Transfer Coefficients is the Wilson plot technique; this method, however, bases its accuracy on the cooling side temperature profile measurement and it does not directly measure the HTC inside the duct.

Some technical articles on condensation inside mini and microchannels are present in the literature.

Cavallini et al. [3] reported a detailed overview about the most recent works on heat transfer and pressure drop with natural refrigerants (such as propane or ammonia), halocarbons and hydrocarbons in minichannels. The reported data are referred to circular channels with inner hydraulic diameter ranges between $0.5 \div 3$ mm. The authors suggest that models for macroscale condensation can still be used in minichannels (down to 1 mm in diameter) provided that the mass velocity is above approximately $200 \text{ kg m}^{-2} \text{ s}^{-1}$ and the channel shape is circular. Furthermore they considered a proper Performance Evaluation Criterion, dubbed Penalty Factor, to compare heat transfer performances of different refrigerants in different channel geometries, such as macrochannel and microchannel. They assessed the superiority of the mini-geometry over the conventional macro-geometry in forced convection condensation (for a given mass velocity and condenser optimized geometry) in terms of heat transfer coefficient, frictional pressure drop and minimization of the refrigerant charge.

Matkovič et al. [4] measured local Heat Transfer Coefficients for condensation of R134a and R32 inside a circular channel with a 0.96 mm inner diameter. The tests were carried out with a saturation temperature of 40°C with mass velocity ranging from $200 \div 1200 \text{ kg m}^{-2} \text{ s}^{-1}$. The authors compared experimental data with theoretical models developed for macrochannels, the better agreement of experimental and predicted values was given by the model developed by Cavallini et al. [5].

Del Col et al. [6] tested the low GWP refrigerant R1234yf during condensation within a circular microchannel with a 0.96 mm inner diameter. The authors measured Local Heat Transfer Coefficients during two-phase flow regime at a saturation

temperature of 40 °C and pressure drop in adiabatic conditions. For all the tests, the mass velocity ranged from $200 \div 1000 \text{ kg m}^{-2} \text{ s}^{-1}$. A good prediction of the HTC was obtained by using the model developed by Cavallini et al. [5] as the disagreement between experimental and predicted points is below 15% for the entire mass velocity span. Furthermore the pressure drop for R1234yf have resulted lower than for R134a at the same operative conditions. The authors made a further investigation on R1234ze(E) [7] with respect to the HTC and the pressure drop inside a 0.96 mm inner diameter microchannel. They conclude that the model developed by Cavallini et al. [5] well predicted the experimental data. The HTCs shown by R1234ze(E) had been resulted comparable with the ones shown by R134a and higher than R1234yf but lower than pure R32. The model developed by Del Col et al. [8] had been used for the frictional pressure drop prediction with a good agreement with the experimental data. The pressure gradient for R1234ze(E) is resulted higher than R32, R134a and R1234yf as it presents the lowest reduced pressure.

Shin and Kim [9] conducted an experimental study of flow condensation Heat Transfer inside circular and rectangular minichannels. The investigated fluid was R134a inside channels with hydraulic diameters of 0.493, 0.691, and 1.067 mm. They compared the experimental data with different correlations, including the Cavallini and Zecchin correlation [10], the Moser correlation [11] and the Dobson and Chato [12] correlation. They pointend out that all the theroetical models used for the comparison strongly underpredict the experimental data for low mass velocities (less than $200 \text{ kg m}^{-2} \text{ s}^{-1}$); so they are not suitable to be used for minichannel flow.

Kim and Mudawar [13] developed a universal technique to predicting the condensation heat transfer coefficient for mini/microchannel flows basing on correlations and databases from by previous authors. They tested 17 different working pure fluids in micnichannels with hydraulic diameter between 0.424 to 6.22 mm, mass velocities from 53 to $1403 \text{ kg m}^{-2} \text{ s}^{-1}$. The model developed by the authors showed good predictive capabilities, with an overall Mean Absolute Error of 16.0% for the entire 4045 point database and 86.8% and 97.8% of the data falling within $\pm 30\%$ and $\pm 50\%$ error bands respectively.

Just a little amount of articles in the technical literature deal about zeotropic mixtures and their behaviour during condensation.

Fronk and Garimella [14] made a detailed review of the most recent developments on experimental condensation of zeotropic mixtures. They reported different theoretical useful approaches as weel as descriptions of technical difficulties encountered in many years of experiments and measurements. The authors conclude that a further investigation on the whole condensation mechanism is needed because heat and mass transfer resistance are strongly coupled but not yet sufficiently investigated during condensation of zeotropic mixtures.

Smit et al. [15] investigated a zeotropic mixture of R22/R142b inside a macrochannel with a 8.11 mm inner diameter. They used the Wilson plot technique in order to have a mean value of the heat transfer coefficient for different separated sections in the test rig. They found that the heat transfer coefficient is influenced by the flow regime type and by the mass velocity. The authors made a comparison between three models, they found that the Dobson and Chato correlation [12] gave the best agreement between measured values and predicted values. This correlation is followed by ths Shah correlation [16] and then by the Cavallini and Zecchin [10] correlation.

Miyara et al. [17] measured the thermal conductivity of the R1234ze(E) and R1234ze(E)+R32 mixture with the transient hot wire method. The tests were carried out at different temperatures from 10 °C to 80 °C with a constant increment of 10 °C. They showed a good agreement of the experimental data with the Refprop (version 9.0) database, proving the data reliability for both the pure fluids and a mixture with a 50% of R32 in mass for the whole temperature span.

In the present work, the treatment of zeotropic mixtures within a single microchannel is a valuable contribution to the understanding of the two-phase flow condensation phenomenon. The mixture in question is seen as a favorable candidate for the replacement of older and most polluting HCFCs. Furthermore the measurement method here adopted represents a significative improvement compared to the most common Wilson plot technique, leading to a more precise calculation of the local Heat Transfer Coefficient.

Chapter 2

Refrigerants

In the last century in parallel with the incoming of new applications in the refrigerating industry and air conditioning fields, several refrigerants able to operate with high performances and safety constraints were introduced into the market.

The appropriate refrigerant is chosen for the particular application taking into account a plenty of variables such as the refrigerant properties themselves and the implant features. Different fluids, in fact, present optimal thermodynamic characteristics under different operating conditions and for different implant designs; therefore, there is not a single refrigerant optimized for all the possible applications. This is the reason why it is very important to choose the proper refrigerant in order to achieve the best implant efficiency coupled with the best working conditions in terms of safety and reliability. A full knowledge of the main properties of refrigerants is critical and necessary to avoid choices that would affect the system efficiency.

In this chapter some of the most important characteristics of today's refrigerants are reported basing on previous databases [2].

2.1 Refrigerants properties

A working fluid in a refrigerating system (such as a vapor compression cycle or alternative cycles) has to satisfy a number of requirements that can be principally divided into two groups as follows:

- the refrigerant should not cause any risk of injuries, panic, fire or property damages in case of leakage;
- the chemical, physical and thermodynamical properties of the refrigerant have to be suitable for the system and the working conditions (at the lowest cost).

These two main groups describe parameters that can be clearly explained taking every single aspect into consideration, this consists in a so called “refrigerant criteria”:

Chemical: stable and inert at the operative conditions;

Health, safety and environmental: non-toxic, non-flamable, environmental friendly;

Thermal: critical and boiling point temperatures appropriate for the application, low vapor heat capacity, low viscosity, high thermal conductivity;

Miscellaneous: satisfactory oil solubility/miscibility, high dielectric strength of vapor, low freezing point, reasonable containment materials, easy leak detection, low cost.

Obviously all these requirements are impossible to fulfill at the same time for a single fluid. The most important characteristic is the chemical stability within the refrigerating system. All the other criteria become meaningless if the refrigerant starts to decompose or reacts with the materials used in the system, this may cause instability and also unsafety conditions. On the other hand the chemical stability may be a backlash if we look at the ambient side. A chemically inert fluid released in the atmosphere may persist for a very long time and then it would be considered a polluting fluid for the environment. So an ideal refrigerant may have a good chemical stability while it is operating within the refrigerating system and would easily decompose once get in contact with the atmosphere. The decomposition has to take place with the elements present in the atmosphere in suitable conditions (such as the presence of ultraviolet radiation) and avoid the formation of harmful substances.

Ensuring the chemical stability, the efforts in developing new refrigerants had been focused on thermal properties but the achievement of good thermodynamic performances are often coupled with the increase of the fluid hazard. Nowadays the trend in chemical research is to create a refrigerant that shows very low polluting characteristics (such as greenhouse effect) maintaining good thermodynamic properties, goals that are very difficult to achieve at the same time.

2.2 A short historical review

Until 1922 the only fluids used in the vapor compression cycles were ammonia (NH_3), carbon dioxide (CO_2), sulfur dioxide (SO_2) and water (H_2O); then around 1922 methyl chloride (CH_3Cl) and ethyl chloride ($\text{C}_2\text{H}_5\text{Cl}$) were introduced as they are not as toxic as ammonia or carbon dioxide but they do not possess the characteristic smell which is useful for leakage detection.

Around 1930 CFCs and later HCFCs fluids replaced ammonia and methyl chloride in refrigerating industry as they present higher performances and safety conditions. In the mid 70's a new theory about the ozone layer depletion caused by these fluids led to the ratification of different protocols which banned the use of CFCs and HCFCs (Montreal 1987, London 1990, Copenhagen 1992 and Kyoto 1997). This pushed the scientific community to create new fluids in substitutions to the previous ones, so HFCs and HFOs fluids were developed as they are less polluting compared with old refrigerants.

The banning of CFCs and HCFCs refrigerants has marked a crucial point in the refrigerating industry. These fluids, in fact, were created "ad hoc" with the main target of high thermodynamic performances and relatively high safety conditions. The new fluids introduced in their place (HFCs), however, have a different main target: a low environmental impact. Consequently, these fluids can not reach the same performances as the previous ones at the same operating conditions. The development and research of new technologies aimed at increasing the heat exchange efficiency, however, has led to the creation of systems that are more efficient and

competitive (as indirect systems and compact heat exchangers), allowing the use of these less polluting fluids against the banned CFCs and HCFCs. Furthermore, the increase of efficiency has made a fundamental benefit i.e. the drastic reduction of the refrigerant charge for the same thermal power demand. A minor amount of refrigerant means less risk in the event of leakages, lower installation and refill costs, smaller implant sizes and less environmental impact. In parallel with the reduction of the amount of refrigerant a reduction in the size of the heat exchangers has been noticed up to the present day in exchangers formed by mini and microchannels, characterized by high efficiency coupled with high HTC.

2.3 Environmental characteristics

With increasingly environmental restrictions in the use of industrial refrigerants, it was necessary to introduce parameters that certify their danger in terms of pollution. The release of these fluids into the atmosphere has been considered dangerous mainly for two aspects:

- the destruction of the atmospheric ozone layer;
- the increase of the greenhouse effect.

The first phenomenon is manifested with a refrigerant containing chlorine (or bromine) and, according to the Rowland-Molina theory¹, is described by a chain reaction. Once the refrigerant molecule reaches a height of about 20 km above the sea level, it is decomposed by the ultra-violet radiation (which is higher than on the ground). The decomposition forms free atoms of chlorine (or bromine) which react with the ozone molecules (O_3) according to the relation:



In this way a continuous destruction of the ozone molecules occurs, since the ClO molecule is not stable and continues to break down into its two components Cl and O; the chlorine attaches again a new ozone molecule according to Equation (2.1), and so on up to the formation of more stable compounds that stop the reaction. The destruction of the ozone layer allows more penetration of ultraviolet rays through the atmosphere; these rays are harmful to the plant species and also for the majority of living beings, reasons why it is important to preserve the ozone layer integrity. To express the damage caused by these fluids to the ozone layer, an index that quantifies the amount of ozone destroyed by a certain amount of the substance in question has been introduced: the Ozone Depleting Potential (ODP). It is defined as the ratio between the amount of ozone destroyed by the substance in question and the amount destroyed by the same quantity of a reference substance; trichlorofluoromethane (R11) is conventionally used as a reference ($ODP_{R11} = 1$).

The contribution that different fluids bring to the greenhouse effect, and thus to global warming, is counted in a similar manner. A very important index has been introduced: the Global Warming Potential (GWP). It expresses the ratio between

¹Frank Sherwood Rowland and Mario Molina, nobel prize in chemistry in 1995.

the amount of heat retained in the atmosphere from a certain quantity of substance with respect to the heat retained by the same amount of a reference substance. It is internationally agreed to use carbon dioxide (CO_2) as a reference ($\text{GWP}_{\text{CO}_2} = 1$). It is necessary to pay attention to the sources from which the different values of GWP are obtained as they can vary both in the calculation algorithm and in the period of time to which the index is referred. Indeed different GWPs are calculated for different periods of time (for example referred to periods of 20, 50 and 100 years of residence of the fluid in the atmosphere). Conventionally it is assumed that the average gas lifetime in the atmosphere is 100 years, and then the index denoted as GWP_{100} is used to express the global warming potential. Given the widespread use of these fluids in the refrigerating industry, it is crucial to adopt environmentally friendly refrigerants as much as possible; hence the need to have fluids with low ODP and low GWP. Nowadays the production of refrigerants with $\text{ODP} = 0$ is possible as many refrigerants are chlorine and bromine free, but many efforts are still underway to bring down the GWP value. Most refrigerants have indeed $\text{GWP} \gg 1$ (order of hundreds) and then it is easy to understand how important it is to contain the effects they may cause to the greenhouse effect if released into the atmosphere.

Chapter 3

R32, R1234ze(E) and their mixtures

To have a better understanding of the results obtained in the study of this mixture, knowing some characteristics of its two components is very useful. They are two very different fluids, created to satisfy different needs in various industrial fields. The following sections report some of their characteristics.

3.1 R32 (Difluoromethane)

Difluoromethane is a refrigerant of the HFCs family, generally used as a component of non-flammable refrigerant mixtures used in appliances and stationary air conditioning. It is currently being considered as pure (unblended) mildly flammable refrigerant so all sources of heat and ignition should be avoided and safety procedure must be respected in its handling. This refrigerant is a colorless and odorless gas at standard temperature and pressure and has a very low toxicity for human beings. Compared with the R1234ze(E) presents higher saturation pressure at the same saturation temperature, so it is called “high pressure fluid”; furthermore for the same values of temperature and pressure, it has lower density and viscosity (see Table 3.1 on the following page). Difluoromethane is a high performance refrigerant, created to accomplish a wide range of industrial and air conditioning applications. Unfortunately these characteristics are coupled with low environmental properties as $GWP_{R32} = 650$; this is the reason why from October 2012 Difluoromethane has not been commercialized as a pure (unblended) refrigerant. Anyway it is still available for some specific applications such as research or high performance implants.

3.2 R1234ze(E) (trans-1,3,3,3-Tetrafluoroprop-1-ene)

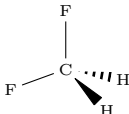
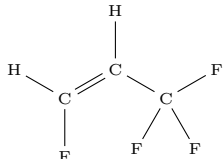
The R1234ze(E) refrigerant belongs to the HFOs family. Its physical characteristics make it suitable for use as refrigerant for applications where non-flammability is a top priority requirement. R1234ze(E) is a fourth generation gas profiting from the HFO technology, i.e. a technology that uses molecules with a double C=C bond, resulting in extremely low $GWP_{R1234ze(E)} = 6$ [18] and $ODP_{R1234ze(E)} = 0$. Besides this important strength, it has many others benefits:

- the fluid does not pose any special problems of compatibility with the materials (plastics and elastomers) and is similar to R134a;
- at the reference ambient temperature (21 °C) R1234ze(E) is non-flammable according to ASTM E-681 and Test EU A-11;
- it is highly suitable to replace R134a and presents a high environmental sustainability.

It is a “low pressure fluid” as it presents lower saturation pressure for the same value of saturation temperature if compared with R32. Viscosity and density are higher than Difluoromethane at the same temperature and pressure.

Table 3.1 reports some significant properties of R32 and R1234ze(E).

Table 3.1: Significant properties of R32 and R1234ze(E) [2],[19].

Property	Unit	R32	R1234ze(E)		
Family	-	HFCs	HFOs		
GWP ₁₀₀	-	650	6		
ODP ₁₀₀	-	0	0		
Molar mass	kg kmol ⁻¹	52.024	114.04		
Triple point temperature	°C	-136.81	-104.53		
Normal boiling point	°C	-51.65	-18.97		
Critical temperature	°C	78.11	109.36		
Critical pressure	MPa	5.782	3.6349		
Critical density	kg m ⁻³	424	489.24		
Chemical formula	-	CH ₂ F ₂	CF ₃ CH=CHF (trans)		
Molecular structure	-				
<i>at a saturation temperature of 40 °C (313.15 K)</i>					
Pressure	bar	24.78	7.66		
Latent heat	kJ kg ⁻¹	237	155		
		liquid	vapor	liquid	vapor
Specific heat	kJ kg ⁻¹ K ⁻¹	2.16	2.00	1.44	1.05
Density	kg m ⁻³	893	73.3	1112	40.6
Viscosity	μPa s	94.9	13.8	167	12.9
Thermal conductivity	mW m ⁻¹ K ⁻¹	114.6	18.7	69.2	15.0

3.3 R32 and R1234ze(E) mixtures

The blending of Difluoromethane and trans-1,3,3,3-Tetrafluoroprop-1-ene leads to a formation of a non-azeotropic mixture (or zeotropic mixture). A zeotropic mixture differs from pure fluids, with regard to the condensation (or evaporation) process, mainly for two aspects:

- the mixture does not evolve (during condensation or evaporation) at a constant temperature but between the bubble point temperature (T_{bub}) and the dew point temperature (T_{dew}); this temperature variation is named temperature glide. The temperature profile during condensation is therefore not constant but varies across the heat exchanger. This profile is then “coupled” with that of the coolant that remains in a single-phase flow regime (it also show a non-constant temperature profile). Figure 3.1 reports the condensation temperature profiles for a pure fluid (left) and for a zeotropic mixture (right).

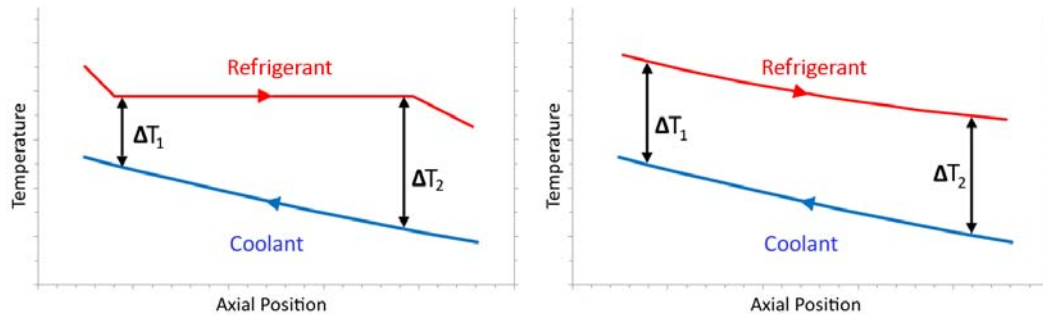


Figure 3.1: Scheme of temperature profiles during condensation of a pure refrigerant (left) and a zeotropic mixture (right).

It can be noticed that for pure fluids the temperature remains constant during condensation, hence the refrigerant to coolant temperature difference increases along the heat exchanger in a counter current configuration: $\Delta T_1 < \Delta T_2$. The zeotropic mixtures give a less variable temperature difference between the refrigerant and the coolant, hence:

$$\left(\frac{\Delta T_2}{\Delta T_1}\right)_{\text{pure}} > \left(\frac{\Delta T_2}{\Delta T_1}\right)_{\text{mixture}} \quad (3.1)$$

The coupling of the two temperature profiles is a benefit to the cycle exergetic efficiency as reduces the mean temperature drop between the refrigerant and the coolant and then losses due to irreversibility;

- the chemical composition of both the liquid and vapor phases changes during the process, according to the specific phase diagram. This variation modifies vapor and liquid properties along the heat exchanger and introduces a further resistance to the heat transfer: the mass transfer resistance. This resistance is related to the diffusion of both the mixture components through the liquid-vapor interface and this inhibits the heat exchange compared to a pure fluid.

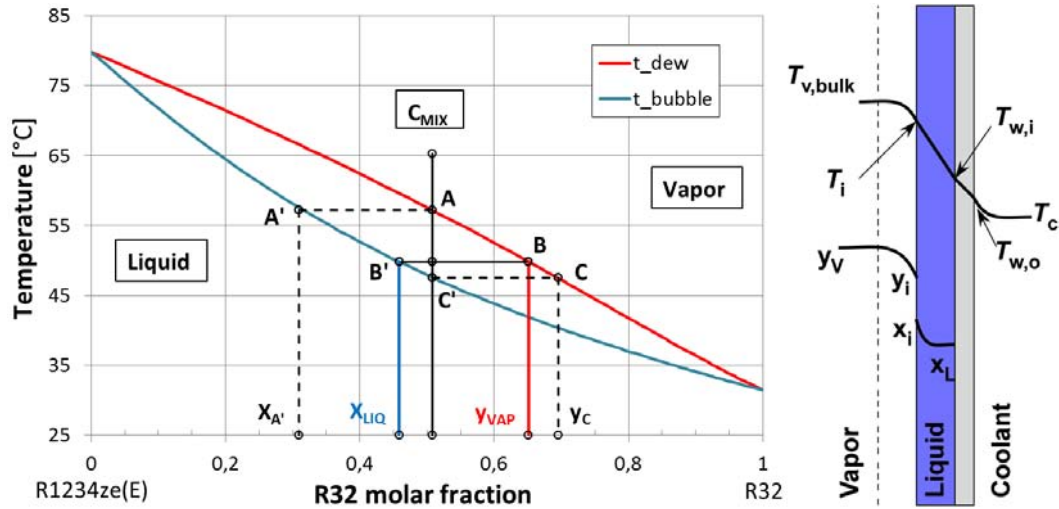


Figure 3.2: Condensation process scheme and phase diagram for a R32/R1234ze(E) zeotropic mixture with a molar fraction of 50/50% at a pressure of 20 bar. The scheme is referred to situation B in the phase diagram.

Consider the R32/R1234ze(E) zeotropic mixture shown in Figure 3.2. The figure shows the phase diagram, the relative condensation process with the concentration profiles inside the bulk vapor and condensing liquid film as well as the temperature profile. By looking at the phase diagram is clear that pure R32 is a more volatile fluid than pure R1234ze(E) as for a fixed pressure it evaporates at a lower temperature (dubbed bubble point T_{bub}). This implies that as pure R32 is added to the mixture, the bubble point and also the dew point decrease according to the relative lines shown in the phase diagram.

For a mixture with an initial composition C_{mix} the condensation process starts with saturated vapor ($x = 1$) at $T = T_{dew} = T_A$ where the first drop of liquid formed has a composition $X_{A'}$. The condensation stops with a saturated liquid ($x = 0$) at $T = T_{bub} = T_C$ where the last vapor that condenses has a composition Y_C . Between these two points the mixture varies its temperature (from T_{bub} to T_{dew}), thus to declare a unique saturation temperature for a zeotropic mixture it is not appropriate. The definition of a mean refrigerant temperature (mean value between the dew and bubble point) during condensation is an acceptable simplification:

$$\bar{T}_r = \frac{T_{dew} + T_{bub}}{2}$$

Between dew and bubble temperatures, vapor and liquid phases change their composition: the liquid phase follows the bubble line from A' to C' while the vapor phase follows the dew line from A to C.

In a middle position ($0 < x < 1$) both phases coexist and if the thermodynamic equilibrium is verified, the relative state is described by position B in Figure 3.2. As heat is removed, the less volatile component (R1234ze(E) in the present case) condenses more readily, resulting in a locally higher concentration of the more volatile component (R32) in the vapor near the interface. It can be noticed, by looking at the phase diagram, that a higher concentration of the more volatile component

in the vapor will result in a lower local saturation temperature. Additionally, the resulting concentration gradient between the vapor interface and vapor bulk results in the back diffusion of the more volatile component towards the bulk and of the less volatile component towards the interface. A similar concentration gradient is present in the liquid film. Thus, the interfacial concentration is governed by the combined effect of the rate of mass transfer in the vapor and liquid film and the rate of condensation. The condensation rate is directly related to the driving temperature difference from the interface to the coolant. Finally, the interface temperature is directly a function of the interfacial concentration; thus, the heat and mass transfer phenomena are strongly coupled. It is clear now that as the condensation proceeds, both the mixture components must diffuse in the vapor and liquid phases. In this terms, the mass transfer is a process that introduces a further resistance to the heat transfer as it requires energy.

Condensation of a zotropic mixture implies the removal of both sensible and latent heat: the sensible heat duty is due to the mixture temperature glide while the latent heat duty is relate to the phase change from vapor to liquid. The part of the latent heat is normally greater than the sensible one but both contributions must be considered in the modeling of the condensation heat duty.

In the development of this work, three mixture have been chosen as representative of all possible compositions, for the whole rest of the document the adopted nomenclature is the following:

- the three mixtures are named by their mass composition, shown in Table 3.2;
- the mass composition of the particular mixture is described as a percentage fraction by weight of the two components as:

$$\text{Mixture Composition} = R32_{\text{mass percentage}}/R1234ze(E)_{\text{mass percentage}} \%$$

Every single mixture is decribed by its proper phase diagram as the bubble point and dew point are a function of composition and pressure. Hence for a single mixture, the change in pressure leads to a change in bubble and dew point, and then in the mean refrigerant temperature. The mean refrigerant temperature chosen for the experimental tests is:

$$\bar{T}_r = 40^\circ\text{C}$$

this is the reason why Table 3.1 reports also some pure fluids properties at this temperature. The value of 40 °C has been chosen as is a very common temperature for condensation in air conditioning and automotive applications, where the condenser rejects the heat duty to the external environment. Thus three different mixtures requires three different saturation pressure values to plot the relative phase diagram. Figure 3.4 shows the phase diagrams for each one of the investigated mixtures described in Table 3.2.

The choice to express the mixture composition by mass fraction instead of molar fraction, is due to the experimental technique adopted for its creation (described in section 5.1 on page 33).

Since there was no available data for properties of R32 and R1234ze(E) mixtures in the utilized Refprop version [19], to calculate the mixture properties with correct

Table 3.2: Mixtures significant properties [19].

Property	Unit	1 st Mixture	2 nd Mixture	3 rd Mixture
Ideal Composition	-	25%/75%	50%/50%	75%/25%
Final Composition	-	23%/77%	46%/54%	76%/24%
Nomenclature	-	Mix 23/77%	Mix 46/54%	Mix 76/24%
<i>at a mean refrigerant temperature of 40 °C (313.15 K) during condensation</i>				
Pressure	bar	13.1	17.4	22.0
Dew Point	°C	45.52	44.3	41.6
Bubble Point	°C	34.55	36.1	38.7
Liquid density	kg m ⁻³	1075.3	1017.7	944.2
Vapor density	kg m ⁻³	56.3	64.6	71.3
Liquid viscosity	μPa s	143.8	121.9	103.6
Vapor viscosity	μPa s	13.8	14.2	14.1
Liquid th. conductivity	mW m ⁻¹ K ⁻¹	83.4	94.4	106.4
Vapor th. conductivity	mW m ⁻¹ K ⁻¹	16.1	16.7	17.8

mixing rules, according to the Akasaka et al. [20] experimental data, the previous equation of state adopted by Refprop has been modified by inserting into the *ASCII* file named *HMX.BNC* placed in the *Refprop\fluids* directory, a series of new coefficients. This equation of state is activated if a mixture of R32 and R1234ze(E) is selected as a predefined mixture, it implements the *Kunz and Wagner 2* mixing rules to evaluate mixture properties.

The six text lines manually added in the *HMX.BNC* file are (including the exclamation mark):

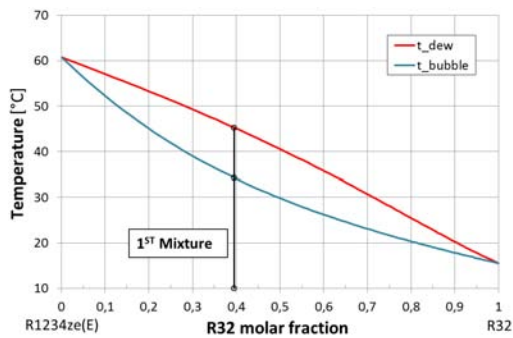
```

?R32/R1234ze      (R32/R1234ze)
?Kunz and Wagner (2007) manually inserted
75-10-5/29118-24-9      KW2  1.00343  0.977857  1.00586  0.982707  -0.265419  0.
                        TC1  0.          0.          0.          0.          0.          0.
                        VC1  0.          0.          0.          0.          0.          0.
!
```

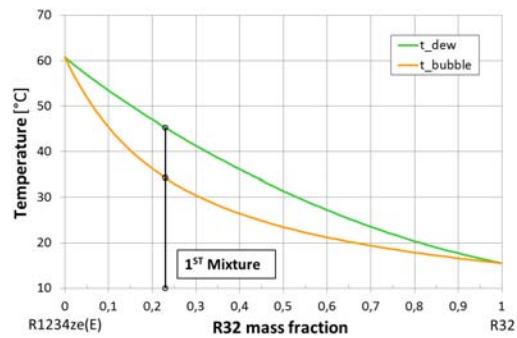
Figure 3.3: Equation of State manually inserted in Refprop [19] to evaluate mixture properties according to the Akasaka et al. [20] database.

The values returned from the Refprop program with these forced mixing rules have been found in a better agreement with the experimental data if compared with values returned with default settings. Hence all the properties of the investigated mixtures have been calculated with these new mixing rules and therefore also the phase diagrams reported in Figure 3.4.

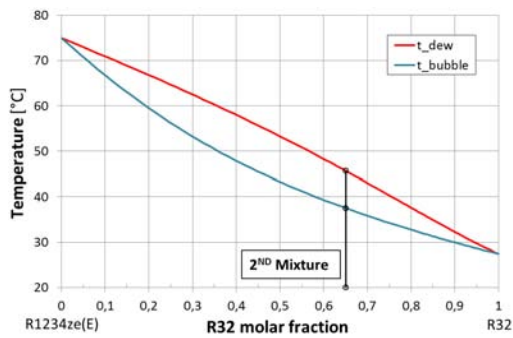
It can be notice, by looking at Figure 3.4, that if the R32 fraction increases, the required pressure to have a 40 °C mean refrigerant temperature increases. This is coherent with the fluids properties as Difluoromethane shows higher pressure than pure R1234ze(E) at the same saturation temperature. Furthermore, proceeding from mixture 23/77% to mixture 76/24%, the glide magnitude decreases from about 11 K down to about 3 K; this means that the sensible contribution to the whole heat duty during condensation decreases.



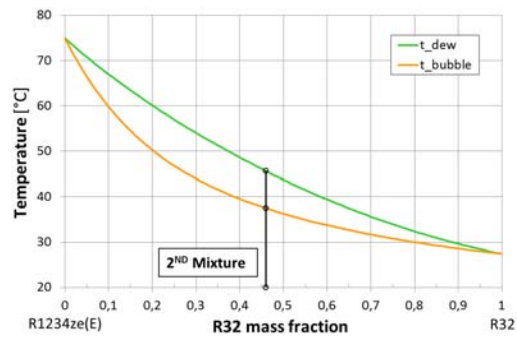
(a) First mixture molar phase diagram at a pressure of 13 bar. The R32/R1234ze(E) mixture has a molar ratio equal to 0.39/0.61.



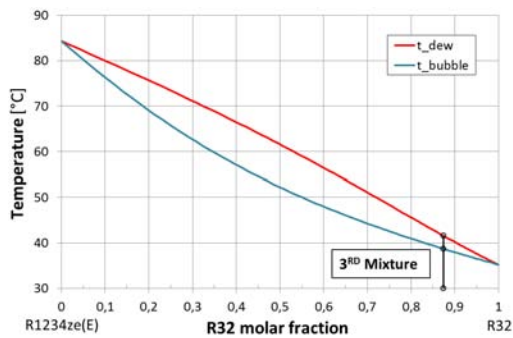
(b) First mixture massive phase diagram at a pressure of 13 bar. The R32/R1234ze(E) mixture has a massive ratio equal to 0.23/0.77.



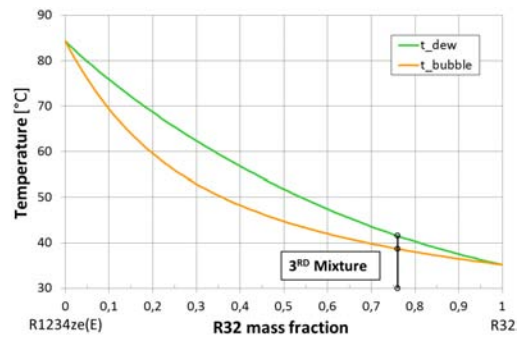
(c) Second mixture molar phase diagram at a pressure of 18 bar. The R32/R1234ze(E) mixture has a molar ratio equal to 0.65/0.35.



(d) Second mixture massive phase diagram at a pressure of 18 bar. The R32/R1234ze(E) mixture has a massive ratio equal to 0.46/0.54.



(e) Third mixture molar phase diagram at a pressure of 22 bar. The R32/R1234ze(E) mixture has a molar ratio equal to 0.87/0.13.



(f) Third mixture massive phase diagram at a pressure of 22 bar. The R32/R1234ze(E) mixture has a massive ratio equal to 0.76/0.24.

Figure 3.4: Molar (left column) and massive (right column) phase diagrams of the investigated mixtures of R32 and R1234ze(E). The diagrams have been obtained according to the Refprop [19] database at different pressures (13, 18 and 22 bar respectively) in order to maintain a mean refrigerant temperature of 40 °C.

Nomenclature

Symbols

C	molar composition [mol _{R32} /mol _{R1234ze(E)}]
T	temperature [K]
x	thermodynamic vapor quality
X	liquid composition [mol _{R32} /mol _{R1234ze(E)}]
Y	vapor composition [mol _{R32} /mol _{R1234ze(E)}]

Superscripts

—	mean value
---	------------

Subscripts

bub	bubble point at the same composition
c	coolant
dew	dew point at the same composition
i	interface
L	bulk liquid
mix	mixture
o	outer surface
r	refrigerant
V	bulk vapor
w	wall

Chapter 4

Experimental apparatus

This section provides a description of the experimental apparatus used for the development of this work. The apparatus here described is located at the Dipartimento di Ingegneria Industriale, Università degli studi di Padova. It has been used for experimental tests both for condensation (in order to investigate the HTC local values) and two-phase pressure drop (in order to investigate pressure drop values in adiabatic conditions).

4.1 Test rig

The system was designed to perform condensation (and evaporation) processes and pressure drop tests, varying the operating conditions. The test rig is shown in Figure 4.1 and consists of four closed circuits:

- the refrigerant loop;
- a hot water loop necessary for the evaporation of the refrigerant;
- a temperature controlled water loop which controls the condensation;
- a cold water loop to subcool the refrigerant.

These three water circuits are coupled and regulated (with appropriate temperatures and flow rates) together with the primary refrigerant circuit, depending on the test that has to be performed.

The subcooled refrigerant from the postcondenser is sent through a mechanical filter and a dehumidifier. Once filtered and dehumidified, the fluid passes through an independently controlled gear pump which regulates the flow rate in the system. The pump is coupled with a variable speed electric motor by means of a magnetic joint, the drag of the gears is therefore accomplished without the use of transmission shafts and related seals, i.e. gears and electric motor are physically separated. The choices of the pump type and magnetic drive imply two significant advantages:

- with a gear pump it is not necessary to use lubricating oil together with the refrigerant, it would in fact contaminate the refrigerant itself and then an oil separator would be necessary. The oil, in fact, would not contribute to the heat exchange but would introduce a further thermal resistance;

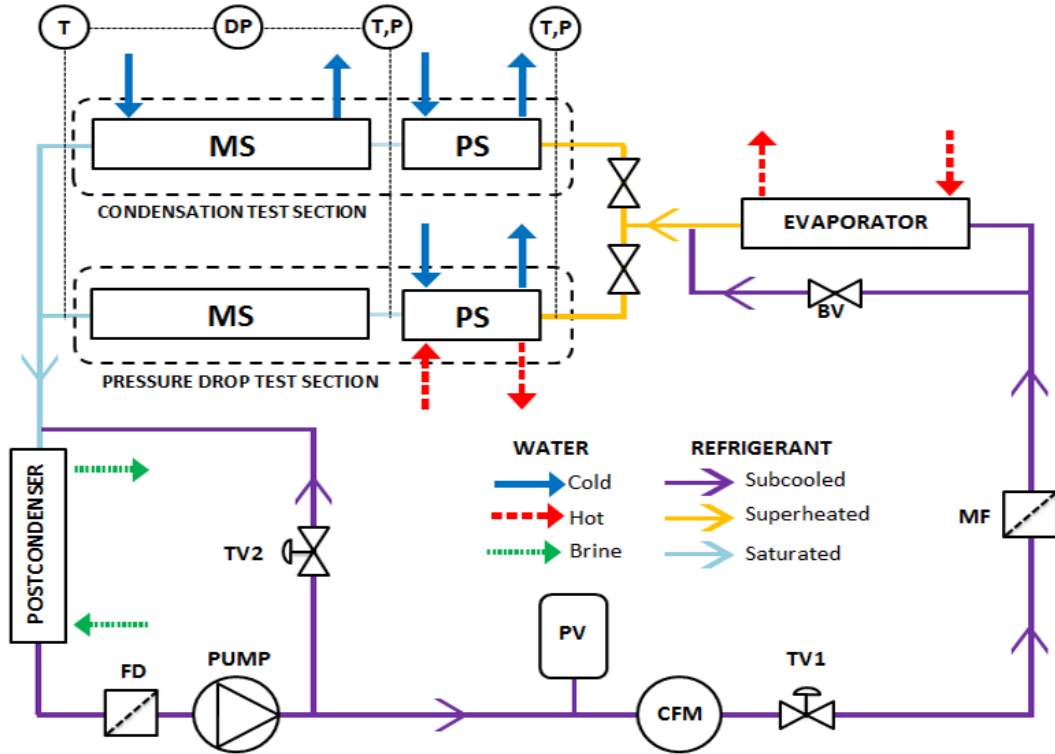


Figure 4.1: Experimental test rig scheme. FD: filter and dehumidifier, PV: pressure vessel, CFM: Coriolis-effect mass flow meter, MF: mechanical filter, PS: pre-section, MS: measuring section, TV: throttle valve, BV: ball valve.

- the absence of seals between moving parts minimizes refrigerant losses that would be problematic for mixtures. The leakage of not perfectly mixed refrigerant would lead to a variation of the composition of the mixture itself with a consequent variation of its physical properties.

In series with the pump there is a Coriolis-effect mass flow meter that measures the mass flow of refrigerant pumped into the evaporator. It is a tube-in-tube heat exchanger where the refrigerant flows in the inner pipe (copper made) while in the outer annulus hot water heated by Proportional, Integrative and Derivative (PID)-controlled electrical heaters flows. The fluid is thus evaporated and superheated so there is the certainty of entering the test section with only the vapor phase.

If a condensation test is carried out, the superheated vapor enters the condensation test section which consists of two tube-in-tube heat exchangers: the first one is an equicurrent desuperheater (technically called pre-section) and is used to obtain the saturation conditions of the fluid which then enters the second countercurrent heat exchanger constituting the actual measuring section. The pressure is gauged through two digital strain gauge pressure (relative and differential) transducers, connected to manometric taps to measure the fluid pressure upstream and downstream of the test tube while the temperature measurements are made using T-type thermocouples; a complete description of the measuring sections is given in section 4.2 on page 25. The cooling water flow rates, in the pre-section and in the measuring section, are measured by means of two Coriolis-effect mass flow meters and the total temperature

gains of the water across both sectors are measured with two copper-constantan four and three junctions thermopiles. Once passed the measuring section, the refrigerant is sent to a post-condenser that subcools it.

If a Pressure Drop (PD) test is carried out, the superheated vapor enters the pressure drop test section. This section is used to investigate the frictional pressure gradient along a 0.96 mm inner diameter microchannel in adiabatic conditions. The pressure drop is measured by relative and differential strain gauge pressure transducers and temperatures are detected by T-type thermocouples. Once the vapour exits the measuring section reaches the post condenser that subcools it. A complete description of the pressure drop measuring section is given in section 4.3 on page 28.

The system pressure is controlled by means of a membrane expansion vessel filled with nitrogen, it is placed in the lower part of the system in contact with the liquid phase in order to obtain a good pressure control with small adjustments. The desuperheater and the measuring section are fed with water as cooling medium by the same thermal bath. Now the three auxiliary circuits are briefly described:

- the evaporator water circuit is built with commercial tubes and has independent pressure vessel and pump as well as dedicated safety devices. The water is heated by a series of electrical resistances with a maximum power of 6 kW controlled by a PID electronic device. The water temperature for the evaporation is set at a temperature of about 70 °C;
- the water circuit of the test section feeds both the pre-section and the measuring section but the two coolant flow rates, as well as temperatures, can be decoupled thanks to the presence of manual throttle valves and an electrical heater placed between the pre-section and the thermal bath. The flow rate is measured by a Coriolis-effect mass flow meter and the water temperature is detected by T-type thermocouples at the inlet and the outlet of the pre-section and the measuring section. The water can be pumped at ambient pressure at a constant temperature inside the range 16 ÷ 69 °C with an accuracy of ± 0.01 °C, before the water inlet and after the water outlet mixing chambers are placed in order to obtain a good mixing of the coolant and implement a precise temperature measurement;
- the third circuit is filled with a mixture of water and propylene glycol and is set at a constant temperature of 5 °C. The mixture feeds the post condenser that complete the refrigerant condensation and keep it subcooled. The subcooling is necessary as the gear pump operates in a stable conditions with fluid in the liquid phase, the presence of some vapor bubbles inside the pump would result in an unstable flow regime.

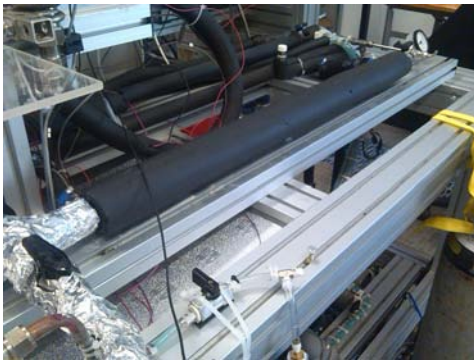
The pictures of the auxiliary elements of the refrigerant loop are reported in Figure 4.2.



(a) Mechanical filter and a dehumidifier.



(b) Magnetic gear pump.



(c) Tube-in-tube evaporator.



(d) Pressure vessel.



(e) Post-condenser.



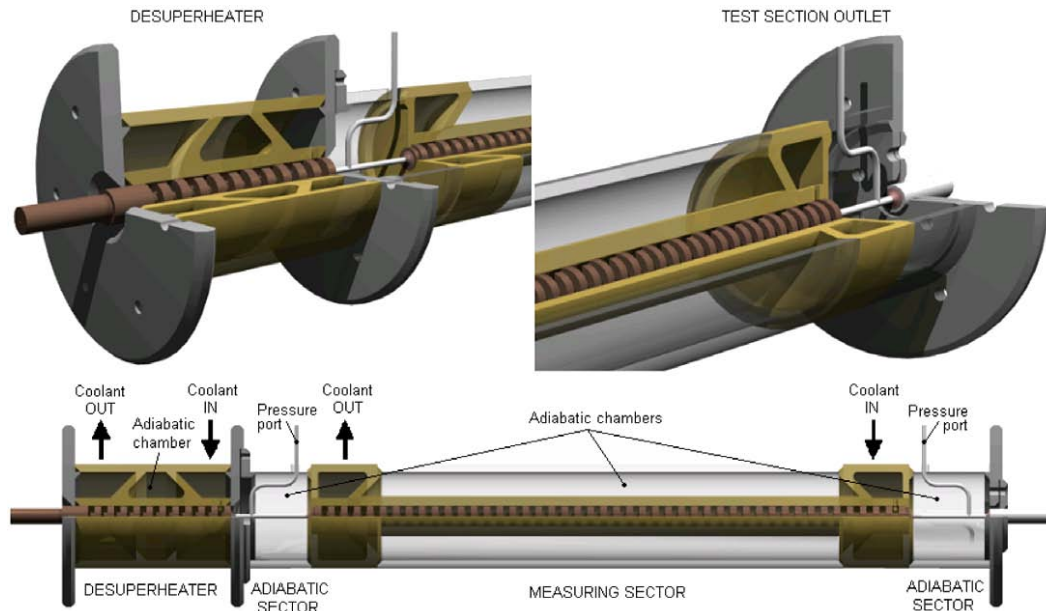
(f) Thermal baths.

Figure 4.2: Experimental apparatus. Refrigerant loop auxiliary elements.

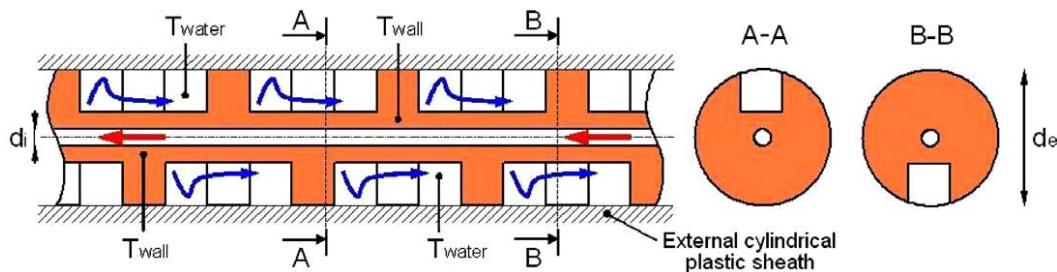
4.2 Heat Transfer test section

The measuring section for the measurement of HTC is a copper circular microchannel with an inner diameter of 0.96 mm and is divided into two parts: the first part (pre-section) serves as a desuperheater and is 0.05 m long, the second part is the actual measuring section in which the saturated vapor condensation takes place and has a length of 0.23 m. The pre-section and the measuring section are connected by a stainless capillary tube (adiabatic sector) and a similar tube connects the inlet and the outlet of the test section to the test rig. The stainless steel capillary tubes, which are 31 mm long, have three main roles:

1. to ensure a good thermal separation between the desuperheater and the measuring section and between the measuring section and the test section outlet;
2. to provide adiabatic sectors where measurement of the saturation temperature can be done with a good accuracy on the outer tube surface;
3. to provide an accommodation for the pressure ports.



(a) Design of the heat transfer test Section.



(b) Details of the coolant flow passage geometry.

Figure 4.3: Heat transfer test section [4].

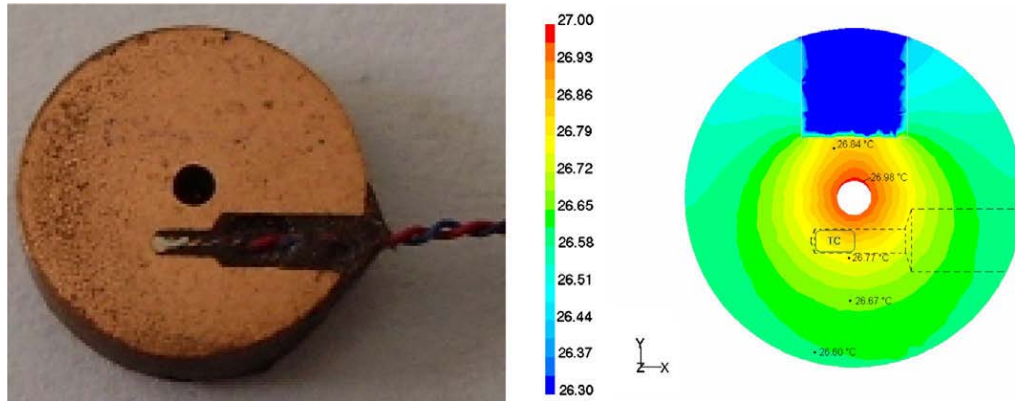
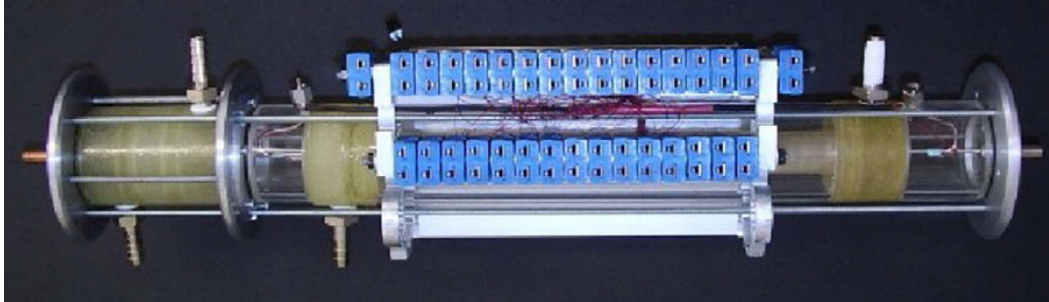


Figure 4.4: Measuring sector cross-section, thermocouple position. (Left) Enlarged image of the cross-section of the fin sample where the wall temperature is measured. The junction of the thermocouple is electrically insulated and glued in its position with high thermally conductive glue. (Right) Contours of wall temperature around the thermocouple in the copper tube [4].

The saturation pressure is measured at the inlet port by an absolute pressure transducers and at the outlet port with a differential pressure transducer, this leads to a pressure distribution (supposed linear) which accounts for the effects of frictional, local and momentum pressure change along the sector. The refrigerant temperature is measured at the inlet and outlet of the measuring section by means of a T-type thermocouple and a three-junctions thermopile soldered to the adiabatic sectors. As is depicted in Figure 4.3(a) the test section is shaped as a counter current flow heat exchanger with the condensing fluid flowing in the inside microchannel and the cooling water flowing in the external annulus. The cores of both the desuperheater and the measuring sector are obtained by proper machining the thick wall of a copper tube for industrial application, with an internal diameter of 0.96 mm and external original diameter of 8 mm. The geometry of the coolant chamber is illustrated in Figure 4.3(b), it allows to increase the external heat transfer area and reduce the related heat transfer resistance. The complex flow passage causes throughout local mixing of the coolant in the channel: by continuously changing the flow direction and disturbing the boundary layer. The major thermal resistance is then located on the refrigerant side, leading to a high difference between the saturation and the wall temperature. This means that the thermocouples uncertainty less affects the temperature measurements.

The measuring section is designed for the measurement of local two-phase Heat Transfer Coefficients by measuring both the local wall temperature and the coolant temperature along the duct. The coolant temperature profile is obtained by the thermocouples placed inside the coolant path and then the local heat flux is calculated. The wall temperatures are measured by the thermocouples placed in contact with the copper tube. They are positioned as closed as possible to the microchannel inner wall, installed inside 0.6 mm diameter holes machined 0.5 mm far from the internal surface as depicted in Figure 4.4. This short distance from the inner surface ensures a good wall temperature detection and consequently a determination of the HTC with a good accuracy. The number of temperature sensors installed in the



(a) Picture of the HTC measuring section [4].



(b) Picture of the HTC test section installed in the test rig.

Figure 4.5: Heat transfer test section pictures.

measuring sector comes up as a compromise between an appropriate temperature profile description and a feasible design; as a result of CFD modelling and prototype testing 13 thermocouples measure the wall temperature and 15 thermocouples are available for coolant temperature detection. So far the test section used in this work represents a unique experimental apparatus for two-phase condensation inside microchannels and its advantages can be schematically summarized as follows:

- it facilitates accurate measurement of local “quasi-mixing cup” temperatures of the water at low flow rates permitting the evaluation of the local heat fluxes;
- it provides improved precision in the evaluation of the HTC owing to the large ratio of heat transfer surface area;
- it allows the insertion of many wall thermocouples without passing through the cooling water, minimizing the error due to conduction along the thermocouple wires, and due to spurious electromagnetic field’s build up for the presence of high temperature gradients in the thermocouples wires.

A picture of the whole heat transfer test section is reported in Figure 4.5.

4.3 Pressure Drop test section

The pressure drop test section is inserted after the evaporator in parallel to the Heat Transfer test section as depicted in Figure 4.1 on page 22. Pressure drop tests have been performed with adiabatic conditions with two-phase flow regime occurring inside the microchannel. The refrigerant enters the test section as superheated vapor or as subcooled liquid depending on whether the vapor quality is obtained with a condensation or evaporation process. The vapor quality is obtained by an heat balance in the pre-section and it is maintained constant along the measuring section in a range between $0.1 \div 0.9$. The pre-section is a mini shell-and-tube heat exchanger and its purpose is to achieve the desired saturated thermodynamic state of the refrigerant at the inlet of the measuring section. The water outlet temperature in the pre-section is detected by a T-type thermocouple and the water temperature difference is measured by a thermopile; static mixers have been positioned upstream of the water temperature sensors in order to measure the mean effective water temperature both at the inlet and outlet.

The measuring section is produced with the same copper channel used for the Heat Transfer test section and it is connected to the test rig by mean of adiabatic stainless steel capillary tubes in order to ensure the adiabatic flow conditions. Two pressure ports are connected to the measuring section positioned at a distance of 220 mm; the pressure lines are heated by electrical resistances in order to avoid the creation of liquid droplets that would create a pressure differential between the two sides of the liquid droplet itself. The inlet pressure is measured by an absolute pressure transducer and the pressure drop between the two ports is gauged by a differential transducer; pressure drop below 0.01 bar can be detected.

A picture of the pressure drop test section inserted in the test rig is reported in Figure 4.6.



Figure 4.6: Picture of the pressure drop test section installed in the test rig.

4.4 Measuring instruments

This section provides a brief description of the characteristics of the measuring instruments installed in the experimental apparatus. The three parameters measured during the experimental tests are: temperature, mass flow rate and pressure. All other parameters such as diameters, roughness or lengths are measured with dedicated instruments whose uncertainty is reported in chapter 6 on page 47.

Thermocouples

All the thermocouples installed in the test rig are T-type thermocouples (copper - constantan junction). The temperature measurement is indirect because it is transduced from an electrical potential difference, such potential difference occurs between the two junctions of the copper and constantan wires and is dependent on their temperature (Seebeck effect). A junction (hot junction) is placed at the point where the temperature has to be detected while the other one (cold junction) is located in a point of known temperature. The reference temperature is achieved by a Kaye instrument that physically maintains a constant temperature of 0°C inside a reference chamber; all the thermocouples installed in the implant are connected to this physical reference. The hot junction was obtained by melting together the two cables by electrical welding, so there are no interpositions of a third material which would have increased the joint size; the cold junction is created inside the Kaye instrument which has separate terminals for copper and constantan wires.



(a) Kaye instrument, reference for 0°C .



(b) Super thermometer for thermocouples calibration.

Figure 4.7: Instruments for thermocouples calibration.

The thermocouples are placed in the following locations:

- at the inlet of the test sections in order to measure the superheating produced by the evaporator. The thermocouple is installed on the outer surface of the adiabatic sector, i.e. the stainless steel tube which has an outer diameter of 0.76 mm;
- at the inlet and outlet of the pre-sections water loop;

- at the inlet of the measuring sections, again on the outer surface of the adiabatic sectors (stainless steel capillary tube);
- 13 thermocouples placed along the HTC measuring section for the wall temperature detection, the accommodation of the hot junctions is depicted in figure 4.4;
- 15 thermocouples placed in the external annulus of the measuring section for the water profile detection;
- at the outlet of the measuring section in the final adiabatic sector;
- a final thermocouple measures the room ambient temperature.

The thermocouples calibration has been done with the use of a super thermometer, reported in Figure 4.7(b), capable of measure temperatures with an uncertainty of ± 0.002 K. The calibration is performed by comparing the values returned by the super thermometer and the temperatures measured by the thermocouples. The difference between the two measures is evaluated at different temperatures in order to get two temperature profiles. Assuming as a reference the one of the super thermometer, the thermocouples temperature curves are corrected retrospectively using coefficients obtained from the temperature interpolation. This procedure allows to obtain an uncertainty equal to ± 0.05 K for the temperature measurements.

Coriolis-effect mass flow meters

Such instruments are constituted by a curved tube put in oscillation with a known frequency. Once the fluid flows, such oscillation is modified by the Coriolis force $\vec{F} = m \cdot 2\vec{\omega} \wedge \vec{v}$ (where m is the mass, $\vec{\omega}$ is the angular velocity and \vec{v} is the fluid velocity). This force deforms the channel and it varies the frequency and the amplitude of oscillation, allowing the measurement of the flow. Inside the plant there are three flow meters: one dedicated to the refrigerant, with a maximum flow rate $\dot{m}_{\max} = 4$ kg h⁻¹ and two placed on the measuring sections and pre-sections water loops with a maximum flow rate of $\dot{m}_{\max} = 80$ kg h⁻¹. A picture of the refrigerant mass flow meter and its relative transducer is reported in Figure 4.8.



(a) Coriolis-effect mass flow meter.



(b) Mass flow rate transducers.

Figure 4.8: Picture of the refrigerant Coriolis-effect mass flow meter and relative transducer installed in the test rig.

Pressure transducers

The absolute pressure is gauged at the inlet both of the test sections and measuring sections, the pressure ports are located in adiabatic sectors (stainless tubes). The two absolute pressure transducers have a maximum operative pressure $p_{\max} = 275.8$ bar and a full-scale pressure $p_{fs} = 50$ bar. The differential pressure transducers measure the pressure difference between the inlet and outlet port of the measuring sections. These two instruments have different full scale pressures in order to measure with a good accuracy different pressure ranges, both the transducers have a maximum pressure $p_{\max} = 20.7$ bar and the two full scale pressure are $p_{fs} = 1$ bar and $p_{fs} = 0.01$ bar. All the pressure lines are heated by electrical resistances in order to avoid the formation of liquid droplets that otherwise would affect the measure by creating a pressure drop in the pressure lines. The relative uncertainty of these instruments is reported in section 6.1 on page 47. A picture of two pressure transducers is reported in Figure 4.9.

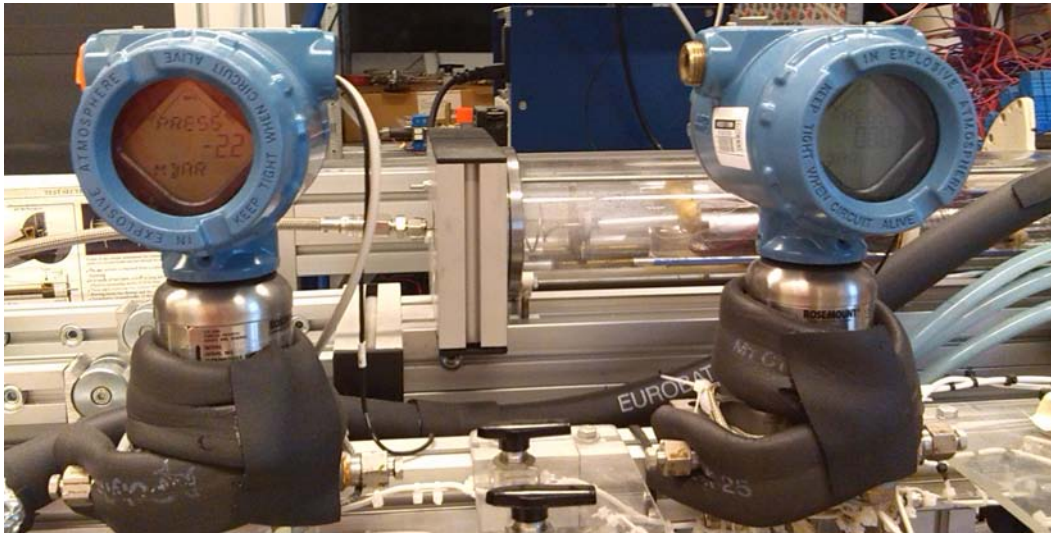


Figure 4.9: Picture of two Rosemount pressure transducers installed in the test rig.

Chapter 5

Experimental tests

A short description of the experimental technique adopted in this work is reported. The procedure includes: mixture preparation, data acquisition and data reduction for both condensation and pressure drop tests.

5.1 Mixture preparation

The two mixture components are contained in two different high pressure tanks and they are blended together inside a third dedicated reservoir (dubbed mixture reservoir). Once knowing the internal capacity of the mixture reservoir, it is possible to calculate the refrigerants amounts (in kg) that has to be put inside in order to avoid too high pressures. The two amounts are in dependence on the mixture that has to be formed.

The following procedure is adopted:

- first of all, the mixture reservoir is connected to both the fluid tank which has the lower saturation pressure and an alternative vacuum pump, the connection is made by using rods and valves. This is necessary in order to have no air contamination as it would change the mixture properties. The lower saturation pressure of the first refrigerant (R1234ze(E) in the present case) will allow an easier charge of the second fluid which has a higher saturation pressure;
- the reservoir is placed on a balance with 0.001 kg sensitivity in order to constantly measure its weight and later the amount of fluid that will be injected inside it;
- after a sufficient vacuum degree is reached, the vacuum pump is disconnected and the mixture reservoir is filled with the first refrigerant by opening the connection between it and the refrigerant tank. The higher pressure inside the tank makes the fluid flow inside the reservoir (that was in vacuum);
- once the calculated amount of fluid is injected, the mixture reservoir is disconnected from the fluid tank and its weight is recorded;
- the mixture reservoir is connected to the second fluid tank (higher saturation pressure) and the vacuum pump by means of rods and valves;

- after a sufficient vacuum degree is created inside rods and valves, the second fluid (R32 in the present case) enters the mixture reservoir by opening the connection between it and the fluid tank. The pressure difference between the two tanks let the second fluid enters the mixture reservoir (that contained the first fluid in equilibrium);
- the mixture reservoir weight is constantly detected in order to have a good approximation of the mixture composition during its formation. After disconnecting the reservoir from the tank, its weight is registered to make a precise calculation of the mixture composition in terms of mass fractions.

Before the mixture is pumped in the test rig, it is cleaned with several washings made with high pressure nitrogen. This is necessary to clean up the ducts from impurities which would contaminate the mixture. The washings are made by filling the apparatus with nitrogen and then ejecting it from different points along the whole test rig leaving the system at ambient pressure.

Once the apparatus is cleaned, the vacuum pump is connected to it and vacuum is made inside the ducts for a sufficient time period. Then the mixture reservoir is connected to the test rig and by means of the pressure difference between them, the mixture is pumped inside the channels.

A picture of the mixture reservoir and the vacuum pump is reported in Figure 5.1.



(a) Mixture reservoir.



(b) Alternative vacuum pump.

Figure 5.1: Picture of the mixture reservoir and the vacuum pump used for the mixture charge.

As the mixture reservoir is easily manageable (it contains about 0.8 kg of mixture), it is possible to turn it upside down in order to place the outlet valve in direct contact with the mixture liquid phase. The test rig, in fact, must be filled with liquid phase to make sure that the mixture composition is as homogeneous as possible.

During the tests, more samples of the investigated mixtures have been taken and then analyzed by using a gas chromatograph in order to know the exact mixture composition.

5.2 Data acquisition

The tests have been carried out by setting the apparatus in a stable condition in terms of temperatures, mass flow rates and pressures. It is important to say that, for both condensation and pressure drop tests, every parameter as well as its relative Standard Deviation σ are recorded as a mean value of $n=50$ readings, done with a frequency of 1 Hz (so every measure lasts 50 seconds). This mean value is then used as a reference in the data reduction and its relative Standard Deviation is used in the uncertainty calculation as explained in section 6.1 on page 47.

5.2.1 Condensation tests

The condensing refrigerant flows inside the Heat Transfer test section while water flows on the external annulus in both pre-section and measuring section.

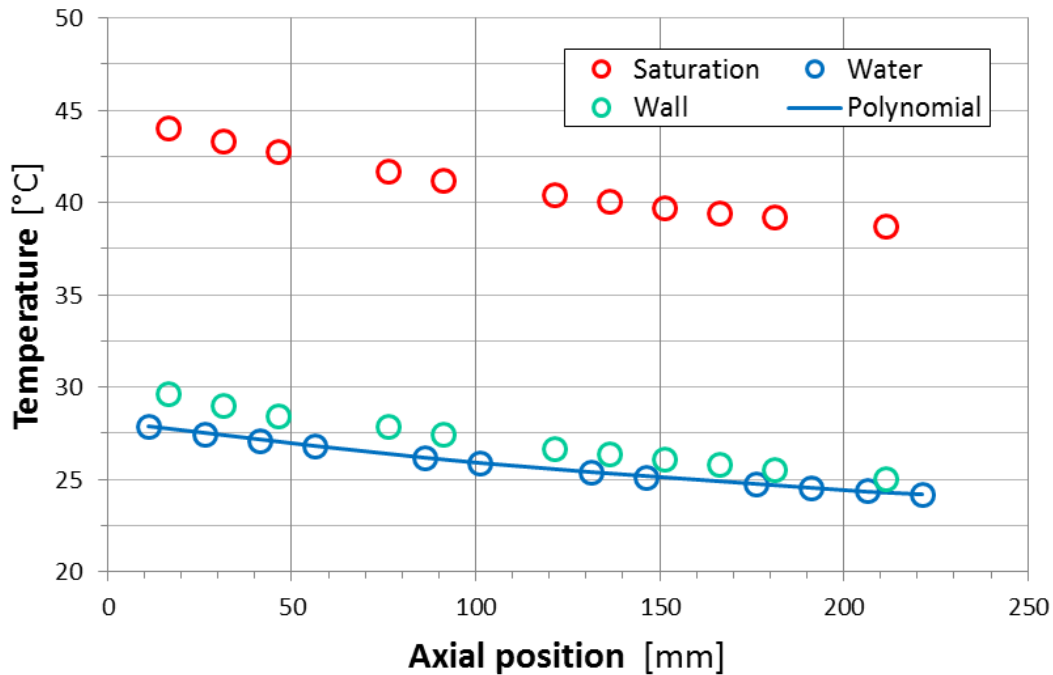


Figure 5.2: Refrigerant, wall and water temperature experimental profiles at $G = 400 \text{ kg m}^{-2}\text{s}^{-1}$ for a R32/R1234ze(E) mixture with a 46/54% mass fraction. The continuous line shows the profile obtained with the water temperatures interpolation by means of a second order polynomial.

During the tests, the following parameters are measured:

- water temperatures: inlet and outlet water temperatures in the pre-section and measuring section are recorded. The water temperature profile in the measuring section is obtained by using 15 T-type thermocouples;
- 13 wall temperatures values by using 13 T-type thermocouples placed in the copper tube as depicted in Figure 4.4 on page 26;
- the refrigerant temperatures on the adiabatic sectors (stainless tubes) i.e. at the pre-section inlet and at the inlet and outlet of the measuring section;

- the ambient temperature;
- the pressure at the inlet of the pre-section and at the measuring section inlet by means of two absolute pressure transducers;
- the pressure drop along the measuring section by means two differential pressure transducers;
- the refrigerant mass flow rate and water mass flow rates (both in the pre-section and measuring section) by means of three Coriolis-effect mass flow meters.

Figure 5.2 shows the temperature profiles obtained in the measuring section for a test carried out at $G = 400 \text{ kg m}^{-2}\text{s}^{-1}$ with mixture 46/54% as operative fluid (R32/R1234ze(E) mass ratio equal to 46/54%). The figure also reports the refrigerant temperature calculated along the test section. It is evident that the condensing fluid is not pure as its saturation temperature varies by about 5°C ; the whole temperature glide for the mixture is about 7°C as shown in Figure 3.4 on page 17. Furthermore, we can note the coupling of the wall and saturation temperature profiles i.e. the difference between the saturation temperature and the wall temperature attests around 14°C with little variations.

5.2.2 Pressure drop tests

Pressure drop tests are conducted with adiabatic flow conditions inside the Pressure Drop test section, the measured parameters are:

- the inlet and outlet refrigerant temperatures in the measuring section as well as in the pre-section on the stainless adiabatic sectors;
- inlet and outlet pressures in the measuring section together with the pre-section inlet pressure;
- the pre-section water mass flow rate and the refrigerant mass flow rate;
- the inlet and outlet water temperature in the pre-section (utilized for the thermal balance).

5.3 Preliminary tests

Preliminary tests are necessary to validate all the measurements carried out in the test sections. They have been performed for both the HTC measuring section and the PD measuring section.

5.3.1 Heat transfer measuring section

A preliminary test of the Heat Transfer measuring section have been carried out before the condensation tests. The check is performed by condensing the mixture from superheated vapor to subcooled liquid. By making a heat balance between the refrigerant and the coolant (water):

$$\dot{m}_r (h_{in} - h_{out}) = \dot{m}_w c_{p,w} (T_{w,out} - T_{w,in}) \quad (5.1)$$

the set-up of the measuring section is verified. The percent deviation between the heat flux on the refrigerant side and on the coolant side is 3.4% for mixture 23/77%, 1.2% for mixture 46/54% and 1.7% for mixture 76/24%. Hence, assuming a maximum deviation of 5%, the heat transfer measuring section is verified.

5.3.2 Pressure drop measuring section

The PD measuring section has been verified by running a test with liquid-phase flow regime in adiabatic conditions. The experimental pressure drop between the two pressure ports of the PD measuring section has been measured in order to obtain the friction factor f defined as:

$$f = \frac{\rho_L D \Delta p}{2G^2 L} \quad (5.2)$$

The verify has been carried out comparing the experimental friction factor with theoretical correlations. For laminar flow regime, the two correlations used for the comparison are the Blasius equation:

$$f = \frac{0.3164}{4} \cdot Re^{-\frac{1}{4}} \quad (5.3)$$

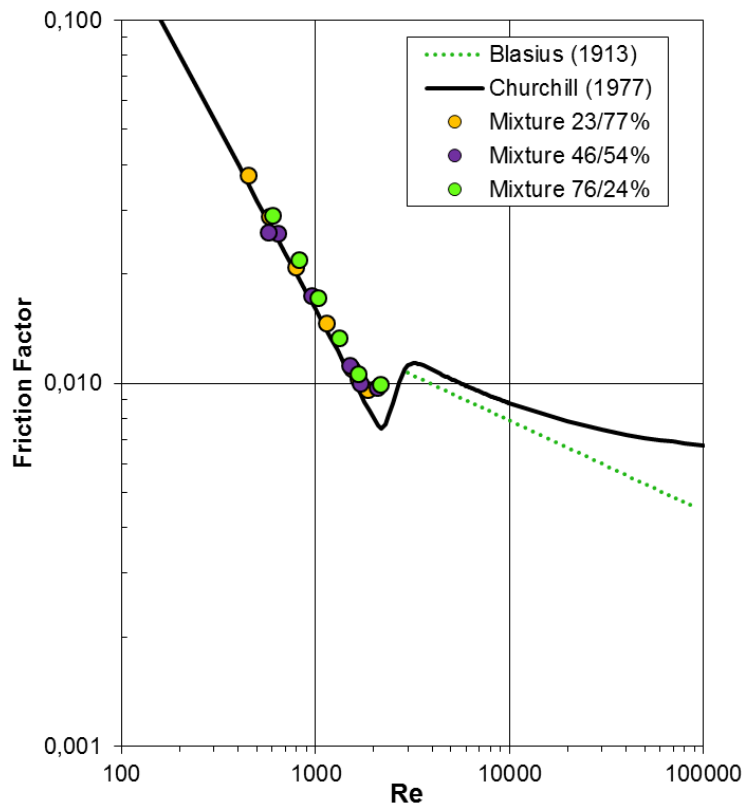


Figure 5.3: Experimental and predicted friction factor at different Reynolds numbers for the investigated mixtures. The experimental points are referred to single-phase flow regime (liquid).

and the Churchill [21] equation:

$$f = 2 \left[\left(\frac{8}{Re} \right)^{12} + \frac{1}{(A+B)^{3/2}} \right]^{\frac{1}{12}} \quad (5.4)$$

where:

$$A = \left[2.457 \ln \left(\frac{1}{(7/Re)^{0.9}} + \frac{0.27 Ra}{D} \right) \right]^{16} \quad (5.5)$$

$$B = \left(\frac{37530}{Re} \right)^{16}$$

The Blasius equation (5.3) is accurate for $Re < 1 \cdot 10^5$ while the Churchill equation (5.4) covers all the Re numbers for laminar, transitional and turbulent flow regimes. The comparison between experimental and predicted friction factors is reported in Figure 5.3. It can be noticed a good agreement between the mixtures data and the theoretical correlations for the laminar region ($Re < 2000$). The experimental points in the transitional region ($2000 \leq Re \leq 4000$) shows a slight deviation from the correlations. The agreement between experimental predicted data guarantees the absence of impurities inside the microchannel and verifies the calibration of the measuring instruments.

5.4 Data reduction for the heat transfer test section

Once the water temperatures in the measuring section are known, a second order polynomial is used to fit them in order to have the water temperature profile in the form of:

$$T_w(z) = a_0 + a_1 z + a_2 z^2 \quad (5.6)$$

Similarly the refrigerant pressure profile is obtained by interpolating the inlet and outlet pressure values with a first order polynomial. So the pressure profile in the measuring section has the form:

$$p_r(z) = b_0 + b_1 z \quad (5.7)$$

where the constants a_0 , a_1 , a_2 and b_0 , b_1 are dependent on the temperatures and pressures values. Two orders have been considered for the water temperature interpolation: the second order and the third order. The second order has been chosen taking account of computational efforts, interpolation accuracy as well as physical aspects. The error committed by the polynomial with respect to the measured temperature is lower than the thermocouples accuracy (i.e. ± 0.05 K), furthermore, the coefficient of determination r^2 shows a value close to unity:

$$r^2 = \frac{\sum_{i=1}^{13} (T_{w,i} - T_{w,i,pol})^2}{\sum_{i=1}^{13} (T_{w,i} - \bar{T}_w)^2} \approx 1 \quad (5.8)$$

where the mean water temperature is defined as:

$$\bar{T}_w = \frac{\sum_{i=1}^{13} T_{w,i}}{13} \quad (5.9)$$

This means that the interpolation of the fitted parameter is done with a good accuracy justifying the choice of the second order polynomial as gives a sufficient accuracy. These interpolations are made up to evaluate all the parameters (wall temperature, water temperature and refrigerant pressure) at the same axial position z_{wall} . In fact the wall thermocouples and water thermocouples are not placed at the same position along the measuring section, so the axial distance between them would lead to an uncorrect local temperature measurements. Furthermore, pressure is known only at the inlet and outlet of the measuring section, so the polynomial (5.7) is necessary to calculate pressure values on intermediate positions.

By deriving the water temperature polynomial equation constructed in (5.6), the slope of the water profile $\partial T_w(z)/\partial z$ is obtained, this is used to calculate the local heat flux as:

$$q(z) = -\dot{m}_w \cdot c_{p,w} \cdot \frac{\partial T_w(z)}{\partial z} \quad (5.10)$$

The local HTC inside the microchannel can be obtained as the ratio of local heat flux to saturation minus wall temperature difference:

$$HTC(z) = \frac{q(z)}{\pi D [T_{sat}(z) - T_{wall}(z)]} \quad (5.11)$$

It should be pointed here that the only unknown value in Equation (5.11) is the saturation temperature $T_{sat}(z)$; in fact the heat removed from the refrigerant is given by (5.10), the inner diameter D is known and the wall temperature T_{wall} is a measured parameter. As previously described in section 3.3 the saturation temperature changes during condensation (see Figure 5.2 on page 35) and its value is dependent on the thermodynamic vapor quality and pressure as well as the mixture itself. Hence by knowing the thermodynamic state of the refrigerant at a certain position along the condenser, the saturation temperature can be evaluated. Two methods have been implemented for its calculation and for the thermodynamic state calculation, such methods are described in the following sections.

5.4.1 First method [22]

This method has been implemented according to the procedure described by Cavallini et al. [22] for condensation of zeotropic mixtures.

For pure refrigerants, the vapor quality change is given as the ratio between the isobaric change in enthalpy Δh_{COND} and the differential latent heat i_{LG} . But condensation of zeotropic mixtures differs from that of a pure refrigerant in that the isobaric process takes place over a temperature range or glide while a pure refrigerant condenses at a fixed saturation temperature. Hence the heat removed from the refrigerant mixture includes both latent heat from the phase change process and sensible heat from cooling. The isobaric change in enthalpy for a zeotropic mixture is then:

$$\Delta h_{COND} = i_{LG} \Delta x + (1 - x)c_{pL} \Delta T_{sat} + xc_{pG} \Delta T_{sat} \quad (5.12)$$

where the values of i_{LG} , c_{pL} and c_{pG} depend on the saturation temperature T_{sat} , as is the case for pure refrigerants. But they are also a function of the local liquid and

vapor compositions. The saturation temperature can be related to the vapor quality by means of the following equation:

$$T_{sat} = T_{dew} - \Delta T_{GL}[1 - f(x)] \quad (5.13)$$

where ΔT_{GL} is the temperature glide (difference between the dew point temperature and bubble point temperature at the same composition) while $f(x)$ is an empirical function for the vapor quality that ranges between $0.0 \div 1.0$. The change in temperature ΔT_{sat} can easily be obtained as:

$$\Delta T_{sat} = \Delta T_{GL}[f(x) - f(x - \Delta x)] \quad (5.14)$$

The value of $f(x)$ is here approximated as a linear function of the x variable:

$$f(x) = x \quad ; \quad x \in [0, 1] \quad (5.15)$$

The combination of Equation (5.15) with Equations (5.12), (5.13) and (5.14) gives a different expression for the Δh_{COND} :

$$\Delta h_{COND} = i_{LG} \Delta x + (1 - x)c_{pL} \Delta T_{GL} \Delta x + x c_{pG} \Delta T_{GL} \Delta x \quad (5.16)$$

the saturation temperature of the refrigerant:

$$T_{sat} = T_{dew} - \Delta T_{GL}(1 - x) \quad (5.17)$$

and finally the saturation change in temperature:

$$\Delta T_{sat} = \Delta T_{GL} \Delta x \quad (5.18)$$

The data reduction procedures are the same for both pre-section and measuring section.

5.4.2 Pre-section

At the pre-section inlet the refrigerant comes as superheated vapor, so as the temperature and pressure values are known, it is possible to obtain its thermodynamic state by using Refprop [19]. Then the refrigerant enters the pre-section where two different processes occur:

1. a desuperheating process i.e. from superheated vapor to saturated vapor ($x = 1$). The heat removed from the desuperheating is easily obtainable by means of the following relation:

$$\dot{q}_{des} = \dot{m}_r (h_{in,ps} - h_{dew,ps}) \quad (5.19)$$

where the two enthalpies are given by the Refprop database [19] knowing the pre-section inlet temperature and pressure, the measuring section inlet pressure and the mixture composition (i.e. the R32 mass fraction in the mixture X_{R32}):

$$\begin{aligned} h_{r,in,ps} &= h_{r,in,ps}(T_{r,in,ps}, p_{r,in,ps}, X_{R32}) \\ h_{r,dew,ps} &= h_{r,dew,ps}(p_{r,in,ms}, x = 1, X_{R32}) \end{aligned} \quad (5.20)$$

2. an initial condensation process that creates the desired thermodynamic state at the outlet of the pre-section. The heat removed during this process is:

$$\begin{aligned}\dot{q}_{\text{COND},ps} &= \dot{m}_{w,ps}(h_{w,out,ps} - h_{w,in,ps}) - \dot{q}_{des} \\ &= \dot{m}_{w,ps} c_{p,w}(T_{w,out,ps} - T_{w,in,ps}) - \dot{q}_{des}\end{aligned}\quad (5.21)$$

This heat flow rate is removed while a phase change occurs, so Equation (5.16) must be used to calculate the pre-section outlet vapor quality $x_{out,ps}$ in the form:

$$\begin{aligned}\Delta h_{\text{COND},ps} &= \frac{\dot{q}_{\text{COND},ps}}{\dot{m}_r} \\ &= i_{\text{LG}}(1 - x_{out,ps}) + (1 - x_{out,ps})^2 c_{pL} \Delta T_{\text{GL}} \\ &\quad + x_{out,ps} c_{pG} \Delta T_{\text{GL}}(1 - x_{out,ps})\end{aligned}\quad (5.22)$$

as the starting value of the vapor quality is equal to 1.

As adiabatic sectors connect the pre-section to the measuring section, the assumption to consider the pre-section outlet thermodynamic state equal to the one on the measuring section inlet is justified. Hence by using Equation (5.17) and (5.18) all the measuring section inlet parameters are now determined: pressure, saturation temperature together with its variation and vapor quality.

5.4.3 Measuring section

Once knowing the refrigerant thermodynamic state at the measuring section inlet, the next ones are calculated for every wall thermocouple placed in the measuring section. Let us assume that the initial thermodynamic state (named with 1 as subscript) of the axial position $z_{wall,1}$ is known; hence parameters such as pressure p_1 , enthalpy $h_{r,1}$ and vapor quality x_1 are known. The following thermodynamic state (named with 2 as a subscript) on $z_{wall,2}$ has now to be determined. The procedure is the following:

- the pressure value p_1 and the mixture composition are inserted into the Refprop [19] database in order to calculate the $T_{dew,1}$ and $T_{bub,1}$ and then obtaining the temperature glide $\Delta T_{\text{GL},1}$;
- the saturation temperature is calculated using equation (5.17) as:

$$T_{sat,1} = T_{dew,1} - \Delta T_{\text{GL},1}(1 - x_1)\quad (5.23)$$

- knowing the saturation temperature $T_{sat,1}$ and the pressure p_1 it is possible to obtain the value of the differential latent heat $i_{\text{LG},1}$. First, the liquid and gas phase compositions are calculated from the Refprop [19] database and then used to obtain the values of $c_{pL,1}$, $c_{pG,1}$. The differential latent heat is calculated as the difference between the gas phase enthalpy and the liquid phase enthalpy at the same saturation temperature $T_{sat,1}$:

$$i_{\text{LG},1} = (h_{rG,1} - h_{rL,1})_{\text{eq}}\quad (5.24)$$

- the local heat flux in the initial position is then calculated using Equation (5.10) as:

$$q_1 = -\dot{m}_{w,ms} \cdot c_{p,w} \cdot \left[\frac{\partial T_w(z)}{\partial z} \right] \Big|_1 \quad (5.25)$$

leading to the experimental HTC_1 calculation by means of Equation (5.11) as:

$$HTC_1 = \frac{q_1}{\pi D (T_{sat,1} - T_{wall,1})} \quad (5.26)$$

- the next vapor quality x_2 is calculated using Equation (5.16) and putting the refrigerant isobaric change in enthalpy equal to the cooling water change in enthalpy between the two position 1 and 2:

$$\begin{aligned} \dot{m}_{w,ms} c_{p,w} (T_{w,pol,1} - T_{w,pol,2}) &= i_{LG,1} (x_1 - x_2) \\ &+ (1 - x_1) c_{pL,1} \Delta T_{GL,1} (x_1 - x_2) + x_1 c_{pG,1} \Delta T_{GL,1} (x_1 - x_2) \end{aligned} \quad (5.27)$$

- now the vapor quality x_2 is know and the pressure on the position $z_{wall,2}$ is evaluated by the polynomial (5.7) on $z = z_{wall,2}$. The procedure is then repeated in order to calculate the thermodynamic states for all the z_{wall} positions.

5.4.4 Second method [23]

This method has been implemented according to the reduction described by Kondou et al. [23] for two-phase heat exchange with zeotropic mixtures as operative fluid and it is the one chosen in this work for the data reduction as it gives lower uncertainty values in the calculation of the mixtures thermodynamic properties.

This method assumes that the thermodynamic equilibrium is present during the whole condensation. It can be applied without distinguish two different algorithms for the pre-section and measuring section as it involves thermal balances derived from the first law of thermodynamics.

According to the procedure performed by Kondou et al. [23] the saturation temperature T_{sat} and vapor quality x can be calculated from pressure, enthalpy and circulating composition, i.e. the R32 mass fraction of the mixture X_{R32} . Hence by using the Refprop [19] database the saturation temperature is obtained as:

$$T_{sat} = T_{sat}(p, h, X_{R32})_{eq} \quad (5.28)$$

and similarly the vapor quality is obtained as:

$$x = x(p, h, X_{R32})_{eq} \quad (5.29)$$

Hence knowing the pressure and enthalpy values on the initial position p_1 and $h_{r,1}$, it is possible to obtain the saturation temperature $T_{sat,1}$ and the vapor quality x_1 . Now the local HTC is given by Equation (5.26). Proceeding along the measuring section, the next enthalpy value $h_{r,2}$ is calculated as:

$$h_{r,2} = h_{r,1} - \frac{\dot{m}_{w,ms}}{\dot{m}_r} c_{p,w} (T_{w,pol,1} - T_{w,pol,2}) \quad (5.30)$$

and then the next saturation temperature $T_{sat,2}$ as well as vapor quality x_2 are calculated referring to Equations (5.28) and (5.29). The procedure is repeated for all the z_{wall} axial position along the measuring section.

5.4.5 Experimental methods corrections [24]

The corrections implemented for the calculation of the experimental HTC was investigated by Matkovič [24] and are related to some technical aspects of the only Heat Transfer measuring section:

- an axial heat flow is present along the measuring section through the copper annulus (that is the tube itself) so its contribution has to be considered. Then it is necessary to interpolate the wall temperatures T_{wall} with a second order polynomial in order to have:

$$T_{wall}(z) = c_1 + c_2z + c_3z^2 \quad (5.31)$$

The order of the polynomial is chosen as it fits with a good accuracy the wall temperature profiles without excessive computational efforts. Now it is possible to calculate the axial heat flow added to the local heat flow as:

$$q_{ax}(z) = 2\lambda_{Cu} A_{cs} \frac{\partial^2 T_{wall}(z)}{\partial z^2} \quad (5.32)$$

where λ_{Cu} is the thermal conductivity of the copper tube and A_{cs} is the axial conductive area of the channel, given by:

$$A_{cs} = \pi \frac{D_e^2 - D^2}{4} \quad (5.33)$$

- a change in temperature between the internal wall surface and the wall thermocouples is present; so a wall temperature correction is necessary. Roughly, the temperature measurement is corrected for the temperature drop obtained from the thermal balance in the radial heat conduction through the tube wall, leading to the following equation:

$$\Delta T_{wall}(z) = \frac{q(z)}{2\pi \lambda_{Cu}} \cdot \ln\left(\frac{D/2 + 0.0005}{D/2}\right) \quad (5.34)$$

- a heat dissipation due to the temperature difference between the water temperature and the ambient temperature is present. Its magnitude has been measured leading to the following expression for the total heat dissipated in the measuring section:

$$\dot{q}_{diss,ms} = 0.1772 \left(T_{amb} - \frac{T_{w,in,ms} + T_{w,out,ms}}{2} \right) + 0.1253 \quad (5.35)$$

the local dissipated heat is given by:

$$q_{diss}(z) = \dot{q}_{diss,ms} \cdot \frac{T_w(z) - T_{amb}}{\int_0^z [T_w(z) - T_{amb}] dz} \quad (5.36)$$

Now the local dissipated heat in the measuring section is computed for each wall position by dividing the total dissipated heat by 13 as this is the number of wall thermocouples. Furthermore, every wall position is characterized by its proper axial flux, then the first member of Equation (5.27) (the isobaric change in enthalpy of the refrigerant) must be corrected as:

$$\dot{m}_r \cdot \Delta h_{\text{COND}}(z) = \dot{m}_{w,ms} c_{p,w}(T_{w,pol,1} - T_{w,pol,2}) + q_{ax}(z) \cdot (z_{wall,2} - z_{wall,1}) - \frac{\dot{q}_{diss,ms}}{13} \quad (5.37)$$

and the second member of Equation (5.30) must be rewritten as:

$$h_{r,2} = h_{r,1} - \frac{1}{\dot{m}_r} \left[\dot{m}_{w,ms} c_{p,w}(T_{w,pol,1} - T_{w,pol,2}) + q_{ax}(z) \cdot (z_{wall,2} - z_{wall,1}) - \frac{\dot{q}_{diss,ms}}{13} \right] \quad (5.38)$$

Hence, the final experimental HTC takes account of all the previous correction and its final formulation is given by:

$$HTC(z) = \frac{q(z) + q_{ax}(z) + q_{diss}(z)}{\pi D [T_{sat}(z) - T_{wall}(z) - \Delta T_{wall}(z)]} \quad (5.39)$$

In this work the second method has been chosen for the data reduction as it presents less uncertainty related to the determination of the thermodynamic state of the refrigerant.

5.5 Data reduction for the pressure drop test section

During the pressure drop tests, adiabatic conditions are maintained along the measuring section. In fact, the condensation (or evaporation) process take place in the pre-section and then the fluid flows trough the measuring section with no heat exchange.

So the reduction regards just the pre-section as it is the only part where a heat exchange takes place while the pressure drop along the measuring section is directly measured (no reduction is needed). Both the two previous methods have been implemented for the calculation of measuring section inlet condition. For the first method, the reduction is the same as decribed above fot the heat transfer pre-section on page 40. For the second method, a symple heat balance is necessary to calculate the measuring section inlet enthalpy and then by knowing the measuring section inlet pressure, the inlet vapor quality is obtained from the Refprop database [19] according to (5.29).

Nomenclature

Symbols

A_{cs}	axial conductive area of the copper channel, Equation (5.33)
c_p	specific heat capacity [$\text{J kg}^{-1} \text{K}^{-1}$]
D_e	channel external diameter [m]
D	channel internal diameter [m]
f	experimental friction factor
h	specific enthalpy [J kg^{-1}]
HTC	Heat Transfer Coefficient [$\text{W m}^{-2}\text{K}^{-1}$]
i_{LG}	differential latent heat [J kg^{-1}]
L	length [m]
\dot{m}	mass flow rate [kg s^{-1}]
p	pressure [bar]
q	heat flow rate per length unit [W m^{-1}]
\dot{q}	heat flow rate [W]
r^2	coefficient of determination, Equation (5.8)
Ra	channel internal roughness [m]
Re	Reynolds number = $\rho v D / \mu$
T	temperature [K]
x	thermodynamic vapor quality
X_{R32}	R32 mass fraction in the mixture
z	axial position [m]

Greek Symbols

Δ	difference
λ_{Cu}	copper channel thermal conductivity [$\text{W m}^{-1}\text{K}^{-1}$]
ρ	density [kg m^{-3}]
σ	Standard Deviation

Superscripts

—	mean value
---	------------

Subscripts

1	initial position
2	final position
<i>amb</i>	ambient

ctd. . .

<i>ax</i>	axial
<i>bub</i>	bubble point ($x = 0$) at the same composition
COND	condensation
<i>des</i>	desuperheating
<i>dew</i>	dew point ($x = 1$) at the same composition
<i>diss</i>	dissipated
eq	equilibrium
G	gas phase
<i>i</i>	i-th
<i>in</i>	inlet
L	liquid phase
<i>ms</i>	measuring section
<i>out</i>	outlet
<i>pol</i>	polynomial
<i>ps</i>	pre-section
<i>r</i>	refrigerant
<i>sat</i>	saturation
<i>w</i>	water
<i>wall</i>	wall

Chapter 6

Experimental uncertainty

Each measurement conducted during the tests is affected by uncertainty. This chapter reports the error analysis and the uncertainty estimation of the parameters involved in the measurements using the same technique adopted in previous analysis [25].

6.1 Uncertainty expression

The nominal experimental heat transfer coefficient uncertainty depends mainly on four parameters:

1. mass flow rate;
2. geometric length (hydraulic diameter);
3. saturation to wall temperature difference;
4. heat flux.

where just the first two are directly measured and their contributions to the overall experimental uncertainty remain rather constant for the entire spans of mass velocities and vapor qualities. The major contribute to the overall HTC uncertainty is given by the uncertainty associated with the calculation of the heat flux, which in turns depends on the coolant temperature profile. The enhanced external surface of the test section (see Figure 4.3 on page 25) allows to reduce the thermal resistance on the coolant side, so the governing thermal resistance is located on the condensing side (internal). With this configuration the saturation minus wall temperature difference does not assume too low values and its contribute to the overall uncertainty is reduced.

The experimental uncertainty is considered made up of two parts:

Type A uncertainty u_A : it is obtained by statistical methods and derives from direct and repeated observations. Its estimation is carried out once in possession of a sufficient number of measurements. In the current case, each measure (temperature, pressure and mass flow rate) is recorded for $n = 50$ times with a

frequency of 1 Hz (i.e. 50 values are recorded) and then the related mean value is calculated. So, as an example, the average temperature value is:

$$\bar{T} = \frac{1}{n} \sum_{i=1}^n T_i = \frac{1}{50} \sum_{i=1}^{50} T_i \quad (6.1)$$

and the standard deviation is:

$$\sigma(T) = \sqrt{\frac{1}{n-1} \sum_{i=1}^n (T_i - \bar{T})^2} = \sqrt{\frac{1}{49} \sum_{i=1}^{50} (T_i - \bar{T})^2} \quad (6.2)$$

According to the UNI CEI ENV 13005:2000 the Type A standard uncertainty is given by the experimental standard deviation of the mean as follows:

$$u_A(T) = \sigma(\bar{T}) = \frac{\sigma(T)}{\sqrt{n}} = \frac{\sigma(T)}{\sqrt{50}} \quad (6.3)$$

so all Type A uncertainties in this work have been calculated using Equation (6.3).

Type B uncertainty u_B : it derives from calibrations of instruments and manufacturers' specifications. Every measuring instrument has its Type B uncertainty depending on its configuration, accuracy and other characteristics. The values of this type of uncertainty are obtainable from the instrument data sheets as well as previous measurements or calibrations. The Type B experimental uncertainties for the measured parameters are reported in Table 6.1.

Table 6.1: Type B experimental uncertainties of measured parameters.

Parameter	Type B uncertainty
Temperature	± 0.05 °C
Refrigerant flow rate	$\pm 0.2\%$ at 2 kg h^{-1}
Water flow rate	$\pm 0.14\%$ at 10 kg h^{-1}
Absolute pressure	± 5 kPa
Pressure difference	± 0.1 kPa
Length and diameter	± 0.02 mm

Combined uncertainty u_c : Once Type A and Type B uncertainties are known, the combined uncertainty u_c of a measured parameter is obtained as:

$$u_c = \sqrt{u_A^2 + u_B^2} \quad (6.4)$$

6.2 Heat Transfer Coefficient uncertainty $u_c(HTC)$

If a parameter can not be directly measured, an indirect measurement based on theoretical correlations is adopted. These correlations are used for the definition of the combined uncertainty as the case of the local Heat Transfer Coefficient $HTC(z)$:

$$HTC(z) = \frac{q(z)}{P[T_{sat}(z) - T_{wall}(z)]} = \frac{-\dot{m}_w c_{p,w} \frac{\partial T_w(z)}{\partial z}}{\pi D [T_{sat}(z) - T_{wall}(z)]} \quad (6.5)$$

that is dependent on water flow rate \dot{m}_w , water temperature gradient $\frac{\partial T_w(z)}{\partial z} = g(z)$, saturation temperature T_{sat} , wall temperature T_{wall} and the internal perimeter πD . To obtain the Heat Transfer Coefficient combined uncertainty, Type A and Type B uncertainties of the five parameters described above must be calculated and then combined in order to have their relative combined uncertainties according to Equation (6.4). Under the assumption that these five variables (named v_i) are uncorrelated, the combined local HTC uncertainty is calculated as:

$$u_c^2(HTC) = \sum_{i=1}^5 \left(\frac{\partial HTC}{\partial v_i} \right)^2 u_c^2(v_i) \quad (6.6)$$

where $\frac{\partial HTC}{\partial v_i}$ are the sensitivity coefficients. In the current case is:

$$u_c(HTC) = \left[\left(\frac{\partial HTC}{\partial \dot{m}_w} \right)^2 u_c^2(\dot{m}_w) + \left(\frac{\partial HTC}{\partial g} \right)^2 u_c^2(g) + \left(\frac{\partial HTC}{\partial T_{sat}} \right)^2 u_c^2(T_{sat}) + \left(\frac{\partial HTC}{\partial T_{wall}} \right)^2 u_c^2(T_{wall}) + \left(\frac{\partial HTC}{\partial P} \right)^2 u_c^2(P) \right]^{\frac{1}{2}} \quad (6.7)$$

where the sensitivity coefficients are calculated referring to Equation (6.5). The five components that contribute to the definition of the Heat Transfer Coefficient uncertainty are now analyzed.

6.2.1 Water flow rate uncertainty $u_c(\dot{m}_w)$

The Type A uncertainty of the water flow rate is calculated according with Equation (6.3), hence:

$$u_A(\dot{m}_w) = \frac{\sigma(\dot{m}_w)}{\sqrt{50}} \quad (6.8)$$

The Type B uncertainty is calculated with the following equation reported from the instrument handbook:

$$u_B(\dot{m}_w) = \left(0.001 + \frac{0.004}{3600 \cdot \dot{m}_w} \right) \frac{\dot{m}_w}{\sqrt{3}} \quad (6.9)$$

now the combined uncertainty is evaluated according to Equation (6.4) as:

$$u_c(\dot{m}_w) = \sqrt{u_A^2(\dot{m}_w) + u_B^2(\dot{m}_w)} \quad (6.10)$$

6.2.2 Water temperature gradient uncertainty $u_c(g)$

A major source of uncertainty is related to the local heat flux that depends on the local water temperature gradient $g(z)$. This means that the heat flux depends on the interpolating function chosen to fit the water temperatures. To evaluate the uncertainty related to the water temperature gradient the Weighted Least Square (WLS) regression method have been implemented as follows:

- The water temperatures T_w for each test run have been fitted with a second order polynomial as:

$$T_w(z) = a_0 + a_1z + a_2z^2 \quad (6.11)$$

where a_0 , a_1 and a_2 are the polynomial coefficients that minimize the merit figure χ^2 with:

$$\chi^2 = \sum_{i=1}^{13} \left[\frac{T_{w,i} - (a_0 + a_1z_i + a_2z_i^2)}{u_i(T_w)} \right]^2 \quad (6.12)$$

i index ranges between 1 and 13 because 13 thermocouples are placed in the Heat Transfer measuring section to detect the wall temperatures and, correspondingly, 13 water temperature values are estimated with the polynomial (6.11) at the same position $z_{wall,i}$.

- A 13×3 matrix called \mathcal{A} and a 13 elements vector named b are defined as:

$$\mathcal{A}_{ij} = \frac{z_{w,i}^{j-1}}{u_i(T_w)} \quad ; \quad b_i = \frac{T_{w,i}}{u_i(T_w)} \quad (6.13)$$

- The minimum of Equation (6.12) occurs when the derivative of χ^2 with respect to all parameters a_0 , a_1 and a_2 is equal to zero. This condition yields the following equation in the matrix form:

$$(\mathcal{A}^T \cdot \mathcal{A}) \cdot a = \mathcal{A}^T \cdot b \quad (6.14)$$

where a is the vector whose components are the parameters to be fitted a_0 , a_1 and a_2 .

- Now it is possible to calculate the inverse matrix \mathcal{C} as:

$$\mathcal{C} = (\mathcal{A}^T \cdot \mathcal{A})^{-1} \quad (6.15)$$

the diagonal elements of \mathcal{C} are the square uncertainties of the fitted parameters:

$$u^2(a_j) = \mathcal{C}_{jj} \implies \begin{cases} u^2(a_0) = \mathcal{C}_{11} \\ u^2(a_1) = \mathcal{C}_{22} \\ u^2(a_2) = \mathcal{C}_{33} \end{cases} \quad (6.16)$$

and the off-diagonal elements of \mathcal{C} are the covariances between the estimated parameters a_j and a_k ; as an example:

$$\text{cov}(a_j, a_k) = \mathcal{C}_{jk} \implies \text{cov}(a_1, a_2) = \mathcal{C}(2, 3) \quad (6.17)$$

so \mathcal{C} is a symmetric matrix and has the form:

$$\mathcal{C} = \begin{bmatrix} u^2(a_0) & \text{cov}(a_0, a_1) & \text{cov}(a_0, a_2) \\ \vdots & u^2(a_1) & \text{cov}(a_1, a_2) \\ \vdots & \vdots & u^2(a_2) \end{bmatrix} \quad (6.18)$$

- the combined uncertainty related to the water temperature gradient $u_c(g)$ is obtained by manipulating the \mathcal{C} matrix elements and by applying the law of propagation of uncertainty for correlated variables as follows:

$$g(z) = \frac{\partial T_w(z)}{\partial z} = a_1 + 2a_2z \quad (6.19)$$

so the combined uncertainty of the water temperature gradient is given by:

$$\begin{aligned} u_c(g) &= u_c\left(\frac{\partial T_w}{\partial z}\right) \\ &= \sqrt{\left(\frac{\partial g}{\partial a_1}\right)^2 u^2(a_1) + \left(\frac{\partial g}{\partial a_2}\right)^2 u^2(a_2) + 2 \cdot \text{cov}(a_1, a_2) \left(\frac{\partial g}{\partial a_1}\right) \left(\frac{\partial g}{\partial a_2}\right)} \\ &= \sqrt{u^2(a_1) + (2z)^2 u^2(a_2) + 2 \cdot \text{cov}(a_1, a_2) \cdot (2z)} \end{aligned} \quad (6.20)$$

If a different polynomial interpolation is chosen to fit the water temperature profile, the procedure remains the same. The second order polynomial have been chosen by taking account of computational efforts and method accuracy. A bigger order would have brought negligible accuracy improvements.

6.2.3 Saturation temperature uncertainty $u_c(T_{sat})$

The saturation temperature is calculated basing on pressure values along the measuring section. The pressure is gauged by an absolute pressure transducer at the measuring section inlet and the outlet pressure is obtained with a differential pressure transducer. The Type A uncertainty for both the transducers is obtained as usual referring to Equation (6.3) on page 48 while Type B uncertainty is given by:

$$u_B(p) = \left[0.015 + 0.05 \left(\frac{p_{max}}{p_{fs}} \right) \right] \cdot \left(\frac{p_{fs}}{100} \right) \cdot \frac{1}{\sqrt{3}} \quad (6.21)$$

where the maximum pressure of the inlet transducer is $p_{max} = 275.8$ bar and its full scale pressure is $p_{fs} = 50$ bar. As the pressure transducer measures the inlet relative pressure of the measuring section, the uncertainty related to the atmospheric pressure has to be considered and combined with the previous uncertainty to obtain the correct value of the Type B inlet pressure uncertainty:

$$u_B(p_{in}) = \sqrt{u_B^2(p) + u_B^2(p_{atm})} = \sqrt{u_B^2(p) + \left(\frac{0.001}{\sqrt{3}} \right)^2} \quad (6.22)$$

For the differential transducer $p_{max} = 20.7$ bar and $p_{fs} = 1$ bar, the Type B differential pressure uncertainty is calculated again with Equation (6.21). The combined uncertainties for the inlet pressure transducer and for the differential pressure transducers are calculated using Equation (6.4). The inlet and outlet saturation temperature uncertainties are calculated as the difference between the saturation temperatures evaluated using pressure values with and without the relative combined uncertainties, hence:

$$\begin{aligned} u_c(T_{sat,in}) &= T_{sat,in}(p_{in}) - T_{sat,in}(p_{in} + u_c(p_{in})) \\ u_c(T_{sat,out}) &= T_{sat,out}(p_{out}) - T_{sat,out}(p_{out} + u_c(p_{in}) - u_c(dp)) \end{aligned} \quad (6.23)$$

The combined uncertainty for every saturation temperature along the measuring section is given considering the error propagation starting from:

$$T_{sat}(z) = m \cdot z + q = \left(\frac{T_{sat,in} - T_{sat,out}}{z_{in} - z_{out}} \right) \cdot z + T_{sat,in} \quad (6.24)$$

under the hypothesis of uncorrelated variables, the error propagation is applied as follows:

$$u_c(T_{sat,z}) = \sqrt{\left[\frac{\partial T_{sat}(z)}{\partial T_{sat,in}} \right]^2 u_c^2(T_{sat,in}) + \left[\frac{\partial T_{sat}(z)}{\partial T_{sat,out}} \right]^2 u_c^2(T_{sat,out})} \quad (6.25)$$

so every saturation temperature measurement is affected by its uncertainty.

6.2.4 Wall temperature uncertainty $u_c(T_{wall})$

This uncertainty is related to both Type A and Type B uncertainties. Knowing that the thermocouples placed in the measuring section has an accuracy of ± 0.05 K, the combined wall temperature uncertainty is:

$$u_c(T_{wall}) = \sqrt{\left[\frac{\sigma(T_{wall})}{\sqrt{50}} \right]^2 + \left(\frac{0.05}{\sqrt{3}} \right)^2} \quad (6.26)$$

6.2.5 Inner perimeter uncertainty $u_c(P)$

The measure of the microchannel inner diameter is affected only by Type B uncertainty. Referring to Table 6.1 on page 48 the combined inner perimeter uncertainty is:

$$u_c(P) = u_B(P) = \frac{0.02}{\sqrt{3}} \quad (6.27)$$

6.2.6 Overall uncertainty

The expanded uncertainty on the heat transfer coefficient U_M is obtained by multiplying the combined standard uncertainty $u_c(HTC)$ by a coverage factor $k = 2$ with an interval having a level of confidence of approximately 95%:

$$U_M = k u_c(HTC) = 2 u_c(HTC) \quad (6.28)$$

6.3 Vapor quality uncertainty

As the vapor quality is calculated basing on the Refprop database [19] as a function of pressure and enthalpy (see section 5.4.4 on page 42), its relative uncertainty depends on the internal algorithms of the program. Thus an uncertainty estimate can be obtained with the difference between the vapor qualities calculated with pressure and enthalpies with and without their relative uncertainties. It is then necessary to obtain the enthalpies uncertainties.

Considering that at the pre-section inlet the refrigerant comes as a superheated vapor, its uncertainty is neglected. The inlet enthalpy in the measuring section is obtained by:

$$h_{in,ms} = h_{in,ps} - \frac{\dot{m}_{w,ps} \cdot c_{p,w} \cdot \Delta T_{ps}}{\dot{m}_r} \quad (6.29)$$

Under the hypothesis of uncorrelated variables the combined uncertainty of the measuring section inlet enthalpy is given by:

$$u_c(h_{in,ms}) = \left[\left(\frac{\partial h_{in,ms}}{\partial \dot{m}_{w,ps}} \right)^2 u_c^2(\dot{m}_{w,ps}) + \left(\frac{\partial h_{in,ms}}{\partial \Delta T_{w,ps}} \right)^2 u_c^2(\Delta T_{w,ps}) + \left(\frac{\partial h_{in,ms}}{\partial \dot{m}_r} \right)^2 u_c^2(\dot{m}_r) \right]^{\frac{1}{2}} \quad (6.30)$$

where the water flow rate uncertainty is calculated with Equation (6.10) while the water temperature drop uncertainty and the refrigerant mass flow rate uncertainty are calculated referring to Equation (6.4) with:

$$u_B(\dot{m}_r) = \left(0.0015 + \frac{0.001}{3600 \cdot \dot{m}_r} \right) \frac{\dot{m}_r}{\sqrt{3}} \quad (6.31)$$

and

$$u_B(\Delta T_{w,ps}) = \frac{0.003}{\sqrt{3}} \quad (6.32)$$

The uncertainty relative to the water specific heat capacity is here neglected. Once the uncertainty of the enthalpy at the inlet of the measuring section is known, the uncertainties related to the following enthalpies must be evaluated. The vapor quality is calculated at $z = z_{wall,i}$, where the wall temperature is directly measured and the water temperature is evaluated with the polynomial (6.11). Thus the uncertainty related to the polynomial water temperatures must be calculated. As the polynomial coefficients a_0 , a_1 and a_2 are correlated variables, the uncertainty on the polynomial water temperatures is calculated as:

$$u_c(T_{w,pol}) = \left\{ \left[\frac{\partial T_w(z)}{\partial a_0} \right]^2 u^2(a_0) + \left[\frac{\partial T_w(z)}{\partial a_1} \right]^2 u^2(a_1) + \left[\frac{\partial T_w(z)}{\partial a_2} \right]^2 u^2(a_2) + 2 \cdot \text{cov}(a_0, a_1) \left[\frac{\partial T_w(z)}{\partial a_0} \right] \left[\frac{\partial T_w(z)}{\partial a_1} \right] + 2 \cdot \text{cov}(a_1, a_2) \left[\frac{\partial T_w(z)}{\partial a_1} \right] \left[\frac{\partial T_w(z)}{\partial a_2} \right] + 2 \cdot \text{cov}(a_0, a_2) \left[\frac{\partial T_w(z)}{\partial a_0} \right] \left[\frac{\partial T_w(z)}{\partial a_2} \right] \right\}^{\frac{1}{2}} \quad (6.33)$$

that leads to:

$$u_c(T_{w,pol}) = [u^2(a_0) + u^2(a_1) \cdot z^2 + u^2(a_2) \cdot z^4 + 2 \cdot \text{cov}(a_0, a_1) \cdot z + 2 \cdot \text{cov}(a_1, a_2) \cdot z^3 + 2 \cdot \text{cov}(a_0, a_2) \cdot z^2]^{\frac{1}{2}} \quad (6.34)$$

where each term is obtained by matrix \mathcal{C} described in (6.18). The next enthalpy uncertainty is calculated starting from the equation:

$$h_{ms,i+1} = h_{ms,i} - \frac{\dot{m}_{w,ms} \cdot c_{p,w} [T_{w,pol}(z_{wall,i}) - T_{w,pol}(z_{wall,i+1})]}{\dot{m}_r} \quad (6.35)$$

and then evaluating:

$$u_c(h_{ms,i+1}) = \left\{ u_c^2(h_{ms,i}) + \left(\frac{\partial h_{ms,i+1}}{\partial \dot{m}_w} \right)^2 u_c^2(\dot{m}_w) + \left[\frac{\partial h_{ms,i+1}}{\partial T_{w,pol}(z_{wall,i})} \right]^2 u_c^2(T_{w,pol}(z_{wall,i})) + \left[\frac{\partial h_{ms,i+1}}{\partial T_{w,pol}(z_{wall,i+1})} \right]^2 u_c^2(T_{w,pol}(z_{wall,i+1})) + \left(\frac{\partial h_{ms,i}}{\partial \dot{m}_r} \right)^2 u_c^2(\dot{m}_r) \right\}^{\frac{1}{2}} \quad (6.36)$$

The pressure uncertainty is evaluated by considering two different pressure values at the same position $z_{wall,i}$. The first one is given by the lectures of the inlet pressure and the pressure drop in the measuring section; supposing a linear trend inside the duct a first order polynomial is used to evaluate the pressure at every position $z_{wall,i}$:

$$p(z) = p_{in,ms} - \frac{\Delta p}{L_{\Delta p}} \cdot z \quad (6.37)$$

The second value is given with a first order polynomial with the uncertainties relative to the inlet pressure $u_c(p_{in,ms})$ and the pressure drop $u_c(\Delta p)$, where the Type B uncertainty for the pressure drop is given by Equation (6.21) with $p_{max} = 20.7$ bar and $p_{fs} = 1$ bar. The second polynomial is:

$$p_{unc}(z) = [p_{in,ms} - u_c(p_{in,ms})] - \frac{\Delta p + u_c(\Delta p)}{L_{\Delta p}} \cdot z \quad (6.38)$$

Now it is possible to calculate two different vapor qualities as:

$$\begin{aligned} x(z_{wall,i}) &= x(h_{ms,i}, p(z_{wall,i}), X_{R32}) \\ x(z_{wall,i})_{unc} &= x(h_{ms,i} + u_c(h_{ms,i}), p_{unc}(z_{wall,i}), X_{R32}) \end{aligned} \quad (6.39)$$

and thus the expanded uncertainty related to the vapor quality is given by:

$$U_M(x) = k \cdot [x(z_{wall,i}) - x(z_{wall,i})_{unc}] \quad (6.40)$$

the coverage factor $k = 2$ is used in order to obtain a level of confidence of approximately 95%.

6.4 Pressure drop uncertainty

The pressure gradient in the Pressure Drop measuring section is obtained as:

$$\left(\frac{dp}{dz} \right)_f = \frac{\Delta p}{L_{\Delta p}} \quad (6.41)$$

where Δp is the pressure drop measured by the differential pressure transducer. Hence under the hypothesis of uncorrelated variables, the combined uncertainty related to the pressure drop is calculated as:

$$\begin{aligned} u_c\left(\frac{dp}{dz}\right) &= \sqrt{\left[\frac{\partial(dp/dz)}{\partial\Delta p}\right]^2 u_c(\Delta p)^2 + \left[\frac{\partial(dp/dz)}{\partial L_{\Delta p}}\right]^2 u_c(L_{\Delta p})^2} \\ &= \sqrt{\left(\frac{1}{L_{\Delta p}}\right)^2 u_c(\Delta p)^2 + \left(\frac{\Delta p}{L_{\Delta p}^2}\right)^2 u_c(L_{\Delta p})^2} \end{aligned} \quad (6.42)$$

6.5 Experimental uncertainties analysis

This section reports the results obtained from the uncertainties analysis.

The uncertainties trends are reported in Figure 6.1 on page 57 for each investigated mixture during condensation tests ran at $G = 400 \text{ kg m}^{-2}\text{s}^{-1}$. The figure reports the percent uncertainty values against vapor quality.

By analyzing the uncertainties trends it is possible to notice that:

- the inner perimeter uncertainty is constant along the duct for every mixture. This is easily understandable looking at the inner perimeter uncertainty definition on section 6.2.5 on page 52;
- saturation and wall temperature uncertainties remains rather constant during the condensation as well as the uncertainty related to the water mass flow rate. Again this is deductible by looking at their definition on sections 6.2.3, 6.2.4 and 6.2.1 on pages 51, 52 and 49 respectively;
- the water temperature gradient uncertainty varies with the vapor quality hence with the position along the measuring section. It presents a near-parabolic trend as its minimum value is located near the middle of the section while tends to increase near the ends (inlet and outlet of the measuring section). This behaviour is strongly dependent on the water temperature profile interpolation: the polynomial function well fits the points in the middle of the section but commits a bigger error at the boundary points, i.e. the inlet and outlet water temperature in the measuring section.

The expanded uncertainty U_M has a similar trend as is obtained by combining the previous uncertainties referring to Equation (6.7). The major contribute is then given by the uncertainty related to the water temperature gradient $g(z)$ while the other parameters produce little variations. Table 6.2 reports the minimum and maximum values of the expanded uncertainty U_M as well as the vapor quality range. The values are reported for each mixture for the whole mass velocity span.

For all the tests, the uncertainty remains below 13.0%. It can be noticed that by increasing the mass velocity, a reduction in the value of the experimental extended HTC uncertainty occurs. This is due to the fact that at lower mass velocities the flow regime is not as stable as at higher ones. This means that higher standard deviations are registered and they raise up the uncertainty. Moreover, with small

Table 6.2: Experimental extended HTC uncertainty and vapor quality ranges of the investigated mixtures for the whole mass velocity span during condensation tests.

G [kg m ⁻² s ⁻¹]	Mix 23/77%		Mix 46/54%		Mix 76/24%	
	$U_M\%$	x	$U_M\%$	x	$U_M\%$	x
150	5.0 ÷ 10.2	0.16 ÷ 0.63	4.6 ÷ 10.2	0.18 ÷ 0.71	4.6 ÷ 12.5	0.16 ÷ 0.74
200	4.5 ÷ 8.8	0.18 ÷ 0.63	3.9 ÷ 10.3	0.2 ÷ 0.74	3.9 ÷ 9.0	0.22 ÷ 0.77
300	3.4 ÷ 8.9	0.17 ÷ 0.71	3.3 ÷ 11.9	0.18 ÷ 0.79	3.2 ÷ 9.9	0.18 ÷ 0.8
400	3.0 ÷ 6.6	0.17 ÷ 0.74	2.9 ÷ 5.4	0.2 ÷ 0.78	2.9 ÷ 7.2	0.2 ÷ 0.82
600	2.7 ÷ 4.2	0.18 ÷ 0.77	2.7 ÷ 5.3	0.2 ÷ 0.83	2.7 ÷ 4.6	0.2 ÷ 0.82
800	2.7 ÷ 3.6	0.2 ÷ 0.8	2.6 ÷ 4.1	0.18 ÷ 0.82	2.6 ÷ 3.7	0.24 ÷ 0.82

Table 6.3: Experimental extended vapor quality uncertainty ranges of the investigated mixtures for the whole mass velocity span during condensation tests.

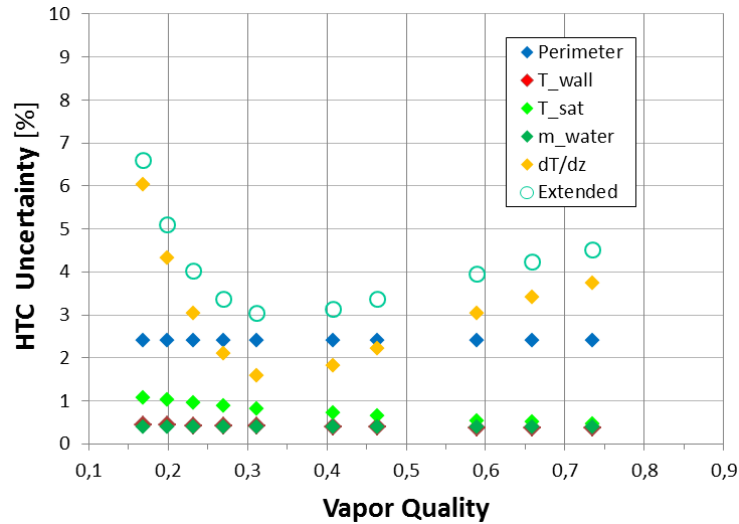
G [kg m ⁻² s ⁻¹]	Mix 23/77%	Mix 46/54%	Mix 76/24%
	$U_x\%$	$U_x\%$	$U_x\%$
150	1.01 ÷ 27.47	0.85 ÷ 27.25	1.02 ÷ 34.06
200	1.01 ÷ 21.31	0.61 ÷ 19.86	0.74 ÷ 18.77
300	0.54 ÷ 15.95	0.38 ÷ 15.18	0.48 ÷ 16.62
400	0.39 ÷ 12.25	0.29 ÷ 9.31	0.36 ÷ 11.18
600	0.25 ÷ 7.61	0.18 ÷ 7.53	0.23 ÷ 7.25
800	0.22 ÷ 5.69	0.16 ÷ 6.12	0.17 ÷ 4.5

flow rates, the heat flux is small and thus the water temperature gradient is small; this turns into a worse interpolation profile compared with higher flow rates.

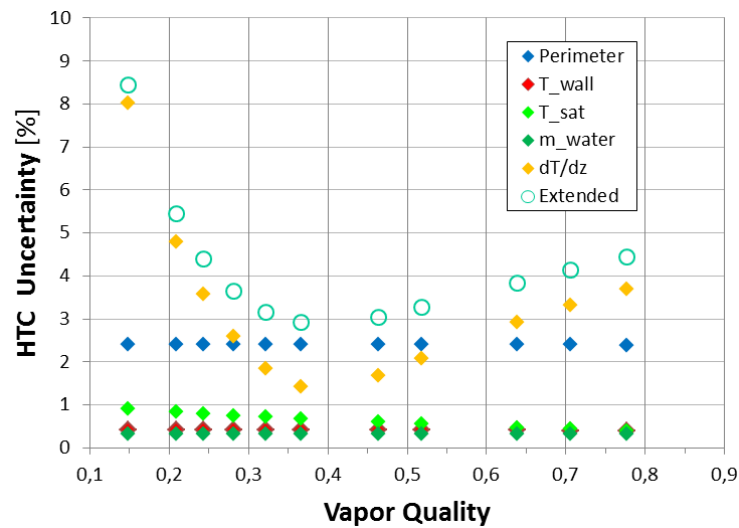
Table 6.3 reports the experimental percentage uncertainties ranges related to the vapor quality. As the method used for its calculation is iterative and based previous values of specific enthalpy in turn affected by uncertainty, the vapor quality uncertainty increases as the condensation proceeds along the measuring section. Hence lower vapor qualities are affected by higher uncertainties. For all the tests carried out 96.15% of all the experimental points fall between $\pm 20\%$ error bands. Table 6.4 reports the maximum uncertainty values returned from the analysis of the Pressure drop tests for all the investigated mixtures (see section 7.2 on page 68).

Table 6.4: Experimental extended vapor quality and pressure drop uncertainties for the investigated mixtures at mass velocity of 200, 400 and 600 kg m⁻²s⁻¹ during pressure drop tests.

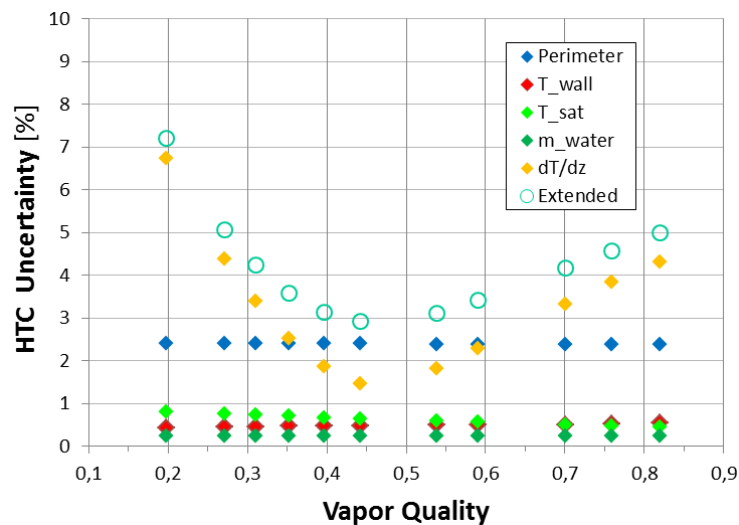
G [kg m ⁻² s ⁻¹]	U_Q -	$U_{dp/dz}$ kPa m ⁻¹
200	<0.005	<0.7
400	<0.007	<0.7
600	<0.006	<0.9



(a) R32/R1234ze(E) mixture with 22/78% mass ratio.



(b) R32/R1234ze(E) mixture with 46/54% mass ratio.



(c) R32/R1234ze(E) mixture with 76/24% mass ratio.

Figure 6.1: Total experimental percentage uncertainties of the Heat Transfer Coefficient and its components. The charts are referred to a condensation test run with a mass velocity equal to $400 \text{ kg m}^{-2}\text{s}^{-1}$ for each one of the three mixtures.

Nomenclature

Symbols

c_p	specific heat capacity [$\text{J kg}^{-1} \text{K}^{-1}$]
D	channel internal diameter [m]
g	water temperature gradient [K m^{-1}]
G	mass velocity [$\text{kg m}^{-2}\text{s}^{-1}$]
h	specific enthalpy [J kg^{-1}]
k	cover factor
$L_{\Delta p}$	pressure ports distance [m]
\dot{m}	mass flow rate [kg s^{-1}]
n	number of readings = 50
p	pressure [bar]
P	internal microchannel perimeter = πD [m]
q	heat flux per length unit [W m^{-1}]
T	temperature [K]
u	uncertainty
U_M	expanded uncertainty
v	generic variable
X_{R32}	R32 mass fraction in the mixture
x	thermodynamic vapor quality
z	axial position [m]

Greek Symbols

Δ	difference
σ	standard deviation
χ^2	merit figure, Equation (6.12)

Superscripts

—	mean value
---	------------

Subscripts

A	Type A
atm	atmospheric
B	Type B
c	combined
f	frictional
fs	full scale

ctd. . .

<i>i</i>	i-th position
<i>in</i>	inlet
<i>j</i>	j-th position
<i>max</i>	maximum
<i>ms</i>	measuring section
<i>pol</i>	polynomial
<i>ps</i>	pre-section
<i>r</i>	refrigerant
<i>sat</i>	saturation
<i>unc</i>	affected by uncertainty
<i>w</i>	water
<i>wall</i>	wall

Chapter 7

Experimental results

The heat transfer and pressure drop tests have been conducted with a mass velocity span of $G = 150 \div 800 \text{ kg m}^{-2}\text{s}^{-1}$ with a mean refrigerant temperature of $\bar{T}_r = 40^\circ\text{C}$. The experimental results are shown for a vapor quality range of $x = 0.15 \div 0.85$.

7.1 Heat Transfer Coefficients

The experimental HTC is plotted against the vapor quality in Figure 7.1 with the relative uncertainty bands; each diagram refers to a mixture.

Obviously, given the fact that the condensation takes place in forced convection, for a given vapor quality the HTC increases as the refrigerant mass velocity increases. It can be noticed that as the condensation proceeds along the measuring section, i.e. the vapor quality decreases, the local HTC decreases. The percentage decrease is included between 40% and 50% for all mixtures at mass velocities ranging from $G = 300 \div 800 \text{ kg m}^{-2}\text{s}^{-1}$. The lowest $G = 200 \text{ kg m}^{-2}\text{s}^{-1}$ and $G = 150 \text{ kg m}^{-2}\text{s}^{-1}$ mass velocities present smaller HTC percent variations, moreover the variation becomes smaller by increasing the R32 mass fraction in the mixture (down to 20% for mixture 76/24%). This behaviour could be justified by the fact that, at higher mass velocities, the condensation process is dominated by the shear stress at the liquid-vapor interface, while gravity and surface tension play a marginal role. In this case the condensation process takes place with annular flow regime, characterized by a liquid film uniformly distributed on the inner channel perimeter. At lower mass velocities, the influence of gravity and surface tension increases as the vapor is unable to sustain the annular liquid film and the shear stress decreases; this leads the liquid film to become thicker on the lower side of the channel leading to a non uniform distribution.

The decreasing trend of the HTC with the vapor quality is due to the fact that, during the condensation, the liquid film forming onto the microchannel internal wall introduces a further thermal resistance to the heat exchange as it is positioned between the vapor core and the wall. As the condensation proceeds, the liquid film becomes thicker and the relative thermal resistance raises up.

Figure 7.2 shows the experimental HTC values of the three mixtures for the whole mass velocity span adopted in this work. It can be noticed that, for given values of specific flow rate and vapor quality, the HTC increases as the R32 mass fraction

in the mixture increases. This is due to the thermodynamic characteristics of the specific fluid as it is known that R32 offers higher performances than R1234ze(E) at the same operative conditions. By looking at Table 3.1 on page 12 it can be noticed that pure R32 has larger latent heat (about 1.53 times) and higher liquid thermal conductivity (about 1.66 times) if compared with pure R1234ze(E) at a saturation temperature of 40 °C.

A further comparison can be made by plotting the HTC against the vapor quality for both pure fluids and mixtures at a constant mass velocity, as shown in Figure 7.3. It is possible to see how mixtures 23/77% and 46/54% achieve lower, or at least equal, HTCs if compared with the pure R1234ze(E), for all the three mass velocities reported; for low vapor qualities these two mixtures are very close to pure R1234ze(E). Only mixture 76/24% shows an intermediate behaviour as it realizes HTCs between pure R32 and pure R1234ze(E) during condensation.

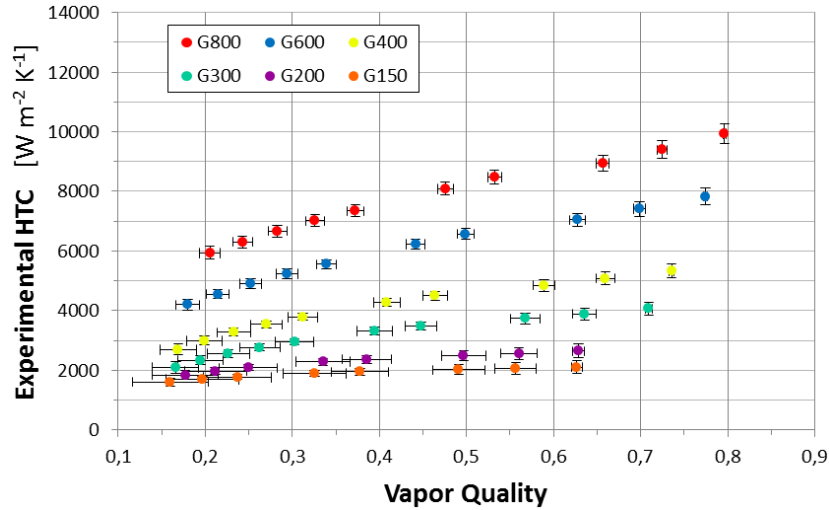
The intermediate behaviour could be roughly predicted for all the investigated mixtures as they are composed by both the two fluids, but this is not confirmed by experimental data. Considering a vapor quality $x = 0.5$, for $G = 800 \text{ kg m}^{-2}\text{s}^{-1}$ mixture 23/77% shows a decrease around 9% with respect to pure R1234ze(E) while mixture 46/54% assumes a comparable value with respect to the same fluid. Only mixture 76/24% shows an improvement on the HTC of about 12% if compared with pure R1234ze(E). All the mixtures show a decrease with respect to pure R32 around 28.7%, 21.7% and 12.3% for mixtures 23/77%, 46/54% and 76/24% respectively. At the same vapor quality $x = 0.5$, for $G = 400 \text{ kg m}^{-2}\text{s}^{-1}$ the decrease with respect to pure R1234ze(E) is 10.8% for mixture 23/77% while mixture 46/54% assumes a comparable value. Only mixture 76/24% shows an increase of about 13.7%. All the mixtures present HTCs lower than pure R32 with deviations of 31.1%, 22.7% and 12.1% for mixtures 23/77%, 46/54% and 76/24% respectively. At $G = 200 \text{ kg m}^{-2}\text{s}^{-1}$ and $x = 0.5$ mixtures 23/77% and 46/54% both show a decrease, if compared to pure R1234ze(E), around 26.5% and 11.8% respectively. Mixture 76/24% shows an increase, with respect to the same fluid, of about 5.8%. All the mixtures present a decrease of the HTC value, if compared to pure R32, around 37.5%, 25% and 10% for mixtures 23/77%, 46/54% and 76/24% respectively.

The deviation from the ideal behaviour could be explained by the mass transfer resistance introduction: during the condensation process, both liquid and vapor phases show a change in composition according to the specific phase diagram (i.e. the mixture is non-azeotropic); the diffusion of both the mixture components through the liquid/vapor interface introduces a further resistance that penalizes the heat exchange as it requires energy and then also the HTC value.

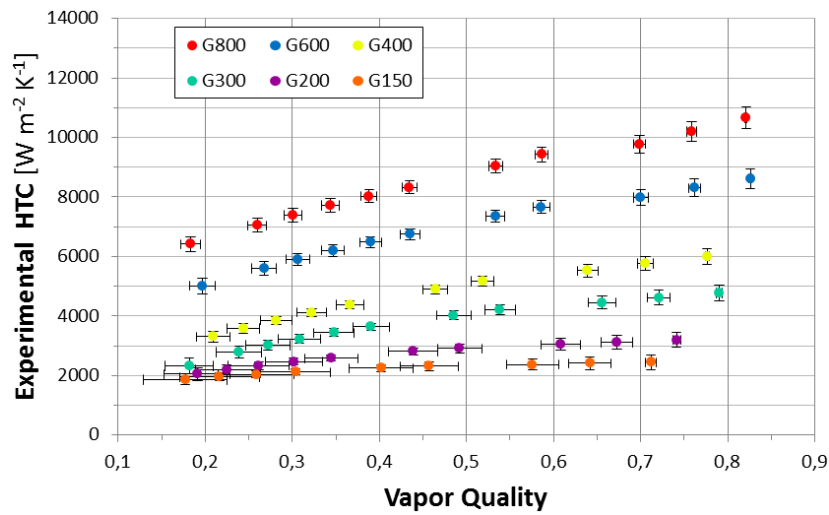
The effect of the mass transfer resistance can be seen also in Figure 7.4 where the HTC is reported against the R32 mass fraction at a constant value of vapor quality for different mass velocities; the dashed lines indicate the ideal intermediate behaviour that a mixture should present. The experimental points show the effect of the mass transfer resistance as the realized HTC is lower than the ideal one. Considering Figure 7.4(b) referred to a vapor quality $x = 0.5$, with a mass velocity of $G = 800 \text{ kg m}^{-2}\text{s}^{-1}$, the HTC decrease from the ideal mixture behaviour attests around 13.2% for mixture 23/77%, 12% for mixture 46/54% and 6.5% for mixture 76/24%. At $G = 400 \text{ kg m}^{-2}\text{s}^{-1}$ the decreases are about 19.3%, 15.6% and 0.8% while at $G = 200 \text{ kg m}^{-2}\text{s}^{-1}$ are 26.8%, 19.2% and 10.8% for mixtures 23/77%,

46/54% and 76/24% respectively.

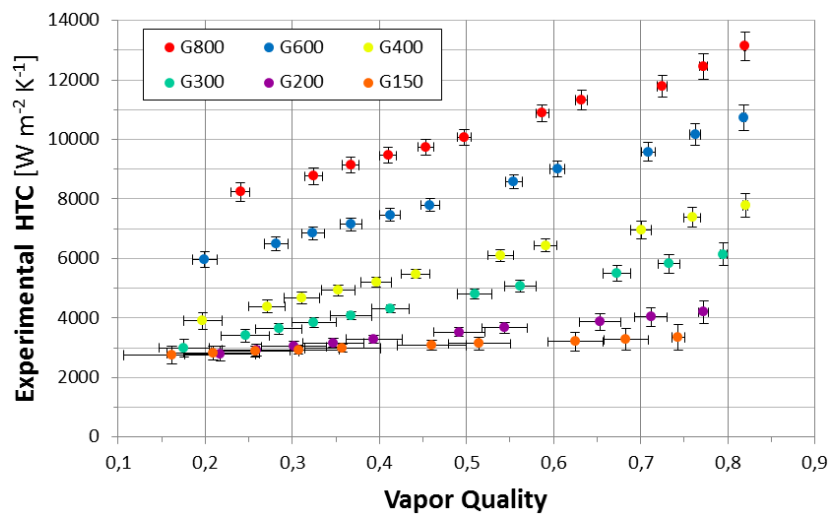
For all the three investigated vapor qualities, the higher penalization is shown by mixture 23/77% while mixture 46/54% and 76/24% shows lower penalizations. This can be explained by the fact that by increasing the R32 mass fraction the glide magnitude decrease as well as the differential latent heat. Thus the difference in composition between the condensing vapor and the liquid is the highest for mixture 23/77% (see Figure 3.4 on page 17) and then the mass transfer resistance gives the highest contribute to the HTC penalization. By analyzing the three charts, it can be noticed that by decreasing the vapor quality, the deviation from the ideal behaviour becomes smaller for all the mixtures, this is understandable by looking at the definition of the mass transfer resistance as shown in section 8.2 on page 79.



(a) R32/R1234ze(E) mixture with 23/77% mass ratio.



(b) R32/R1234ze(E) mixture with 46/54% mass ratio.



(c) R32/R1234ze(E) mixture with 76/24% mass ratio.

Figure 7.1: Experimental HTC vs vapor quality diagrams at mass velocities ranging from 150 to 800 $\text{kg m}^{-2}\text{s}^{-1}$ with HTC and vapor quality uncertainty bands.

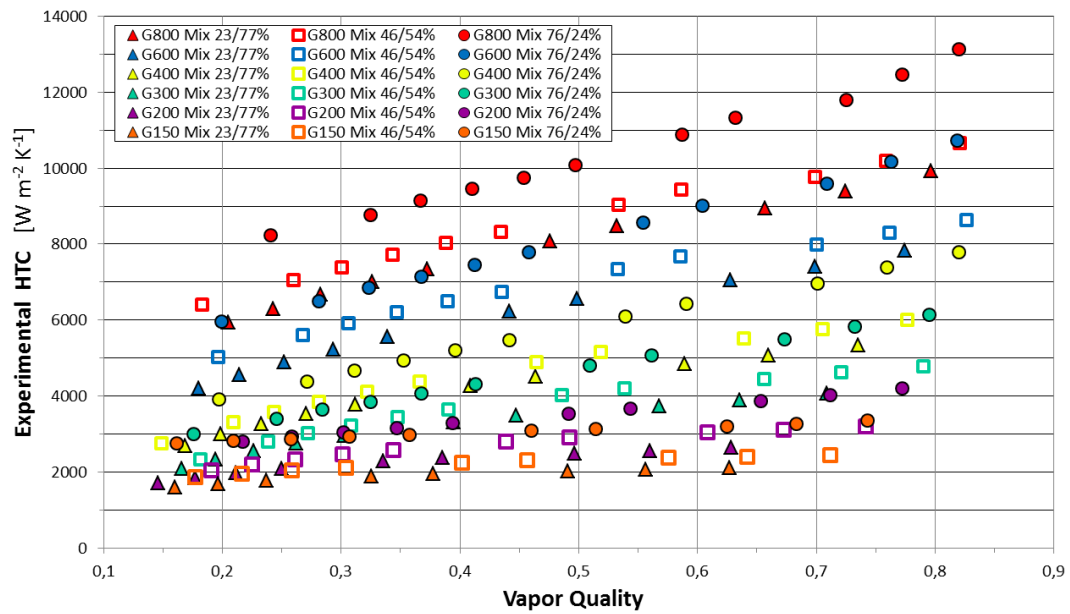


Figure 7.2: Experimental HTC vs vapor quality for the investigated R32/R1234ze(E) zeotropic mixtures. The mass velocity ranges from 150 to 800 kg m⁻²s⁻¹.

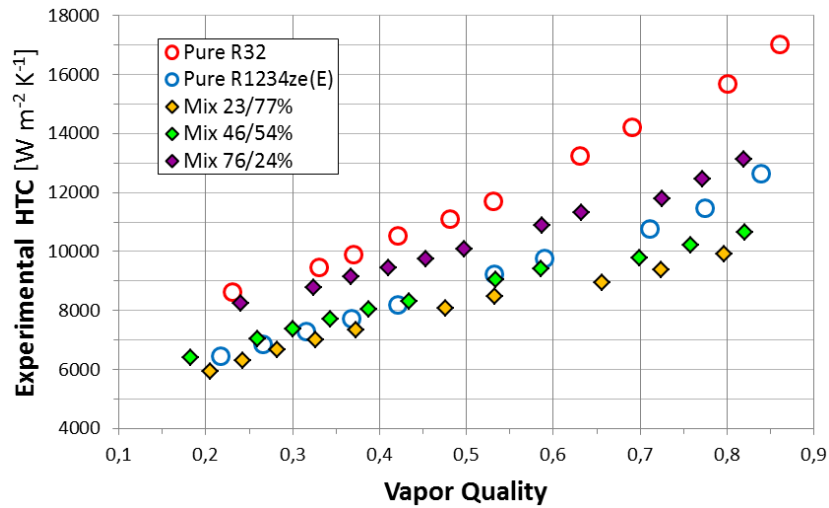
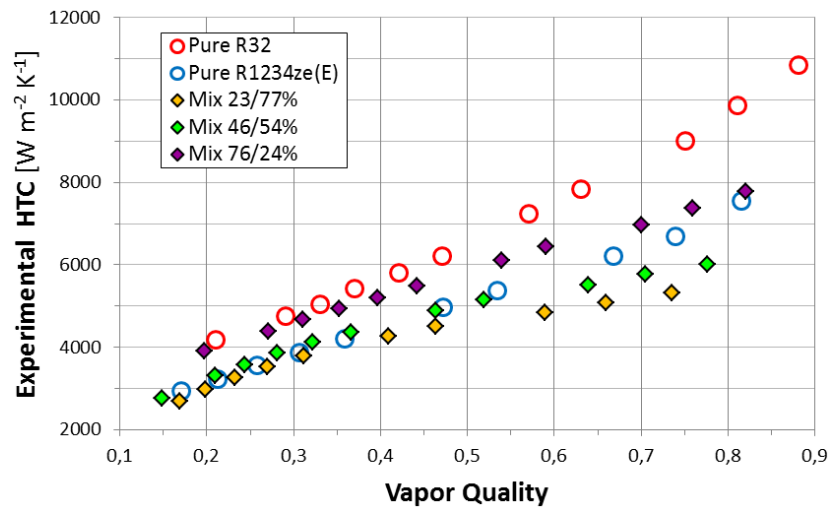
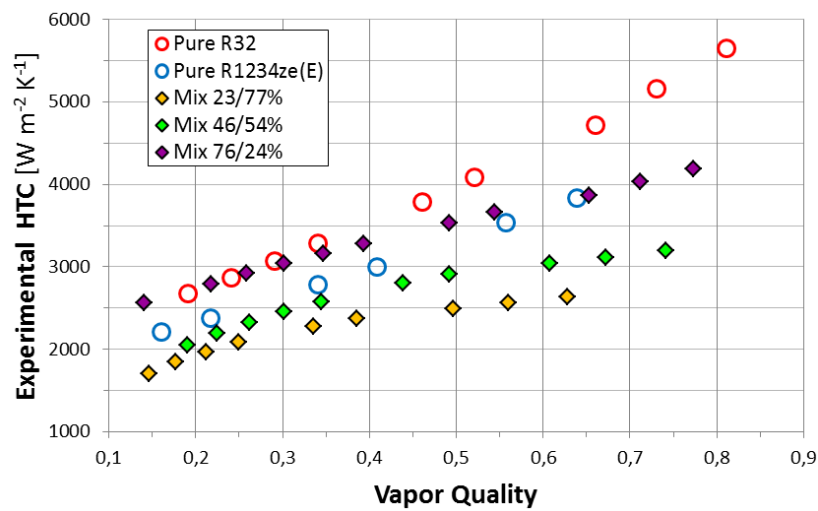
(a) Mass velocity $G = 800 \text{ kg m}^{-2}\text{s}^{-1}$.(b) Mass velocity $G = 400 \text{ kg m}^{-2}\text{s}^{-1}$.(c) Mass velocity $G = 200 \text{ kg m}^{-2}\text{s}^{-1}$.

Figure 7.3: Experimental HTC vs vapor quality at mass velocities of 800, 400 and 200 kg m⁻²s⁻¹ for pure R32 and R1234ze(E) fluids and the investigated mixtures.

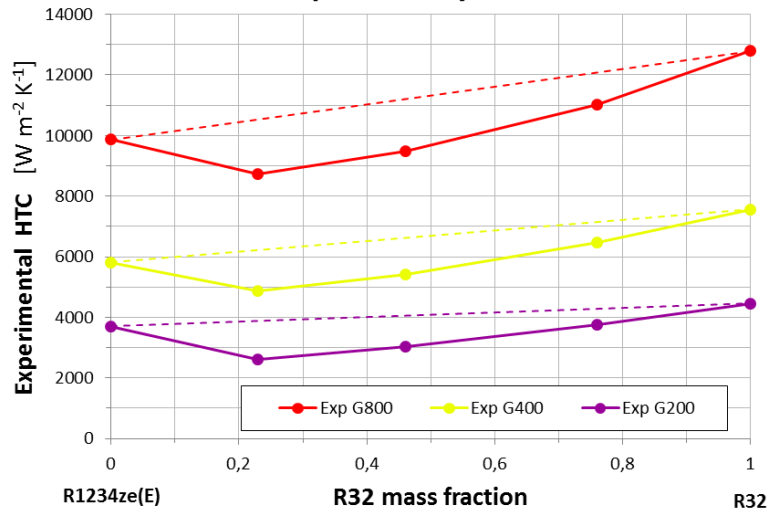
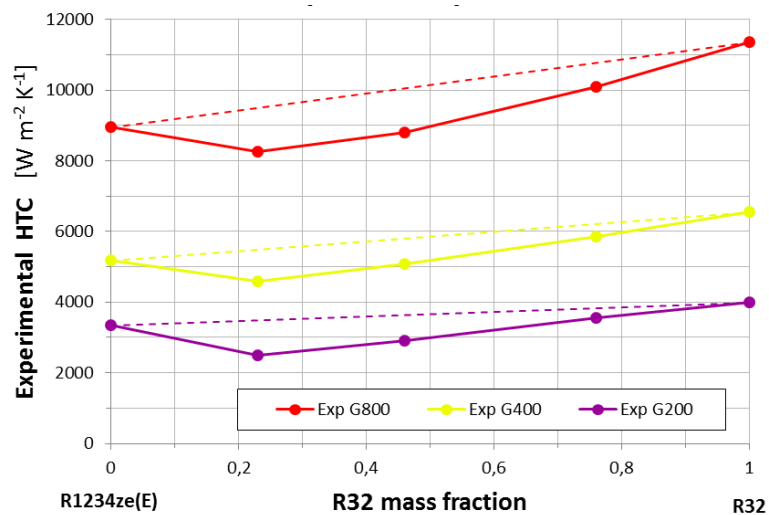
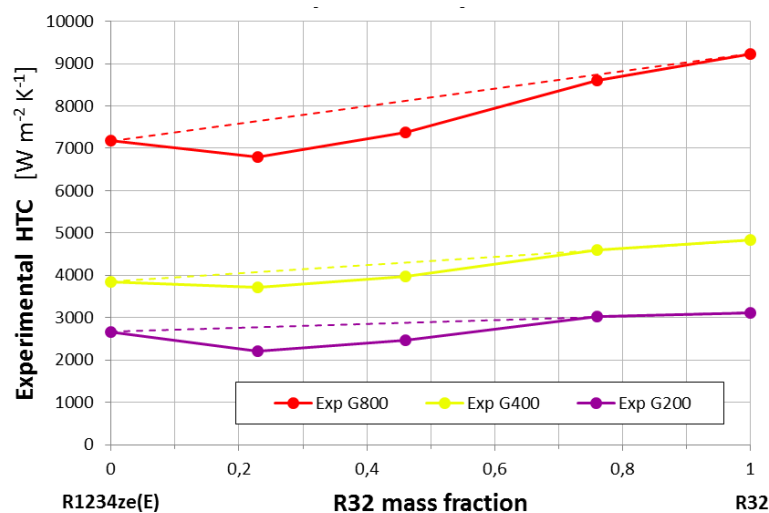
(a) Vapor quality $x = 0.6$.(b) Vapor quality $x = 0.5$.(c) Vapor quality $x = 0.3$.

Figure 7.4: Experimental HTC vs R32 mass fraction in the mixture at constant vapor qualities for different values of mass velocities: 200, 400 and 800 kg m⁻²s⁻¹.

7.2 Pressure Drops

Figure 7.5 shows the experimental pressure drop versus vapor quality for the three investigated mixtures and for pure R1234ze(E). The pressure gradient shows a typical trend as for the pure fluid: it increases with the increase of the vapor quality up to $x \approx 0.85$ where it reaches the maximum value. Then the pressure drop shows a decrease for vapor qualities greater than about 0.85.

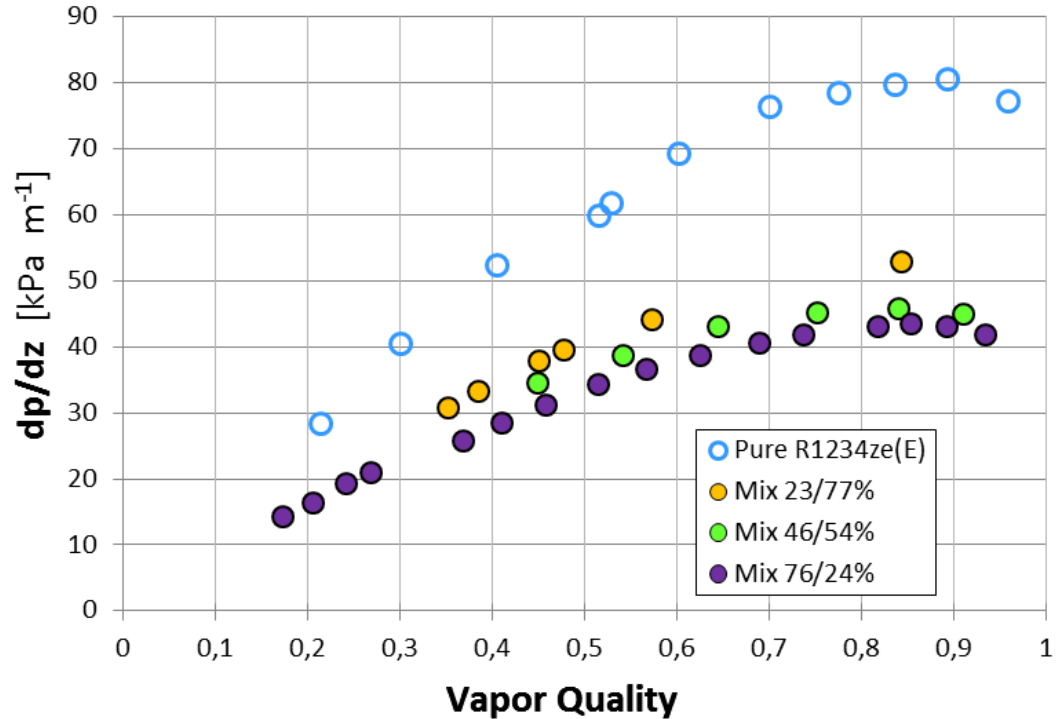


Figure 7.5: Experimental pressure gradient vs vapor quality of pure R1234ze(E) and the investigated mixtures for a mass velocity equal to $400 \text{ kg m}^{-2}\text{s}^{-1}$.

It can be noticed (referring to the mixtures) how the highest difference is showed by mixture 23/77% that reaches the highest value of dp/dz for $x = 0.84$ while mixtures 46/54% and 76/24% show very close behaviours. In fact, for example at $x = 0.84$, passing from mixture 23/77% to mixture 46/54% leads to a pressure drop decrease of about 15% while from mixture 46/54% to mixture 76/24% the decrease is just 5%. The higher variation in the linear pressure drop is evident comparing the mixtures with the pure fluid; in fact the decrease from the values showed by pure R1234ze(E) is significant even adding a small amount of R32 in the mixture. Thus for a vapor quality $x = 0.85$ mixture 23/77% shows a decrease in the pressure drop around 33.6%; the difference is in evidence for the whole vapor quality span. The experimental points trend suggests that for $x < 0.3$ the three mixtures would show a very similar behaviour. The slight difference between the curves can be explained by looking at liquid density and liquid viscosity of the mixtures in Table 3.2 on page 16. From mixture 23/77% to mixture 46/54% the liquid density and viscosity variations are quite small (5.4% and 15% respectively) as well as from mixture 46/54% to mixture 76/24% (7.2% and 15% respectively).

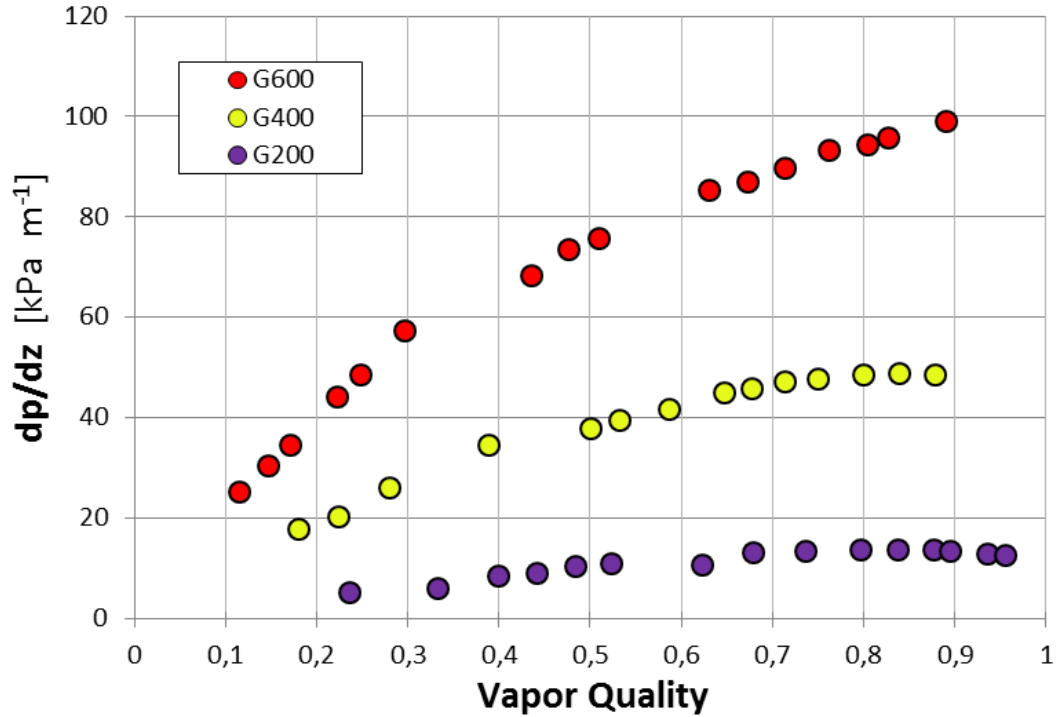


Figure 7.6: Experimental pressure gradient vs vapor quality for mixture 50/50% at mass velocities equal to 200, 400 and 600 $\text{kg m}^{-2}\text{s}^{-1}$.

Therefore the considerable increase of the R32 mass fraction in the mixture does not involve a strong variation of the pressure drop. Hence, in order to have a good description of the mixtures behaviours (in terms of pressure gradient), a mixture with an intermediate composition is suitable to be considered as representative of the investigated mixtures. A mixture with the intermediate composition 50/50% has been investigated for the evaluation of the pressure drop at different mass velocities. It has been found that varying the mixture mass velocity a high variation of the pressure gradient occurs, the variation is much higher than the one obtained varying the mixture composition. The results are plotted in Figure 7.6. The figure shows the experimental pressure drop against vapor quality for the R32/R1234ze(E) mixture with 50/50% mass fraction at three different mass velocities. From 200 $\text{kg m}^{-2}\text{s}^{-1}$ to 400 $\text{kg m}^{-2}\text{s}^{-1}$, the pressure gradient increase at $x = 0.9$ is about 257%; at the same vapor quality from 400 $\text{kg m}^{-2}\text{s}^{-1}$ to 600 $\text{kg m}^{-2}\text{s}^{-1}$ the variation attests around 108%. These differences between the three curves become lower as the vapor quality decrease. The experimental trend is in fact the same for all the three specific flow rate: as the vapor quality increases the pressure gradient increases with a non-linear trend till $x \approx 0.85 \div 0.9$ where it reaches the maximum value. A further increase in the vapor quality leads to a decrease of the pressure drop as can be seen for $G = 200 \text{ kg m}^{-2}\text{s}^{-1}$ and slightly for $G = 400 \text{ kg m}^{-2}\text{s}^{-1}$. For $G = 600 \text{ kg m}^{-2}\text{s}^{-1}$ the decrease is not shown as it would be occurred for vapor qualities higher than the last experimental point. The uncertainties related to vapor quality and linear pressure drop are not reported in the charts; the maximum values are reported in Table 6.4 on page 56.

Nomenclature

Symbols

G	mass velocity [$\text{kg m}^{-2}\text{s}^{-1}$]
p	pressure [bar]
T	temperature [K]
x	thermodynamic vapor quality
z	axial position [m]

Superscripts

—	mean value
---	------------

Subscripts

r	refrigerant
-----	-------------

Chapter 8

Theoretical models

In addition to the experimental results, it is very important to verify the validity of theoretical models developed for condensation. In fact, the ability to predict the condensation HTC is very useful, for example, to design new heat exchangers or verify the heat exchange in a condensation/evaporation process.

In this work three models have been taken into consideration to compare measured data and predicted data with respect to the HTC investigation: the Cavallini et al. model [5], the Moser et al. model [11] and the Shah model [16]. The choice to apply these three particular models is justified by the fact that their quality have been proved by different authors.

Furthermore, a pressure drop model is used to compare experimental data and predicted data. The model was developed by Del Col et al. [8] and has been chosen because it is suitable for analysis of flow regimes within microchannels.

This chapter describes the theoretical models used for the comparison between experimental and theoretical data at the same flow conditions.

8.1 HTC theoretical models

It is important to say that the three models considered have been developed for pure fluids. Anyway, as stated in the results section, the models ability to predict the mixture behaviour is quite good if appropriate correction is applied to the model itself. The correction is described in section 8.2 and adds only a mass transfer resistance on the final HTC calculation. Thus all the parameters have been calculated with the original model algorithm and then the final values have been corrected taking into account a zeotropic mixture as operative fluid.

8.1.1 Cavallini et al. model [5]

This model, developed by Cavallini et al. [5], subdivides the range of flow categories, not considering the observed configurations but the parameters that influence the condensation HTC. For a given fluid, mass velocity, saturation temperature, vapor quality and duct geometry influence the HTC, but a ΔT dependence is not always verified. In a horizontal tube, the ΔT dependence occurs only when gravity is the prevailing force.

The experimental data range used for the validation of the model is reported in Table 8.1:

Table 8.1: Cavallini et al. model [5] experimental ranges.

Authors	Points	Fluids	D [mm]	T _{sat} [°C]	ΔT [°C]	G [kg m ⁻² s ⁻¹]
Cavallini et al. [5]	1007	R22, R134a, R410A, R125, R32, R236ea, R407C, R125/236ea	>3.0	24 ÷ 302	2.4 ÷ 18.4	18 ÷ 2240

Thus the authors consider in this model two categories: a ΔT -dependent flow regime and a ΔT -independent flow regime, requiring only one transition criterion. The criterion adopted to find the transition curve between the two regimes involves mainly two parameters: the dimensionless gas velocity J_G and the Martinelli Parameter X_{tt} (dimensionless also) respectively reported in Equations (8.1) and (8.2):

$$J_G = \frac{xG}{[gD\rho_G(\rho_L - \rho_G)]^{0.5}} \quad (8.1)$$

$$X_{tt} = \left(\frac{\mu_L}{\mu_G}\right)^{0.1} \left(\frac{\rho_G}{\rho_L}\right)^{0.5} \left(\frac{1-x}{x}\right)^{0.9} \quad (8.2)$$

They obtained a transition line in terms of dimensionless gas velocity J_G versus the Martinelli Parameter and they maintained the use of J_G as a transition indicator even though its value might depend on the fluid considered. The transition line between the two flow regimes is described by Equation (8.3) which returns the values of the transition dimensionless gas velocity J_G^T as a function of X_{tt} and a C_T coefficient. As stated in Equation (8.4), this coefficient is introduced taking into account different types of working fluids (depending on the chemical composition). This simple relation for the transition value J_G^T well reflects the analysis conducted by the authors with available data:

$$J_G^T = \left[\left(\frac{7.5}{4.3X_{tt}^{1.111} + 1} \right)^{-3} + C_T^{-3} \right]^{-1/3} \quad (8.3)$$

$$\begin{aligned} C_T &= 1.6 \quad \text{for hydrocarbons} \\ C_T &= 2.6 \quad \text{for other refrigerants} \end{aligned} \quad (8.4)$$

The transition lines for the above described C_T are reported in a $J_G - X_{tt}$ diagram shown in Figure 8.1. For the ΔT -independent flow regime, a simple two-phase multiplier that corrects the liquid phase HTC is proposed; the heat transfer coefficient α_A is given in Equation (8.5). For the ΔT -dependent flow regime, the heat transfer coefficient α_D is given in Equation (8.6); it is related to α_A and to fully-stratified flow heat transfer coefficient α_{STRAT} described in Equation (8.7). Thus Equation (8.6) includes a progressive transition from the wavy-stratified to the smooth stratified flow.

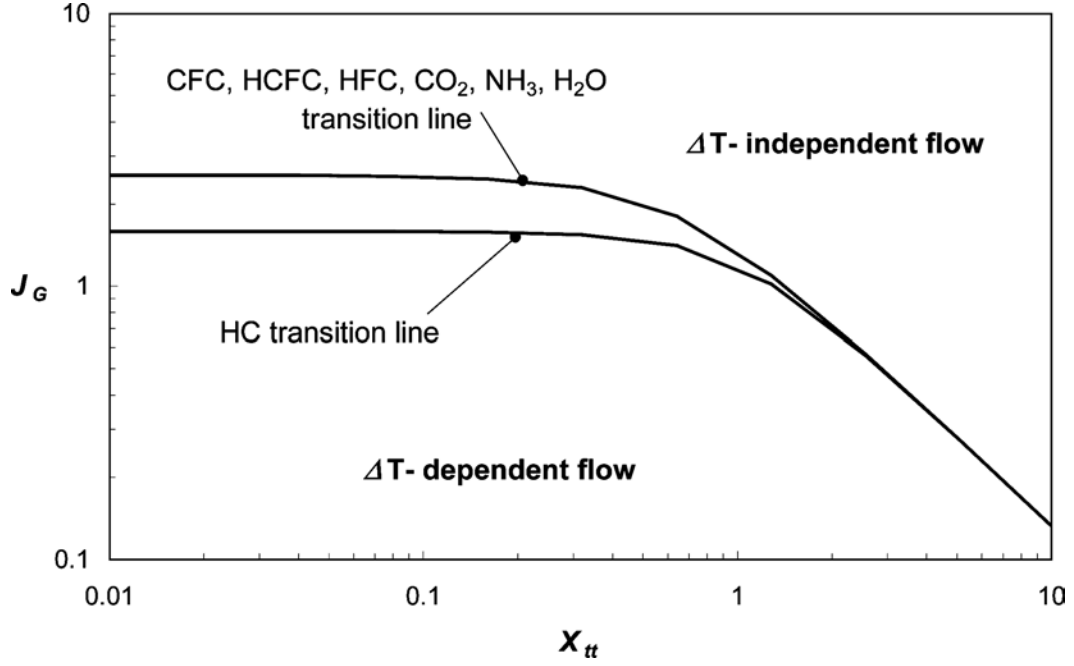


Figure 8.1: Transition between ΔT -dependent and ΔT -independent flow regime, Equation (8.3)

ΔT -independent flow regime ($J_G > J_G^T$):

$$\alpha_A = \alpha_{LO} \left[1 + 1.128x^{0.8170} \left(\frac{\rho_L}{\rho_G} \right)^{0.3685} \left(\frac{\mu_L}{\mu_G} \right)^{0.2363} \left(1 - \frac{\mu_G}{\mu_L} \right)^{2.144} Pr_L^{-0.1} \right] \quad (8.5)$$

ΔT -dependent flow regime ($J_G \leq J_G^T$):

$$\alpha_D = \left[\alpha_A \left(\frac{J_G^T}{J_G} \right)^{0.8} - \alpha_{STRAT} \right] \left(\frac{J_G}{J_G^T} \right) + \alpha_{STRAT} \quad (8.6)$$

where

$$\alpha_{STRAT} = 0.725 \left[1 + 0.741 \left(\frac{1-x}{x} \right)^{0.3321} \right]^{-1} \left[\frac{\lambda_L^3 \rho_L (\rho_L - \rho_G) g h_{LG}}{\mu_L D \Delta T} \right]^{0.25} + (1-x^{0.087}) \alpha_{LO} \quad (8.7)$$

and

$$\alpha_{LO} = 0.023 Re_{LO}^{0.8} Pr_L^{0.4} \frac{\lambda_L}{D} \quad (8.8)$$

It is important to notice that, as declared by the authors, all possible flow regimes observed during the condensation process are included in the model:

- annular flow is covered by Equation (8.5) and is typically forced convection structured;
- stratified-wavy flow is represented by Equation (8.6);

- stratified-smooth flow as the stratified-wavy flow is represented by Equation (8.6). Instead of a marked transition line, the progressive passage from wavy to smooth stratified flow is given by the linear interpolation included in Equation (8.6), and when smooth flow occurs, the ΔT -dependent component prevails;
- slug flow is included in both Equations (8.5) and (8.6). Being a ΔT -independent flow, the transition line described by Equation (8.3) is conceived to include a weak effect of T in Equation (8.6) when slug flow develops.

In addition to pure fluids, this model can also be applied to compute the thermal resistance of the liquid film during condensation of zeotropic mixtures. In this work the Cavallini et al. model has been applied with the Silver, Bell and Ghaly correction [26] in order to obtain the total heat transfer coefficient of the refrigerant.

8.1.2 Moser et al. model [11]

Many of the existing in-tube condensation correlations are based on the annular flow. These correlations can be classified into three categories: shear-based correlations, boundary layer-based correlations and two-phase multiplier-based correlations.

An interesting two-phase multiplier-based correlation was developed by Akers et al. (1959) [27] and became known as the “equivalent Reynolds number” model. This model defines the all-liquid flow rate that provides the same HTC as an annular condensing flow. This liquid flow rate was expressed by this equivalent Reynolds number Re_{eq} and used in a single phase, turbulent flow equation to predict the condensation HTC. Akers et al. [27] proposed that the resulting Nusselt number should be equal to the Nusselt number of the condensing flow.

Moser et al. [11] showed that the assumptions on which the equivalent Reynolds number is defined are faulty and proposed a correlation for a new equivalent Reynolds number that fix them. The operative ranges used for the verification of this model are reported in Table 8.2.

Table 8.2: Moser et al. model [11] experimental ranges.

Authors	Fluids	D [mm]	T_{sat} [°C]	Vapor quality	G [kg m ⁻² s ⁻¹]
Moser et al. [11]	R22, R134a, R410A, R12, R113	4.57 ÷ 12.7	21 ÷ 56	0.1 ÷ 1.0	148 ÷ 1482

This new Re_{eq} is showed in Equation (8.9) and the two-phase multiplier Φ_{LO}^2 given in Equation (8.10):

$$Re_{eq} = \Phi_{LO}^{8/7} Re_{LO} \quad (8.9)$$

$$\Phi_{LO}^2 = A_1 + \frac{3.24A_2}{Fr^{0.045} We^{0.035}} \quad (8.10)$$

where Fr and We are:

$$Fr = \frac{G^2}{gD\rho_{tp}^2} \quad ; \quad We = \frac{G^2D}{\sigma\rho_{tp}} \quad (8.11)$$

with

$$\rho_{tp} = \left(\frac{x}{\rho_G} + \frac{1-x}{\rho_L} \right)^{-1} \quad (8.12)$$

and

$$A_1 = (1-x)^2 + x^2 \left(\frac{\rho_L}{\rho_G} \right) \left(\frac{f_{VO}}{f_{LO}} \right) \quad (8.13)$$

$$A_2 = x^{0.78} (1-x)^{0.24} \left(\frac{\rho_L}{\rho_G} \right)^{0.91} \left(\frac{\mu_G}{\mu_L} \right)^{0.19} \left(1 - \frac{\mu_G}{\mu_L} \right)^{0.70} \quad (8.14)$$

Moser et al. [11] developed a correlation to express the local heat transfer coefficient for two-phase annular condensing flow in a form of a Nusselt number as:

$$\alpha_{tp} = \left(\frac{\lambda_L}{D} \right) \left[\frac{0.0994 C_1 Re_L^{C_2} Re_{eq}^{1+0.875 C_1} Pr_L^{0.815}}{(1.58 \ln Re_{eq} - 3.28)(2.58 \ln Re_{eq} + 13.7 Pr_L^{2/3} - 19.1)} \right] \quad (8.15)$$

where the exponents C_1 and C_2 are:

$$C_1 = 0.126 Pr_L^{-0.0448} \quad ; \quad C_2 = -0.113 Pr_L^{-0.563} \quad (8.16)$$

They found that the model underpredicts the experimental Nusselt number more often than it overpredicts it and the model range validity can be extended to as small as 3.14 mm tube internal diameters.

The two-phase multiplier Φ_{LO}^2 can be also calculated as suggested by Ming Zhang and Ralph L. Webb [28]. They developed a new correlation by testing three tubes to determine the single-phase and two-phase pressure drop of refrigerants R134a, R22 and R404a. Two copper tubes with inner diameter of 6.20 mm and 3.25 mm was used, the third tube was a multi-port, flat extruded aluminium tube with an hydraulic diameter of 2.13 mm. The tests were carried out also to investigate the validity of previous developed two-phase multiplier-based correlations. The test experimental conditions are reported in Table 8.3.

Table 8.3: Zhang and Webb two-phase multiplier experimental ranges.

Authors	Fluids	D [mm]	T_{sat} [°C]	Vapor quality	G [kg m ⁻² s ⁻¹]
Ming Zhang and Ralph L. Webb. [28]	R22, R134a, R404A	2.13 ÷ 6.20	20 ÷ 65	0.2 ÷ 0.89	200 ÷ 1 000

The proposed a new equation for the the two-phase multiplier that is suitable to be used for microchannels:

$$\Phi_{LO}^2 = (1-x)^2 + 2.87x^2 p_r^{-1} + 1.68x^{0.8} (1-x)^{0.25} p_r^{-1.64} \quad (8.17)$$

thus the value returned from the Equation (8.17) has been inserted inside the Moser et al. model in order to have a more correct value of Φ_{LO}^2 for the HTC calculation inside the microchannel.

8.1.3 Shah model [16]

This model consists in an improved version of the previous correlation for heat transfer during film condensation, developed by the same author. Shah decided to extend his correlation to a wider range of parameters such as lower flow rates, different refrigerants and a wider reduced pressure range (if compared with the previous database). He developed and verified a new correlation tested with a parameter ranges shown in Table 8.4.

Table 8.4: Shah model [16] experimental ranges.

Authors	Fluids	D [mm]	p_r	Vapor quality	G [kg m ⁻² s ⁻¹]
M. Mohammed Shah [16]	Water, R11, R12, R22, R32, R113, R123, R125, R134a, R142b, R404a, R410A, R502, R507, isobutane, propylene, propane, benzene, ethanol, methanol, toluene and downtherm 209	2 ÷ 49	0.0008 ÷ 0.905	0.01 ÷ 0.99	4 ÷ 820

For horizontal tubes, two flow regimes were described by the author. To identify the flow regime the dimensionless gas velocity J_G , described by Equation (8.1), is adopted. By comparing this value with the the transition dimensionless gas velocity J_G^T , defined by Shah as:

$$J_G^T = 0.98(\mathcal{Z} + 0.263)^{-0.62} \quad (8.18)$$

with

$$\mathcal{Z} = \left(\frac{1}{x} - 1\right)^{0.8} p_r^{0.4} \quad (8.19)$$

it is possible to know which flow regime occurs during the condensation. For the two regimes, the author considered two contributes for the calculation of the total HTC, the first one is:

$$\alpha_I = \alpha_{LO} \left(\frac{\mu_L}{14\mu_G}\right)^n \left[(1-x)^{0.8} + \frac{3.8x^{0.76}(1-x)^{0.04}}{p_r^{0.38}} \right] \quad (8.20)$$

where α_{LO} is described in Equation (8.8) and the n exponent is defined as:

$$n = 0.0058 + 0.557p_r \quad (8.21)$$

The second one is:

$$\alpha_{Nu} = 1.23Re_L^{-1/3} \left[\frac{\rho_L(\rho_L - \rho_G)g\lambda_L^3}{\mu_L^2} \right]^{1/3} \quad (8.22)$$

Thus the model predicts the condensation heat transfer coefficient basing on the two regimes criteria as:

$$\alpha_{tp} = \begin{cases} \alpha_I & \text{for } J_G \geq J_G^T \\ \alpha_I + \alpha_{Nu} & \text{for } J_G < J_G^T \end{cases} \quad (8.23)$$

8.2 Silver, Bell and Ghaly models correction for condensation of zeotropic mixtures [26]

Mixture condensation differs from pure vapor condensation in two ways:

- the temperature of refrigerant changes through the condenser (temperature glide);
- mass transfer effects are introduced in addition to those of heat transfer.

The resistance to mass transfer in the vapor phase is a critical aspect in the condensation process, where the lack of applicable mass transfer data and the complexity of the computational procedure are big obstacles for the search of exact solutions. Silver, Bell and Ghaly made the assumption that the effect of the mass transfer resistance in the vapor phase can be replaced by a conservative estimate of the heat transfer resistance in the vapor. Their assumption has led to writing the overall thermal resistance as a sum of two thermal resistances in series. The first one is for convective heat transfer in the vapor phase from the bulk vapor temperature to the temperature at the interface; the second one is across the condensate film itself.

For the first component, a pure fluid model can be used in the calculation. The second component is obtained from the ratio of the sensible to total heat duty that can be expressed as:

$$\frac{dq_s}{dq_T} \approx x c_{p,G} \frac{dT_{sat}}{dh} \quad (8.24)$$

If the ratio dT_{sat}/dh remains approximately constant during the condensation process, it can be re-written as a function of the temperature glide and the isobaric change in enthalpy as:

$$\frac{dT_{sat}}{dh} \approx \frac{\Delta T_{gl}}{\Delta h_{LG}} \quad (8.25)$$

Hence naming the first resistance $1/\alpha_{tp}$ where α_{tp} is the heat transfer coefficient computed by a pure fluid model using the mixture properties, the corrected total thermal resistance suggested by Silver, Bell and Ghaly [26] is given as:

$$R_T = \frac{1}{\alpha_{tp}} + x c_{p,G} \left(\frac{\Delta T_{gl}}{\Delta h_{LG}} \right) \frac{1}{\alpha_G} \quad (8.26)$$

where

$$\alpha_G = 0.023 Re_G^{0.8} Pr_G^{0.33} \frac{\lambda_G}{D} \quad (8.27)$$

Thus the final value of the HTC is simply given by:

$$HTC = \frac{1}{R_T} \quad (8.28)$$

The authors suggest a second correction that needs additional assumptions concerning the flow pattern developed inside the condenser. The estimate of these additional parameters have not been taken into consideration in this work, mainly due to the measurement difficulties implied in the condensation process. Furthermore the experimental and predicted data calculated with this simplified correction were found to be in a good agreement (as stated in the results section).

8.3 Pressure Drop theoretical model

As stated for the HTC models, the model here considered for pressure drop prediction has been developed for pure fluids. The tests for the investigation of pressure drops have presented some difficulties because the experimental points were acquired in several days and with different test rig set points. However, experimental data and model data are in a good agreement within the limits of uncertainty, as described in the results section.

8.3.1 Del Col et al. model [8]

This model is an update of the previous one presented by Cavallini et al. [29], [30] through the introduction of a parameter that takes into account the effect of the channel surface roughness depending on the flow regime that is formed. This model has been taken into account as it has been developed and validated for flow patterns inside microchannels. Table 8.5 shows the experimental ranges used for microchannel flow.

Table 8.5: Del Col et al. model [8] experimental ranges for microchannels.

Authors	Fluids	D_h [mm]	R_a [μm]	T_{sat} [$^{\circ}\text{C}$]	G [$\text{kg m}^{-2}\text{s}^{-1}$]
Del Col et al. [8]	R134a, R1234yf, R32, R245fa	$0.96 \div 2$	$1.02 \div 2.0$	$26 \div 50$	$200 \div 800$

The previous model developed by Cavallini et al. [29] and [30] tends to overestimate the data at low liquid-only Reynolds number, with an error increasing as Re_{LO} decreases. The new model considers that the effect of the surface roughness on the fluid flow, and thus on the frictional pressure drop, should be smaller at lower mass velocities and higher liquid-phase viscosity μ_L , and thus lower liquid-only Reynolds number Re_{LO} .

Then the liquid-only friction factor correlation has been modified with the parameter X that takes into account of the wall superficial roughness:

$$f_{LO} = 0.0046(Re_{LO})^{-0.2} + 0.7RR \cdot X \quad (8.29)$$

where

$$X = \begin{cases} 0, & \text{if } Re_{LO} \leq Re_{LO}^+ \\ 1, & \text{if } Re_{LO} \geq 3500 \\ 1 + \frac{A - 0.046Re_{LO}^{-0.2}}{0.7 \cdot RR}, & \text{if } Re_{LO}^+ < Re_{LO} < 3500 \end{cases} \quad (8.30)$$

$$A = 0.0046(3500)^{-0.2} = 8.9938 \cdot 10^{-3} \quad (8.31)$$

and

$$Re_{LO}^+ = \left(\frac{A + 0.7 \cdot RR}{0.046} \right)^{-5} \quad (8.32)$$

The equation to investigate the linear pressure drop is reported as:

$$\left(\frac{dp}{dz}\right)_f = \Phi_{LO}^2 \left(\frac{dp}{dz}\right)_{f,LO} = \Phi_{LO}^2 \frac{2f_{LO}G^2}{D_h\rho_L} \quad (8.33)$$

where the two-phase multiplier is

$$\Phi_{LO}^2 = Z + 3.595 \cdot F \cdot H \cdot (1 - E)^W \quad (8.34)$$

with

$$W = 1.398 p_r = 1.398 \frac{p}{p_{crit}} \quad (8.35)$$

$$Z = (1 - x)^2 + x^2 \frac{\rho_L}{\rho_G} \left(\frac{\mu_G}{\mu_L}\right)^{0.2} \quad (8.36)$$

$$F = x^{0.9525} (1 - x)^{0.414} \quad (8.37)$$

and

$$H = \left(\frac{\rho_L}{\rho_G}\right)^{1.132} \left(\frac{\mu_G}{\mu_L}\right)^{0.44} \left(1 - \frac{\mu_G}{\mu_L}\right)^{3.542} \quad (8.38)$$

The entrainment ratio E is calculated as:

$$\begin{cases} E = 0.015 + 0.44 \log_{10} \left[\left(\frac{\rho_{GC}}{\rho_L}\right) \left(\frac{\mu_L j_G}{\sigma}\right)^2 \cdot 10^4 \right] \\ E = 0, & \text{if } E \leq 0 \\ E = 0.95, & \text{if } E \geq 0.95 \end{cases} \quad (8.39)$$

and the homogeneous gas core density ρ_{GC} is given by:

$$\rho_{GC} = \left(\frac{x + (1 - x)E}{\frac{x}{\rho_G} + \frac{(1+x)E}{\rho_L}} \right) \quad (8.40)$$

As can be seen from the Equations (8.39) and (8.40) the model requires a recursive algorithm for the determination of the two parameters E and ρ_{GC} .

The model presented above for the frictional pressure gradient can be extended to lower vapor qualities and mass velocities ($J_G < 2.5$), with the constraint to take the higher value between $(dp/dz)_f$ from the Equation (8.33) and the all-liquid frictional pressure gradient $(dp/dz)_{f,LO}$ for the considered channel geometry as described in Equations (8.41) and (8.42)

$$\left(\frac{dp}{dz}\right)_{f,LO} = \frac{2f_{LO}G^2}{D_h\rho_L} \quad (8.41)$$

$$\begin{cases} f_{LO} = 0.046 \left(\frac{GD_h}{\mu_L}\right)^{-0.2} & \text{if } Re_{LO} > 2000 \\ f_{LO} = \frac{C}{\left(\frac{GD_h}{\mu_L}\right)} & \text{if } Re_{LO} < 2000 \end{cases} \quad (8.42)$$

where

$$\begin{aligned} C &= 16 && \text{for circular cross section} \\ C &= 14.3 && \text{for square cross section} \end{aligned} \quad (8.43)$$

Nomenclature

Symbols

A_1	single-phase surface area [m ²]
A_2	two-phase surface area [m ²]
c_p	specific heat capacity [J kg ⁻¹ K ⁻¹]
D	inner tube diameter [m]
D_h	hydraulic diameter [m]
Fr	Froude number, Equation (8.11)
f	Fanning friction factor
g	standard gravitational acceleration [m s ⁻²]
G	mass velocity [kg m ⁻² s ⁻¹]
h	specific enthalpy [J kg ⁻¹]
h_{LG}	differential latent heat [J kg ⁻¹]
J_G	dimensionless gas velocity, Equation (8.1)
J_G^T	transition dimensionless gas velocity, Equation (8.3)
j_G	superficial gas velocity = xG/ρ_G
Nu	Nusselt number = $\alpha D/\lambda_L$
Pr	Prandtl number = $\mu c_p/\lambda$
p_r	reduced pressure = p/p_{crit}
p_{crit}	critical pressure [bar]
q	heat flux [W]
R	thermal resistance [m ² K W ⁻¹]
Ra	arithmetical mean deviation of the assessed profile (according to ISO 4287:1997) [m]
Re	Reynolds number = $\rho v D/\mu$
Re_{eq}	equivalent Reynolds number for the Moser et al. model, Equation (8.9)
Re_L	Reynolds number assuming liquid phase flowing alone = $GD(1-x)/\mu_L$
Re_{LO}	liquid-only Reynolds number = GD/μ_L
RR	relative roughness of the channel = $2Ra/D_h$
T_s	saturation temperature [K]
T_w	tube internal wall temperature [K]
We	Weber number, Equation (8.11)
X	dimensionless parameter for roughness, Equation (8.30)
X_{tt}	Martinelli parameter, Equation (8.2)
x	thermodynamic vapor quality
z	axial position [m]
Z	Shah's correlating parameter, Equation (8.19)

ctd . . .

Greek Symbols

α	heat transfer coefficient [$\text{W m}^{-2}\text{K}^{-1}$]
α_{Nu}	Nusselt relation heat transfer coefficient, Shah model Eq 8.22
α_I	heat transfer coefficient given by Equation (8.20)
ΔT	saturation to wall temperature difference = $T_S - T_W$ [K]
ΔT_{gl}	temperature glide = $T_{DEW} - T_{BUBBLE}$ [K]
λ	thermal conductivity [$\text{W m}^{-1}\text{K}^{-1}$]
μ	dynamic viscosity [$\text{kg m}^{-1}\text{s}^{-1}$]
ρ	density [kg m^{-3}]
σ	liquid surface tension [N m^{-1}]
Φ^2	dimensionless two-phase multiplier

Subscripts

A	ΔT independent flow regime (Cavallini et al. model)
D	ΔT dependent flow regime (Cavallini et al. model)
f	frictional
G	gas phase
GC	gas core
L	liquid phase
LO	liquid phase with total flow
S	sensible
sat	saturation
$STRAT$	fully stratified flow regime (Cavallini et al. model)
tp	two-phase flow
T	total
VO	vapor phase with total flow

Chapter 9

Data comparisons

The experimental data are now compared against the theoretical models which include both Heat Transfer models and a Pressure Drop model. The comparison includes also a database of the two pure fluids R32 and R1234ze(E) which have been created basing on experimental tests carried out in the same test rig and at the same operative conditions used for the investigated mixtures.

9.1 Comparison against theoretical models

The models here considered are described in section 8 on page 73, the comparison is subdivided by HTC models and the PD model.

9.1.1 Heat Transfer Coefficients comparison

The models considered for the comparison are corrected with the Silver, Bell and Ghaly correction for zeotropic mixtures [26] and they are evaluated imposing the local thermodynamic equilibrium during condensation. A final comparison is made without considering the Silver, Bell and Ghaly correction in the Cavallini et al. model [5] in order to point out the mass transfer resistance contribution on the HTC prediction. The experimental points available for the comparison for the whole mass velocity span are: 56 points for mixture 23/77%, 63 points for mixture 46/54% and 64 points for mixture 76/24% leading to a database of 183 points for each model.

Figure 9.1 reports the comparison between the experimental HTC and the Heat Transfer Coefficients predicted by the model developed by Cavallini et al. [5] for the whole mass velocity span $150 \leq G \leq 800 \text{ kg m}^{-2}\text{s}^{-1}$; each diagram refers to a mixture. It can be noticed that, in general, the correlation slightly underpredicts the HTC value for all the mass velocities except for the last mixture 76/24% for which experimental data show the best agreement with the predicted data. The deviation magnitude is indeed reduced by increasing the R32 mass fraction in the mixture, from mixture 23/77% to mixture 76/24%. In fact the model gives an Absolute Mean Deviation (e_{AB}) of 9.9% for mixture 23/77% while for mixtures 46/54% and 76/24% the e_{AB} are respectively 7.5% and 5.7%. This correlation seems to well predict the mixtures HTC as 97.8% of the experimental points fall within $\pm 20\%$ error bands with low values of Standard Deviation (σ): for mixture 23/77% the σ is 4.4% , 4.3% for mixture 46/54% and 4.7% for mixture 76/24%.

Figure 9.2 shows the comparison between the experimental points and the points predicted with the model developed by Moser et al. [11]. The model shows, in general, an underprediction of the HTC for all the mass velocities and for all the investigated mixtures. The experimental points deviation from the model tends to be lower by increasing the R32 mass fraction in the mixture, hence by passing from mixture 23/77% to mixture 76/24%. This trend is confirmed by the e_{AB} values: 11.5% for mixture 23/77%, 10.3% and 7.3% for mixture 46/54% and mixture 76/24% respectively. The prediction of the experimental points is quite good as 97.3% of them fall between $\pm 20\%$ error bands. The σ are 4.9% for mixture 23/77% , 4.8% for mixture 46/54% and 4.1% for mixture 76/24%.

Figure 9.3 reports the comparison between the experimental HTC and the HTC predicted by the Shah correlation [16]. The model gives, in general, a good prediction of the HTC for all the mass velocities and for all the investigated mixtures. It can be noticed that all the points are very close to the ideal line except for mixture 76/24% for which the model shows a slight overprediction. In fact the e_{AB} for mixture 23/77% is equal to 5.0%, for mixture 46/54% is 4.9% while for mixture 76/24% raises up to 10.9%. The correlation seems to give a good prediction of the HTC since 97.8% of the experimental points fall between $\pm 20\%$ error bands. The σ values are: 5.5% for mixture 23/77%, 5.4% and 5.9% for mixtures 46/54% and 76/24% respectively.

Table 9.1 summarizes the models accuracy by reporting their absolute mean deviations and the standard deviations both computed for the whole database.

Table 9.1: Absolute Mean Deviations and Standard Deviations of the three theoretical models used for the comparison against experimental data.

Parameter	Unit	Cavallini et al. [5]	Moser et al. [11]	Shah [16]
e_{AB}	%	7.7	9.7	6.9
σ	%	4.5	4.6	5.6
PP ₂₀ ^a	%	97.8	97.3	97.8

^a Points within a $\pm 20\%$ error bands.

It can be noticed that the model developed by Moser et al. [11] gives the worst result in terms of e_{AB} as it assumes the higher value compared with the other two correlations. Furthermore, it predicts the lower percentage of experimental points between $\pm 20\%$ error bands so it is the less accurate correlation. The model developed by Cavallini et al. [5] and the model by Shah [16] predict the same points number within the $\pm 20\%$ uncertainty bands. However the second one shows the lower e_{AB} but the higher σ so far. Between the three models, the one developed by Cavallini et al. [5] shows the lowest σ (4.5%) and an e_{AB} of 7.7% that is just 11% greater than the lowest value. So this correlation seems to be suitable to be used for the HTC prediction of zeotropic mixtures flowing inside microchannels.

By looking at Figures 9.1, 9.2 and 9.3, it can be seen that the points that overcome the error band of -20% are mainly the ones for which the mass velocity is equal to 200 and 150 kg m⁻²s⁻¹, especially for mixture 76/24%. This could be explained as the models make a significant error in the HTC prediction at low mass velocities and low vapor qualities. In particular the Cavallini et al. model [5] it has been tested for pure R32 and Matkovič et al. [4] reported that the correlation gives an underprediction

for low mass velocities ($G < 200 \text{ kg m}^{-2}\text{s}^{-1}$) and low vapor qualities.

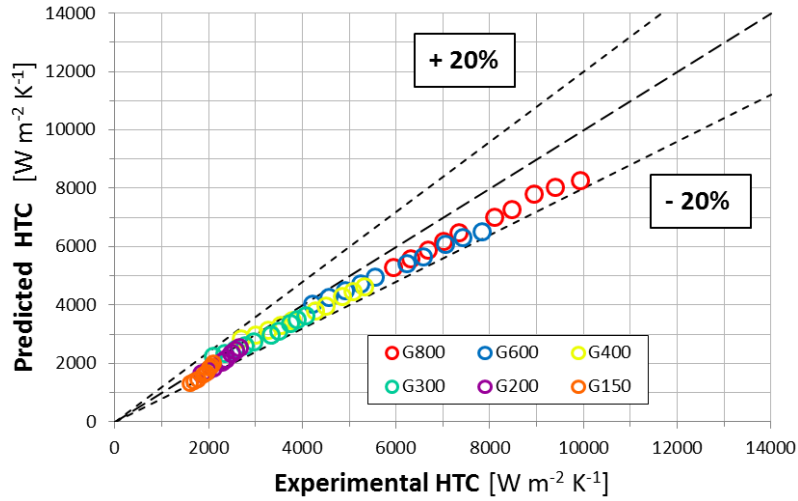
A further analysis is made by comparing experimental data against the data predicted by the Cavallini model [5] without the Silver, Bell and Ghaly correction [26] for zeotropic mixtures. Figure 9.4 reports this comparison. By comparing it with Figure 9.1 it is clear the significant contribution of the mass transfer resistance on the local HTC prediction. The introduction of this further resistance lead to a variation of the HTC up to -40% for mixture 23/77%, -30% and -10% for mixtures 46/54% and 76/26% respectively. Furthermore, the absence of the correction afflicts the model accuracy as the e_{AB} are now raised up to 13.1% for mixture 23/77%, 13.4% and 10.6% for mixtures 46/54% and 76/24% respectively. The σ are 7.1% for mixture 23/77%, 6.6% for mixture 46/54% and 5.4% for mixture 76/24%.

The total e_{AB} is raised up to 12.4% and the total σ is equal to 6.3%. Now the experimental points falling between $\pm 20\%$ error bands are 90.2% of the total. With respect to the same correlation shown in Figure 9.1, the absence of the correction for the mass transfer lead to a mean HTC variation of 24.3% for mixture 23/77%, 20.3% for mixture 46/54% and 8.1% for mixture 76/24%. This significant variations lead the model to overpredict, in general, all the HTC of the three investigated mixtures. Table 9.2 summarizes the Cavallini et al. [5] model accuracy by reporting its absolute mean deviations and the standard deviations computed with and without the Silver, Bell and Ghaly correction [26] for zeotropic mixtures.

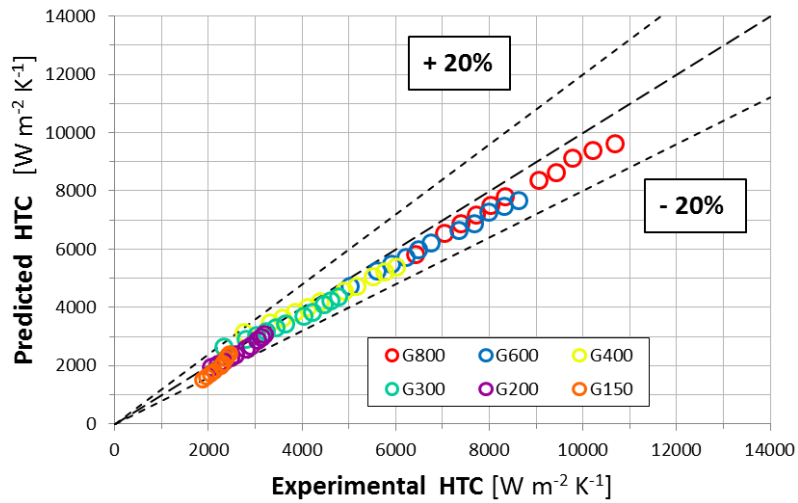
Table 9.2: Absolute Mean Deviations and Standard Deviations of the model developed by Cavallini et al. [5] with and without the Silver, Bell and Ghaly correction [26] for zeotropic mixtures.

Parameter	Unit	With correction	Without correction
e_{AB}	%	7.7	12.4
σ	%	4.5	6.3
PP ₂₀ ^a	%	97.8	90.2

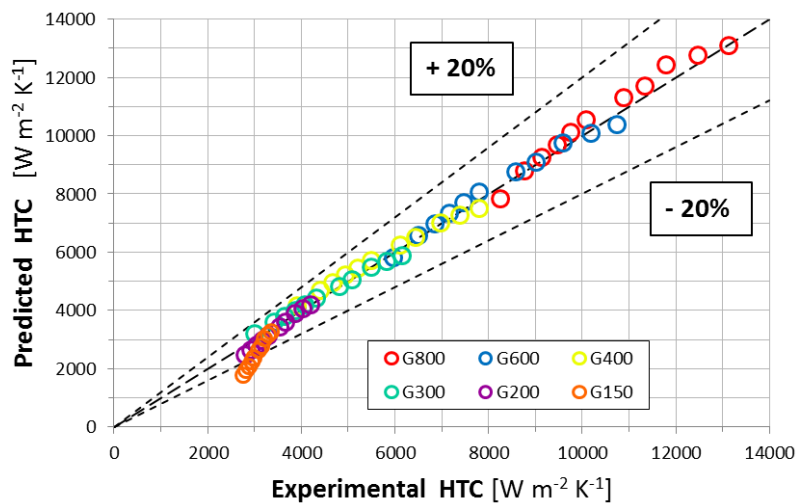
^a Points within a $\pm 20\%$ error bands.



(a) R32/R1234ze(E) mixture with 23/77% mass ratio.

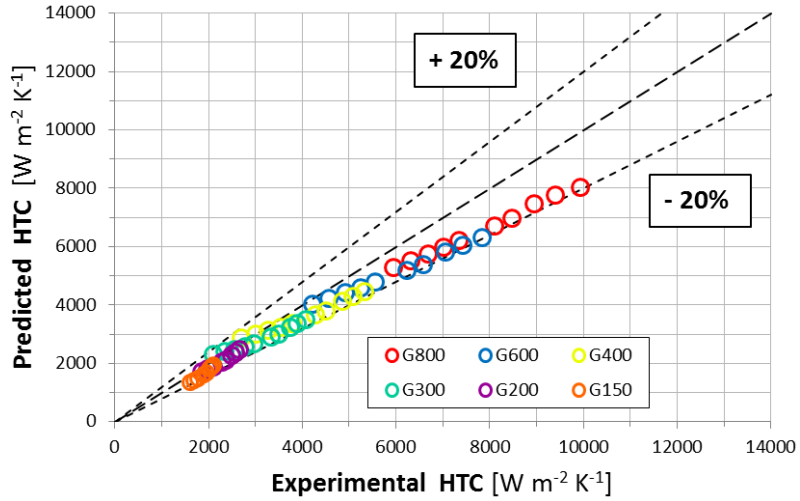


(b) R32/R1234ze(E) mixture with 46/54% mass ratio.

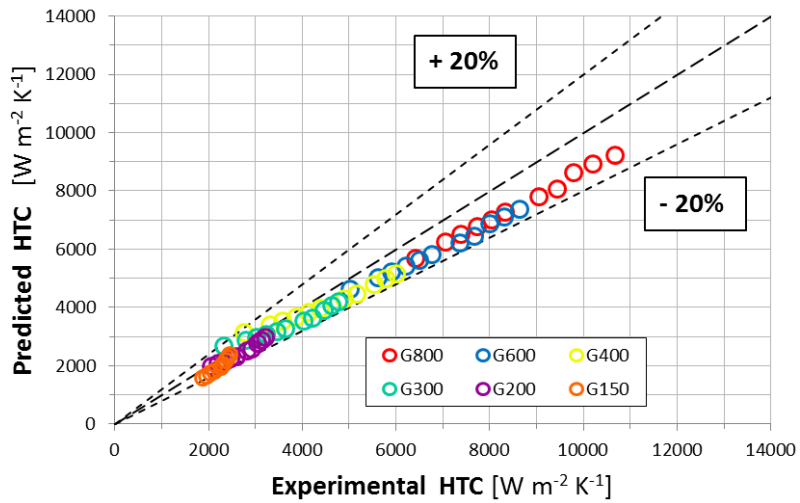


(c) R32/R1234ze(E) mixture with 76/24% mass ratio.

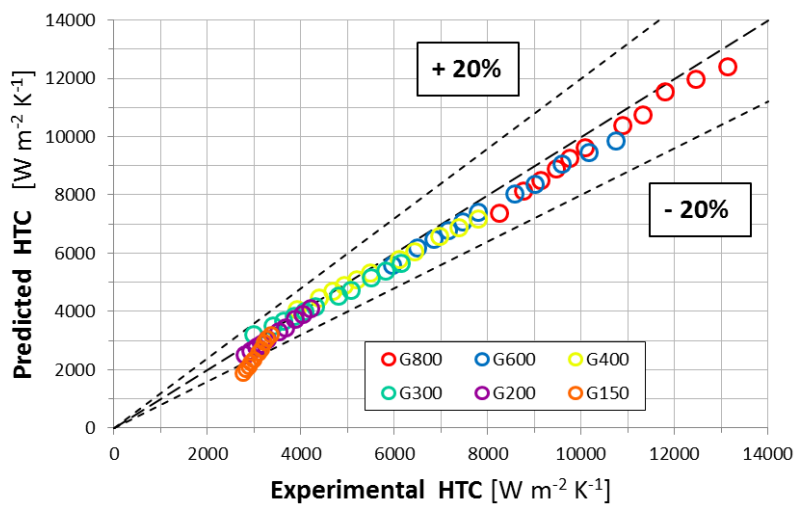
Figure 9.1: Experimental vs calculated HTC predicted by the Cavallini et al. model [5] at mass velocities ranging from 150 to 800 $\text{kg m}^{-2} \text{s}^{-1}$. The model implements the Silver, Bell and Ghaly correction [26] to account for the zeotropic characteristics of the mixture.



(a) R32/R1234ze(E) mixture with 23/77% mass ratio.

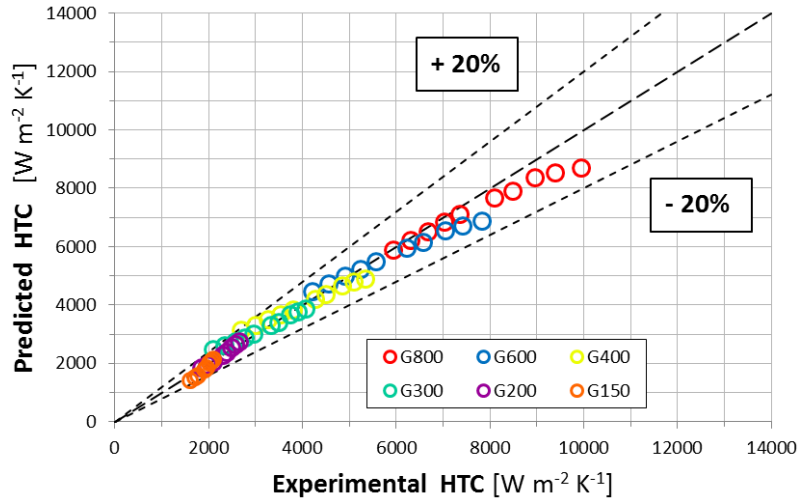


(b) R32/R1234ze(E) mixture with 46/54% mass ratio.

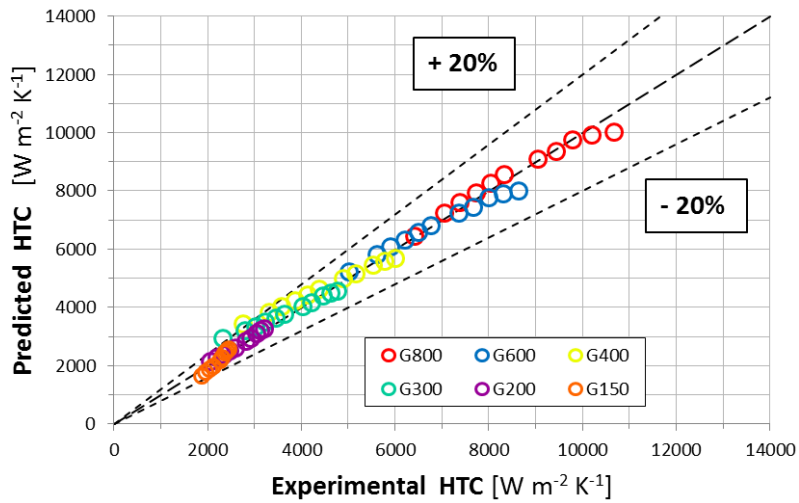


(c) R32/R1234ze(E) mixture with 76/24% mass ratio.

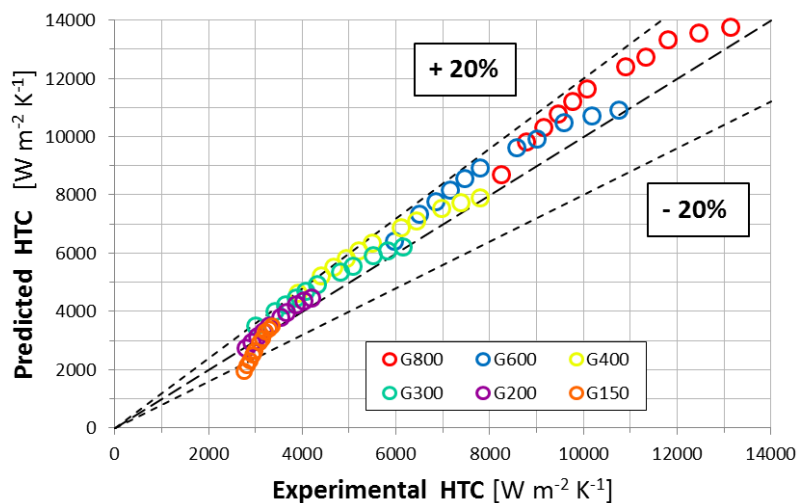
Figure 9.2: Experimental vs calculated HTC predicted by the Moser et al. model [11] at mass velocities ranging from 150 to 800 kg m⁻²s⁻¹. The model implements the Silver, Bell and Ghaly correction [26] to account for the zeotropic characteristics of the mixture and the correction by Zhang and Webb [28] for minichannel flow.



(a) R32/R1234ze(E) mixture with 23/77% mass ratio.

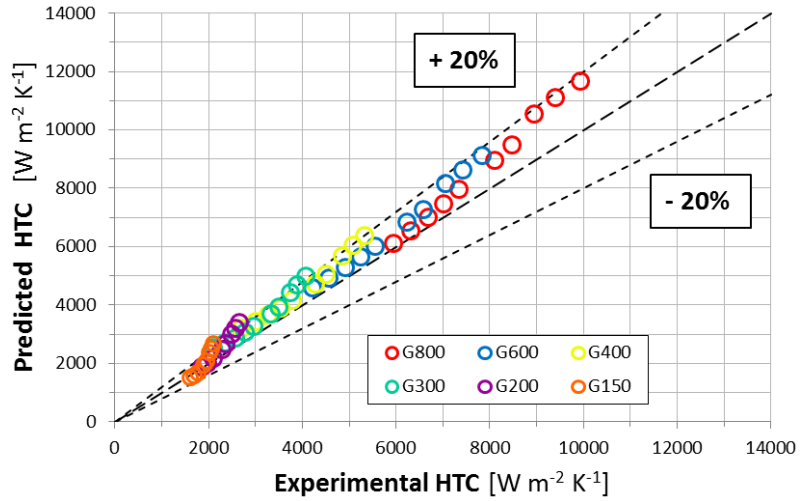


(b) R32/R1234ze(E) mixture with 46/54% mass ratio.

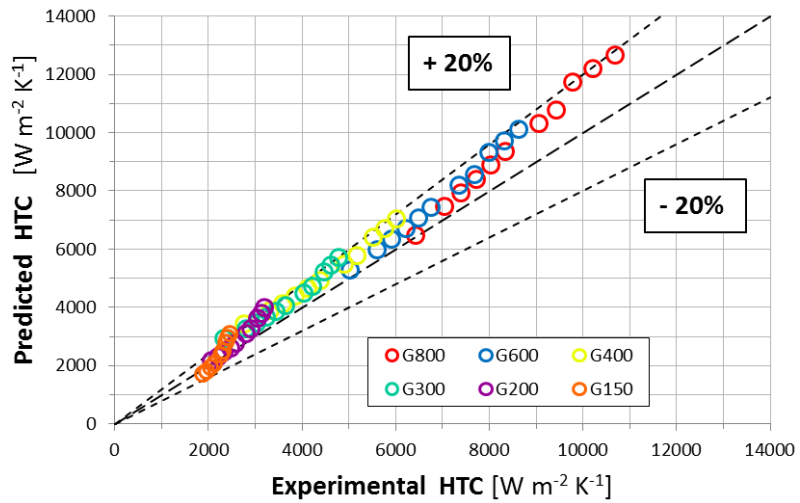


(c) R32/R1234ze(E) mixture with 76/24% mass ratio.

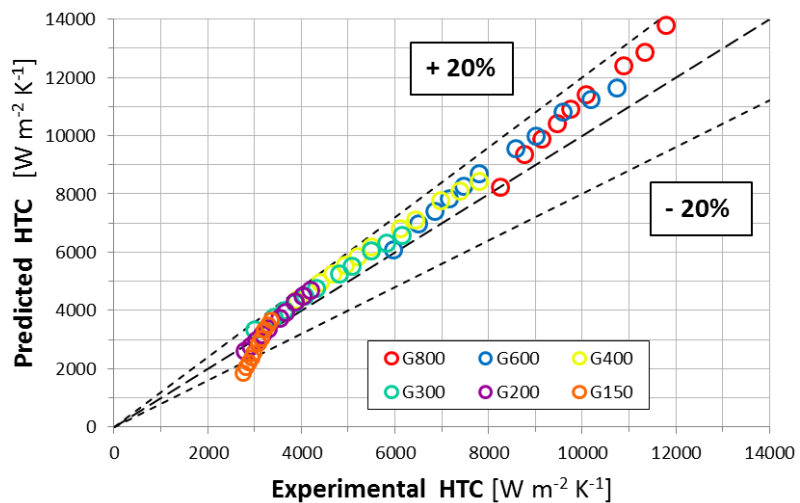
Figure 9.3: Experimental vs calculated HTC predicted by the Shah model [16] at mass velocities ranging from 150 to 800 $\text{kg m}^{-2} \text{s}^{-1}$. The model implements the Silver, Bell and Ghaly correction [26] to account for the zeotropic characteristics of the mixture.



(a) R32/R1234ze(E) mixture with 23/77% mass ratio.



(b) R32/R1234ze(E) mixture with 46/54% mass ratio.



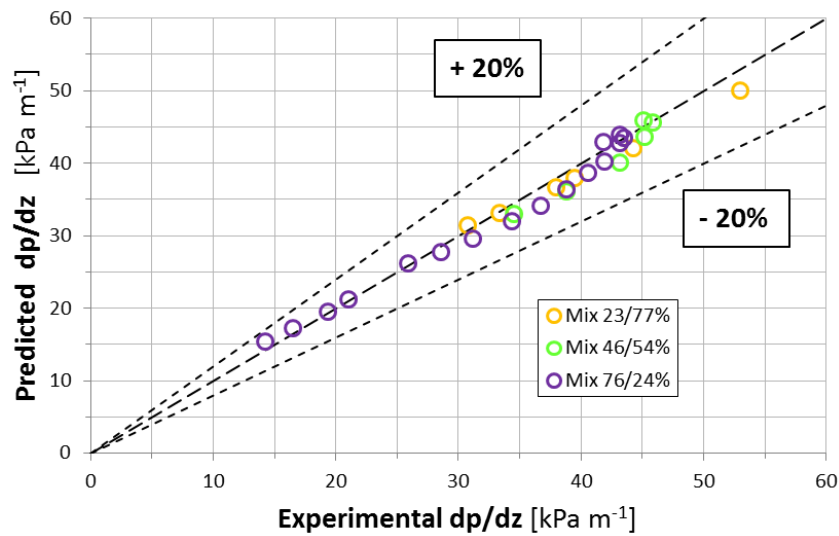
(c) R32/R1234ze(E) mixture with 76/24% mass ratio.

Figure 9.4: Experimental vs calculated HTC predicted by the Cavallini et al. model [5] without the Silver, Bell and Ghaly correction [26] at mass velocities ranging from 150 to 800 $\text{kg m}^{-2}\text{s}^{-1}$.

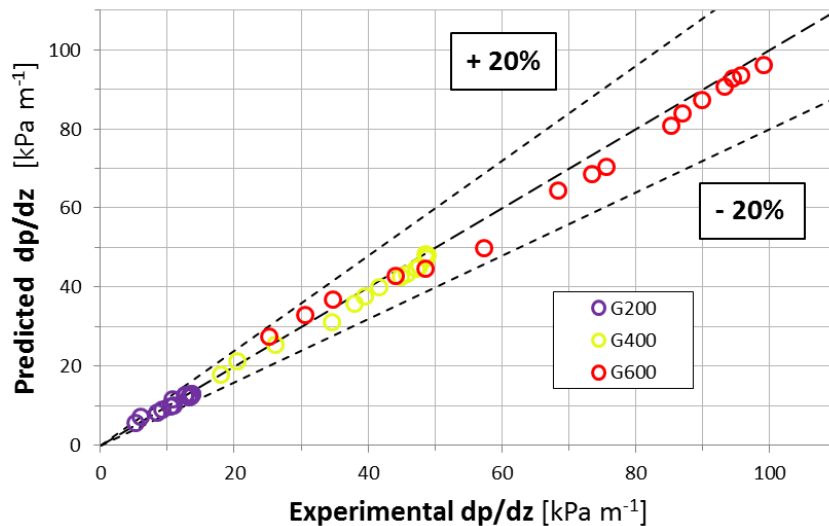
9.1.2 Pressure Drops comparison

The model developed by Del Col et al. [8] is used for the comparison; the pressure drop prediction is made with the hypothesis of thermodynamic equilibrium for each refrigerant state. The experimental points available for the comparison of the investigated mixtures are: 6 points for mixture 23/77%, 6 points for mixture 46/54% and 16 points for mixture 76/24% leading to a database of 28 points.

Figure 9.5(a) shows the predicted and the experimental pressure drop for the investigated mixtures for a mass velocity of $400 \text{ kg m}^{-2}\text{s}^{-1}$. The experimental data show a good agreement with the theoretical model as the e_{AB} are 3.2% for mixture



(a) Investigated mixtures at $G = 400 \text{ kg m}^{-2}\text{s}^{-1}$.



(b) Mixture with a mass ratio of 50/50% for mass velocities of 200, 400 and 600 $\text{kg m}^{-2}\text{s}^{-1}$.

Figure 9.5: Experimental vs calculated pressure drop predicted by the model developed by Del Col et al. [8].

23/77%, 3.9% for mixture 46/54% and 3.7% for mixture 76/24%. The σ are equal to 3.1% for mixture 23/77% , 3.6% and 4.5% for mixtures 46/54% and 76/24% respectively. The total e_{AB} is then equal to 3.6% while the total σ is equal to 3.7%. The model shows a good accuracy as all the experimental points fall between $\pm 20\%$ error bands.

Figure 9.5(b) reports the predicted and the experimental pressure drop for a mixture 50/50% for three mass velocities: 200, 400 and 600 $\text{kg m}^{-2}\text{s}^{-1}$. As it can be seen, the model gives a good prediction of the experimental pressure gradient as the model e_{AB} are 5.3% for $G = 200 \text{ kg m}^{-2}\text{s}^{-1}$ with a σ of 7.6%, 3.8% for $G = 400 \text{ kg m}^{-2}\text{s}^{-1}$ with a σ of 3.3% and 4.0% for $G = 600 \text{ kg m}^{-2}\text{s}^{-1}$ with a σ of 1.8%. The total e_{AB} of the model is equal to 4.4% while the total σ is equal to 4.3%. Also in this case the model shows a good accuracy as 97.4% of the experimental points fall between $\pm 20\%$ error bands.

Nomenclature

Symbols

e_{AB}	Absolute Mean Deviation
G	mass velocity [$\text{kg m}^{-2}\text{s}^{-1}$]
p_r	reduced pressure = p/p_{crit}
z	axial position [m]

Greek Symbols

σ	Standard Deviation
----------	--------------------

Chapter 10

Penalty Factor [31]

To allow the ranking of refrigerants for condenser applications based on their heat transfer potential, a Performance Evaluation Criterion (PEC) is now adopted, referring to the analysis conducted by Cavallini et al. [31]. A complete comparison between different refrigerants during convective forced condensation should consider not only the HTC, but also the pressure drop that affects the refrigerant saturation temperature and then the mean effective temperature difference. A larger saturation temperature drop implies that an additional compressor work will be needed in a refrigeration or air conditioning equipment to maintain a suitable value of the driving temperature difference. Thus, the local saturation temperature drop with respect to the vapor quality can be expressed as:

$$\frac{dT_{sat}}{dx} = \frac{dT_{sat}}{dp_f} \cdot \frac{dp_f}{dz} \cdot \frac{dz}{dx} \quad (10.1)$$

By using the Clausius-Clapeyron equation:

$$\frac{dT}{dp} = \frac{T(v_v - v_L)}{h_v - h_L} \quad (10.2)$$

and applying an energy balance to an elementary length dz of a round tube undergoing condensation from $x = 1$ to $x = 0$, the previous equation becomes:

$$\frac{dT_{sat}}{dx} = \frac{G \cdot D \cdot T_{sat}}{4\alpha \cdot \Delta T_{dr}} \left(\frac{1}{\rho_L} - \frac{1}{\rho_V} \right) \frac{\partial p_f}{\partial z} \quad (10.3)$$

Equation (10.3) contains two energy penalization terms: the first one is dT_{sat}/dx which is associated with the frictional pressure drop of the condensing refrigerant, the second one is ΔT_{dr} which is associated with the driving temperature difference for the heat transfer process:

$$\Delta T_{dr} = T_{sat} - T_{wall} \quad (10.4)$$

The two terms reported in Equation (10.3) and (10.4) adversely affect the compressor power consumption as their increase implies and increase in the compression ratio. Furthermore, Cavallini et al. [31] proved that they both are exergy losses

which penalize the cycle efficiency. To take account of these losses in a condensation process, the Penalty Factor (PF) is now defined as:

$$\text{PF} = \left(\frac{dT_{sat}}{dx} \right) \Delta T_{dr} = \Delta T_{sr} \cdot \Delta T_{dr} \quad (10.5)$$

by combining Equations (10.5) and (10.3) the Penalty Factor can be rewritten as:

$$\text{PF} = \frac{G \cdot D \cdot T_{sat}}{4\alpha} \left(\frac{1}{\rho_L} - \frac{1}{\rho_V} \right) \frac{\partial p_f}{\partial z} \quad (10.6)$$

now it is clear that the application of this methodology requires that both the heat transfer coefficient and the frictional pressure gradient have to be known at given operating conditions.

It can be noticed that the PF combine the two exergy losses terms in order to have a direct comparison between two different refrigerants at the same operative conditions. In fact, when the PF is computed for the same value of α for a given pipe geometry, it can be directly used as a quantitative criterion to rank the heat transfer performance of different working fluids: the smaller the PF, the better is the performance potential of the refrigerant.

This method have been applied to the pure fluids R32, R1234ze(E) and their mixtures in order to make a comparison between them in terms of heat transfer performances.

10.1 Comparison against pure fluids

The aim of this analysis is to compare mixtures and pure fluids R32, R1234ze(E) Heat Transfer performances with an appropriate PEC. To evaluate mixtures and pure fluids performances, the Penalty Factor (PF) is used as a comparative index, so the comparison is made imposing a constant PF and evaluating the particular operative conditions of each investigated pure fluid or mixture.

As reported in chapter 10 on the previous page the PF evaluation requires the use of accurate predicting models for HTC and frictional Pressure Drop at given operating conditions. For the HTC prediction, the model by Cavallini et al. [5] (described in section 8.1.1 on page 73) is used while the frictional pressure drop prediction is performed using the model developed by Del Col et al. [8] (described in section 8.3.1 on page 80).

Imposing a saturation temperature for the pure fluids and a mean refrigerant temperature for the mixtures both equal to 40 °C, the PF has been evaluated for a constant value of mass velocity $G = 400 \text{ kg m}^{-2}\text{s}^{-1}$; the results are reported in Figure 10.1. It can be noticed that the low GWP refrigerant R1234ze(E) shows the highest PF in the vapor quality span $0.1 \leq x \leq 0.9$ while the high GWP refrigerant R32 shows the lowest. This is coherent with the fluids properties as at the same saturation temperature, R32 has lower liquid density than R1234ze(E) as can be seen in Table 3.1 on page 12; this leads to a lower frictional Pressure Drop at the same mass velocity and hence in a lower saturation temperature drop. Furthermore, as R32 has a higher reduced pressure p_r compared with R1234ze(E), the predicted frictional Pressure Drop is lower than the pure R1234ze(E) (see section 8.3.1 on page 80).

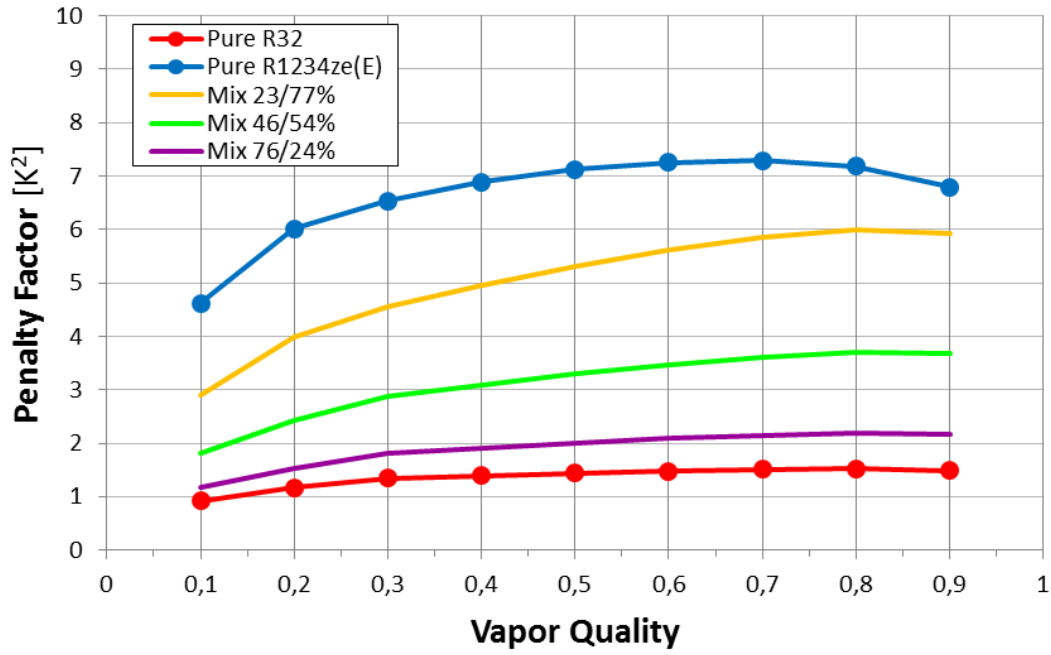


Figure 10.1: Penalty Factor and vapor quality for pure R32, pure R1234ze(E) and the investigated mixtures. The PF is evaluated at $G = 400 \text{ kg m}^{-2}\text{s}^{-1}$ with $T_{sat} = \bar{T}_r = 40^\circ\text{C}$ and $T_{sat} - T_{wall} = \bar{T}_r - T_{wall} = 10^\circ\text{C}$.

The three mixtures curves stand between the pure fluids and as the R32 mass fraction increases, the PF decreases. The mixtures present PF trends not equally distributed between the two pure fluids lines.

Now the same operative conditions are realized in terms of same PF, so the constant value of the PF = 5 K^2 is imposed for a mean vapor quality of $x = 0.5$. By looking at the PF definition, see Equation (10.6) on page 98, it clear that this leads to the definition of a certain mass velocity for both pure fluids and mixtures; in fact the mass velocity influences both the HTC and the frictional Pressure Drop. The particular mass velocity has been evaluated for R32, R1234ze(E) and the investigated mixtures (by using a recursive algorithm) with the constraints:

$$\begin{aligned}
 T_{sat} &= \bar{T}_r = 40^\circ\text{C} \\
 \text{PF} &= 5 \text{ K}^2 \text{ for } x = 0.5 \\
 T_{sat} - T_{wall} &= \bar{T}_r - T_{wall} = 10^\circ\text{C}
 \end{aligned} \tag{10.7}$$

These particular mass velocities are the ones that lead the fluids to show the same energy penalizations during a condensation process with the abovementioned constraints. Figure 10.2 shows that for pure R32 the mass velocity is the highest ($815 \text{ kg m}^{-2}\text{s}^{-1}$) and for pure R1234ze(E) is the lowest ($337 \text{ kg m}^{-2}\text{s}^{-1}$).

Coherently with what stated before, the three mixtures show mass velocities between the ones of the pure fluids. The mixtures mass velocities are $G = 441 \text{ kg m}^{-2}\text{s}^{-1}$ for mixture 23/77%, $G = 557 \text{ kg m}^{-2}\text{s}^{-1}$ for mixture 46/54% and $G = 700 \text{ kg m}^{-2}\text{s}^{-1}$ for mixture 76/24%; the more the R32 is added to the mixture, the more the mass velocity increases. It can be seen how all the PF trends are practically

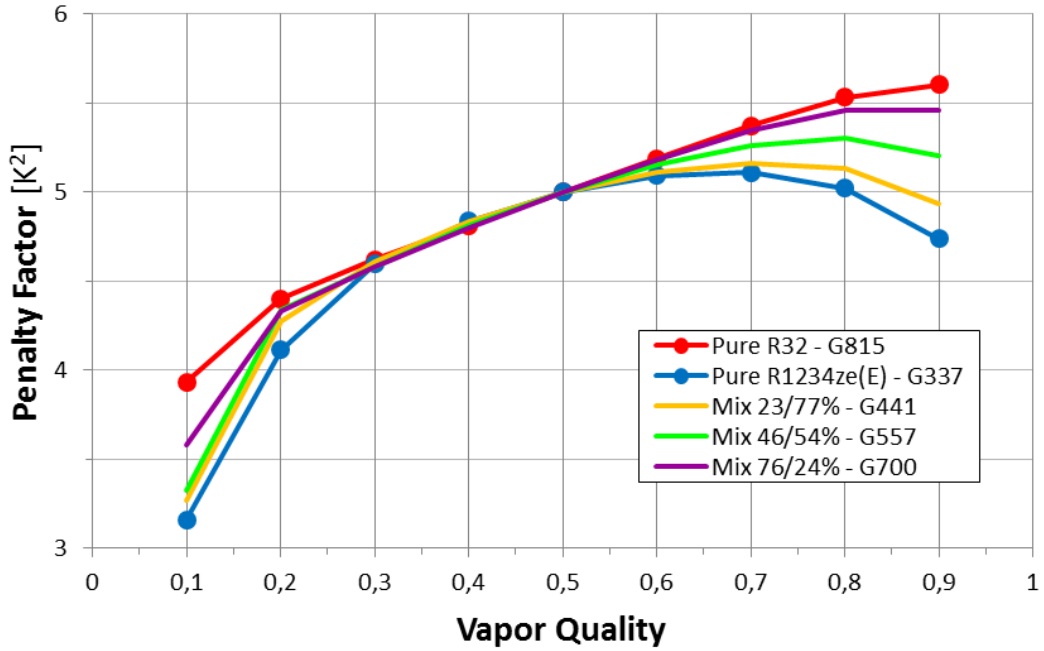


Figure 10.2: Penalty factor and vapor quality for pure R32, pure R1234ze(E) and the investigated mixtures considering a specific mass velocity for each fluid. The specific mass velocity is obtained by imposing the constraints reported in (10.7).

superimposed except for low and high vapor qualities, where a slight difference is in evidence.

It has to be pointed here that the assumption of a constant saturation to wall temperature difference $T_{sat} - T_{wall}$ and mean refrigerant to wall temperature difference $\bar{T}_r - T_{wall}$, as declared in (10.7), is verified a posteriori by evaluating the flow regime type with the fluid particular mass velocity and comparing it with the flow map reported by Cavallini et al. [5]. The resulting points fall always in the ΔT -independent flow region (see Figure 8.1 on page 75), so the assumption of a constant driving temperature difference for both pure fluids and mixtures is justified.

A further comparison is made by plotting the predicted HTC versus vapor quality for the particular mass velocities of pure fluids and mixtures, the results are shown in Figure 10.3. It is evident that pure R32 reaches the highest Heat Transfer Coefficients while pure R1234ze(E) shows the lowest ones. The three mixtures show intermediate values, increasing with the R32 mass fraction.

It can be noticed that a constant increase of the R32 mass fraction in the mixture leads to a non-constant increase in the heat transfer performances of the mixture itself. In fact mixture 23/77% is very close to pure R1234ze(E) in terms of HTC for the same value of PF at $x = 0.5$: the HTC increase is 21.6%. A mixture of intermediate composition between the two pure fluids does not lead to an intermediate heat transfer performance, in fact mixture 46/54% is again closer to pure R1234ze(E) in terms of HTC as the increase from mixture 23/77% is equal to 29.8% at $x = 0.5$. Only mixture 76/24% shows values of HTC closer to pure R32 but slightly higher than the intermediate values between the two pure fluids, the HTC increase from mixture 46/54% at $x = 0.5$ is equal to 35.7%. This penalization could be explained

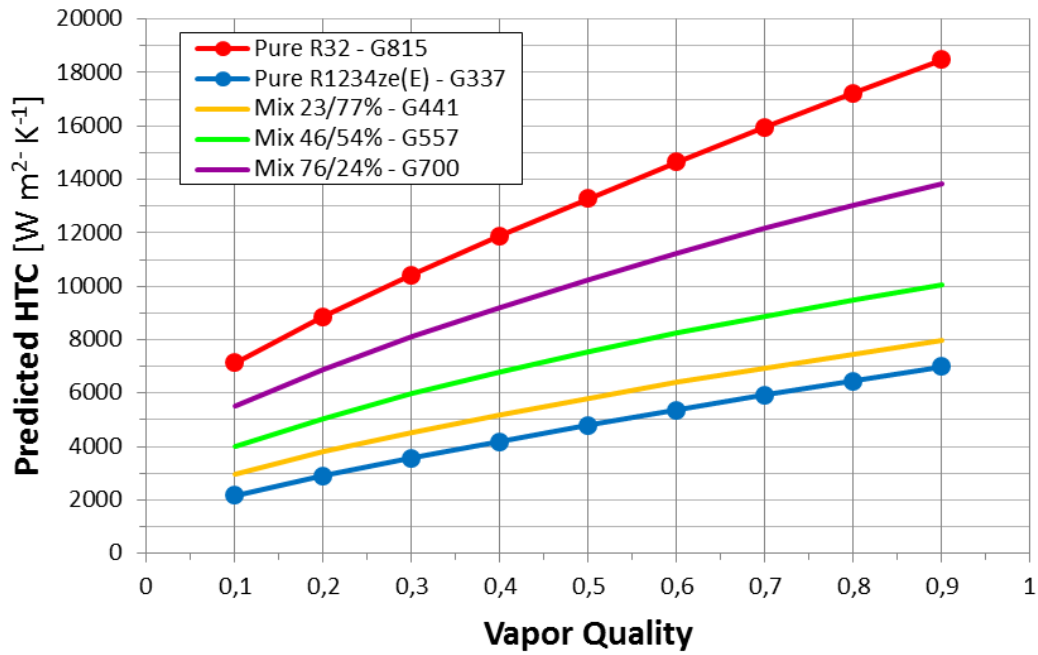


Figure 10.3: Heat Transfer Coefficient and vapor quality for pure R32, pure R1234ze(E) and the investigated mixtures considering a specific mass velocity for each fluid. The specific mass velocity is obtained by imposing the constraints reported in (10.7).

with the resistance introduced by the mass transfer, characteristic of the zeotropic mixtures. The present variation of the HTC increases from mixture 23/77% to mixture 76/24% because the mass velocity increases and also the glide magnitude and the differential latent heat magnitude decrease as can be seen in Figure 3.4 on page 17.

Thus the increase in heat exchange performances due to the addition of R32 to the mixture is reduced by the introduction of the mass transfer resistance that inhibits the heat exchange leading to lower values of HTCs.

Nomenclature

Symbols

D	inner channel diameter [m]
G	mass velocity [$\text{kg m}^{-2}\text{s}^{-1}$]
h	specific enthalpy [J kg^{-1}]
p	pressure [bar]
p_r	reduced pressure = p/p_{crit}
PF	Penalty Factor [K^2]
T	temperature [K]
v	specific volume [$\text{m}^3 \text{kg}^{-1}$]
x	thermodynamic vapor quality
z	axial position [m]

Greek Symbols

α	Heat Transfer Coefficient [$\text{W m}^{-2}\text{K}^{-1}$]
Δ	difference
ρ	density [kg m^{-3}]

Superscripts

—	mean value
---	------------

Subscripts

dr	driving
f	frictional
L	liquid phase
r	refrigerant
sat	saturation
sr	saturation, associated with the frictional pressure drop
V	vapor phase
$wall$	wall

Chapter 11

Conclusions

The heat transfer coefficients during condensation and the two-phase pressure drop in adiabatic flow conditions of R32/R1234ze(E) zeotropic mixture inside two different test sections made by a 0.96 inner diameter circular microchannel have been investigated in this work.

Three R32/R1234ze(E) mixtures with different mass composition have been tested: mixture 23/77%, mixture 46/54% and mixture 76/24%. The condensation tests have been carried out for mass velocity ranging from 150 to 800 kg m⁻²s⁻¹ with a mean refrigerant temperature of 40 °C at a constant pressure. The pressure drop tests have been performed at mass velocities of 200, 400 and 600 kg m⁻²s⁻¹ in adiabatic conditions for vapor quality ranging from 0.15 to 0.95.

Before conducting the tests, the measuring instruments have been calibrated and the acquisition system have been validated. Preliminary tests have been conducted in the measuring sections in order to ensure the validity of the experimental data: the HTC measuring section have been tested to verify that the heat losses to external environment were negligible; the pressure drop measuring section have been tested with single-phase flow regime in adiabatic conditions in order to verify the absence of obstructions and impurities inside the microchannel.

During the condensation tests, the wall temperatures and the coolant water temperatures are detected using 15 and 13 thermocouples respectively. From the measured water temperatures a profile is obtained and the local heat flux is calculated from the slope of this water temperature profile. Knowing the heat flux, the local heat transfer coefficient can be calculated from the temperature difference between the refrigerant and the wall.

The experimental technique adopted for the pressure drop tests consists in achieving the desired thermodynamic conditions of temperature, pressure and vapor quality at the measuring section inlet. The state of the refrigerant is then maintained constant along the measuring section and the pressure drop is measured by differential pressure transducers.

An accurate uncertainty analysis has been carried out focusing on the uncertainty related to the heat transfer coefficient. For all the tests carried out the expanded overall uncertainty of the HTC remains lower than 13% increasing with the decrease of the mass velocity; the maximum calculated value is 12.5% at the lowest mass velocity of 150 kg m⁻²s⁻¹. The analysis conducted on the pressure drop uncertainties has given low values.

By comparing the HTC of the two pure fluids and the investigated mixtures at the same operative conditions (mass velocity, mean condensing temperature and vapor quality) is evident that the mass transfer resistance negatively affects the HTC. In fact, the ideal mixtures behavior, that would present averaged characteristics with respect to the pure fluids concentrations, is not verified by the experimental data. The experimental HTCs result lower than the ones that the mixture would present in ideal conditions. An higher penalization has been found for mixtures with high temperature glide and differential latent heat. Hence mixture 23/77% shows the highest penalization, achieving HTCs even lower than the pure R1234ze(E) except for low vapor qualities where the two fluids are comparable. Mixture 76/24% shows the lowest penalization achieving HTCs between the two pure fluids at the same operative conditions and getting very close to the ideal behaviour at low vapor qualities.

By comparing the two-phase pressure drop of the investigated mixtures, it has been found that the mixture composition has a lighter influence on the pressure gradient if compared to the mass velocity. A significant variation of the mass velocity leads to a significant variation of the pressure drop as expected. The effect of the mass composition is less significant, in fact passing from mixture 23/77% to mixture 76/24% the pressure drop variation is 22% as maximum value. A greater variation occurs by comparing the pure R1234ze(E) with the investigated mixtures, in fact a small composition variation of the mixture causes a significant variation of the pressure gradient: mixture 23/77% shows a pressure drop decrease around 33.6% with respect to pure R1234ze(E).

The experimental data for condensation tests have been compared with three different theoretical models with the Silver, Bell and Ghaly correction [26] for zeotropic mixtures. Such models show a good HTC prediction and, among them, the model developed by Cavallini et al. [5], which presents an e_{AB} of 7.7%, and the model developed by Shah [16], which presents an e_{AB} of 6.9% have given the best predictions.

The Cavallini et al. model [5] has been taken as a reference for the penalty factor comparison since its e_{AB} is low and it presents the lowest standard deviation ($\sigma = 4.5\%$). This comparison between the investigated mixtures and the two pure fluids R32 and R1234ze(E) has been conducted at the same operative conditions in terms of energy penalizations; the Penalty Factor (PF) has been used as index to rank the pure fluids and the mixtures.

The experimental pressure drop tests have been compared against the theoretical correlation developed by Del Col et al. [8] for two-phase flow of pure fluids inside microchannels. The model gives a very good prediction of the experimental points also with the mixture as operative fluid, in fact the e_{AB} is equal to 3.6% with a σ of 3.7%.

The comparison between the mixtures and the two pure fluids allows to rank the investigated refrigerants using the PF, where R32 showed the best performances and R1234ze(E) the worst ones. The same operative conditions are realized in terms of energy penalization by imposing the same PF at the mean vapor quality $x = 0.5$. It has been found that the heat transfer performances of the investigated mixtures are between the two pure fluids and the increase of R32 mass fraction in the mixture leads to an increase of the HTCs achieving higher mass velocities.

Even if the mass transfer resistance negatively affects the heat transfer coefficient with significant contributes at every mixture composition, adding a small amount of R32 in the mixture brings a significant decrease of the pressure drop with respect to pure R1234ze(E). This leads to a decrease of the mixture Penalty Factor at the same operative conditions in terms of energy penalization during condensation and higher heat transfer performances. Furthermore a small amount of R32 in the mixture can lead to a mixture with low GWP, as is the case for mixture 23/77%, making it suitable to be used in several common refrigerating applications.

References

- [1] Koyama S., Takata N., and Fukuda S. “Drop-in experiments on heat pump cycle using HFO-1234ze(E) and its mixtures with HFC-32”. In: *International Refrigeration and Air Conditioning Conference at Purdue* 2514 (2010), pp. 1–8.
- [2] Granryd Eric et al. *Refrigerating Engineering*. Stockholm Sweden, 2011.
- [3] Cavallini Alberto, Del Col Davide, and Rossetto Luisa. “Heat transfer and pressure drop of natural refrigerants in minichannels (low charge equipment)”. In: *International Journal of Refrigeration* 36 (Nov. 2012), pp. 287–300.
- [4] Matkovič Marko et al. “Experimental Study on Condensation Heat Transfer Inside a Single Circular Minichannel”. In: *International Journal of Heat and Mass Transfer* 52 (Nov. 2009).
- [5] Cavallini Alberto et al. “Condensation in Horizontal Smooth Tubes: A New Heat Transfer Model for Heat Exchangers Design”. In: *Heat Transfer Engineering* 27.8 (2006), pp. 31–38.
- [6] Del Col Davide, Torresin Daniele, and Cavallini Alberto. “Heat Transfer and Pressure Drop during Condensation of the low GWP Refrigerant R1234yf”. In: *International Journal of Refrigeration* 33 (July 2011), pp. 1307–1318.
- [7] Del Col Davide et al. “Condensation Heat Transfer and Pressure Drop in a Single Minichannel with R1234ze(E) and Other Refrigerants”. In: *4th IIR Conference on Thermophysical Properties and Transfer Processes of Refrigerants* (2013).
- [8] Del Col Davide et al. “Experiments and updated model for two phase frictional pressure drop inside minichannels”. In: *International Journal of Heat and Mass Transfer* 67 (2013), pp. 326–337.
- [9] Seob Shin Jeong and Hwan Kim Moo. “An Experimental Study of Flow Condensation Heat Transfer Inside Circular and Rectangular Mini-Channels”. In: *heat transfer engineering* 26 (2005), pp. 36–44.
- [10] Cavallini Alberto and Zecchin Roberto. “A Dimensionless Correlation for Heat Transfer in Forced Convection Condensation”. In: *5th International Heat Transfer Conference* 2 (1974), pp. 309–313.
- [11] Moser K.W., Webb Ralph L., and B.Na. “A New Equivalent Reynolds Number Model for Condensation in Smooth Tubes”. In: *Journal of Heat Transfer* 120 (May 1998), pp. 410–417.
- [12] Dobson M. K. and Chato J. C. “Condensation in Smooth Horizontal Tubes”. In: *ASME Journal of Heat Transfer* 120 (1998), pp. 193–213.

- [13] Kim Sung-Min and Mudawar Issam. “Universal Approach to Predicting Heat Transfer Coefficient for Condensing mini/micro-channel Flow”. In: *International Journal of Heat and Mass Transfer* 56 (2013), pp. 238–250.
- [14] Fronk Brian M. and Garimella Srinivas. “In-tube Condensation of Zeotropic Fluid Mixtures: a review”. In: *International Journal of Refrigeration* 36 (2013), pp. 534–561.
- [15] Smit F. J., Thome J. R., and Meyer J.P. “Heat Transfer Coefficients During Condensation of the Zeotropic Mixture HCFC-22/HCFC-142b”. In: *Journal of Heat Transfer* 124 (Dec. 2002), pp. 1137–1146.
- [16] Shah M. Mohammed. “An Improved and Extended General Correlation for Heat Transfer During Condensation in Plain Tubes”. In: *HVAC&R Research* 15.5 (Sept. 2009), pp. 889–913.
- [17] Miyara A. et al. “Thermal Conductivity of Saturated Liquid of HFO-1234ze(E) and HFO-1234ze(E)+HFC-R32 mixture”. In: *23rd IIR International Congress of Refrigeration* (Aug. 2011).
- [18] Bortolin Stefano and Del Col Davide. *Flow Boiling of a New Low-GWP Refrigerant Inside a Single Square Cross Section Microchannel*. 32nd UIT Heat Transfer Conference. Pisa: Dipartimento di Ingegneria Industriale - Università degli Studi di Padova, 2014.
- [19] NIST National Institute of Standard Technology, ed. *Refprop Version 9.1*. Applied Chemicals and Materials Division, Boulder Colorado, 2013.
- [20] Akasaka Ryo. “Thermodynamic property models for the difluoromethane (R32) +trans-1,3,3,3-tetrafluoropropene (R1234ze(E)) and difluoromethane +2,3,3,3-tetrafluoropropene (R1234yf) mixtures”. In: *Fluid Phase Equilibria* 358 (July 2013), pp. 98–104.
- [21] Churchill Stuart W. “Friction-factor equation spans all fluid-flow regimes”. In: *Chemical Engineering* (July 1977), pp. 91–92.
- [22] Cavallini Alberto et al. “Analysis and prediction of condensation heat transfer of the zeotropic mixture R-125/236ea”. In: *IMECE’00* (2000), pp. 1–8.
- [23] Kondou Chieko et al. “Flow boiling of non-azeotropic mixture R32/R1234ze(E) in a horizontal microfin tubes”. In: *International Journal of refrigeration* (2013), pp. 1–13.
- [24] Matkovič Marko. “Experimental Study on Condensation Inside a Single Circular Minichannel”. Mechanical Engineering PhD Thesis. Università degli Studi di Padova, 2008. Chap. 5, pp. 149–151.
- [25] Del Col Davide et al. “Effect of cross section al shape during condensation in a single square minichannel”. In: *International Journal of Heat and Mass Transfer* 54 (May 2011), pp. 3909–3920.
- [26] Del Col Davide, Cavallini Alberto, and Thome John R. “Condensation of Zeotropic Mixtures in Horizontal Tubes: New Simplified Heat Transfer Model Based on Flow Regimes”. In: *Journal of Heat Transfer* 127 (Mar. 2005), pp. 221–230.

- [27] Akers W.W., Deans H.A., and Crosser O.K. “Condensing Heat Transfer Within Horizontal Tubes”. In: *Chemical Engineering Progress Symposium Series* 55.29 (1959), pp. 171–176.
- [28] Zhang Ming and Webb Ralph L. “Correlation of Two-Phase Friction for Refrigerants in Small-Diameter Tubes”. In: *Experimental Thermal and Fluid Science* 25 (June 2001), pp. 131–139.
- [29] Cavallini Alberto, Matkovič Marko, and Rossetto Luisa. “Frictional pressure drop during vapor-liquid flow in minichannels: modelling and experimental evaluation”. In: *International Journal Heat Fluid Flow* 30 (2009), pp. 131–139.
- [30] Cavallini Alberto et al. “Pressure drop during two-phase flow of R134a and R32 in a single minichannel”. In: *Journal Heat Transfer ASME* 131 (2009).
- [31] Cavallini Alberto et al. “In-tube condensation performance of refrigerants considering penalization terms (exergy losses) for heat transfer and pressure drop”. In: *International Journal of Heat and Mass Transfer* 53 (2010), pp. 2885–2896.
- [32] MathWorks Inc., ed. *Matlab R2009b*. 2009.

Thanks

I would like to express my warmest thanks to my parents. Their support has never failed in these years of study and thanks to them I always had all the means to achieve this important goal. I couldn't have asked for a better father and mother. Many thanks to Miriam for her precious help in writing this thesis and for all her tips on the English language during my University career. I thank my family, who spent time and energy to help me, as well as those who want to share my happiness with this degree.

My heartfelt thanks to Professor Davide De Col for giving me the wonderful opportunity of working on this thesis, joined by his collaborators. In the laboratory I found the same complicity and esteem that there was between the University benches, as well as a stimulating and professional environment.

Particular thanks are due to Engineer Marco Azzolin and Engineer Stefano Bortolin, who followed me day after day during the development of this work. They answered all my nagging questions with infinite patience and above all, they treated me as their equal and not as a substitute for any.

My thanks also go to the four crazy guys in my band with whom I have lived some of the most beautiful experiences in my life. I still share with them my biggest passion and even if combining music and University has not been always easy, their understanding was an important base during these years.

Sincere thanks to Enrico, Riccardo, Lorenzo and Helene, friends rather than classmates, with whom I shared endless hours of teaching and study, notes, texts, sleepy afternoons after heavy meals in the cafeteria, gallons of coffee as well as countless "spritizes" before and after my exams. Many thanks also to Michele and Niccoló for the invaluable help with L^AT_EX.

Thanks to all my old and new friends, with no exceptions. Thanks for all the stupid things and for making me feel your friend in my turn.

Let me conclude by expressing my thanks to all those who today are happy for me and with me.

17th July 2014

Appendix A

Reduction codes

This section provides the program codes which were implemented to operate the data reduction: the codes reported are in Matlab[®] [32] language. All the programs developed for the reduction can implement the Silver, Bell and Ghaly correction [26] to take into account the mass transfer resistance that characterizes the zeotropic mixtures studied in this work.

The listed programs include the main reduction program and the functions required for the reduction: the theoretical models functions and the function developed for uncertainty calculation.

To run all the programs correctly a Matlab[®] path connecting to the Refprop database is required, the instructions for the path creation are available on the website:

http://www.boulder.nist.gov/div838/theory/refprop/Frequently_asked_questions.htm

The modified equation of state, manually inserted into the *Refprop* \fluids directory as described in section 3.3, is here reported again:

?R32/R1234ze	(R32/R1234ze)						
?Kunz and Wagner (2007)	manually inserted						
75-10-5/29118-24-9	KW2	1.00343	0.977857	1.00586	0.982707	-0.265419	0.
	TC1	0.	0.	0.	0.	0.	0.
	VC1	0.	0.	0.	0.	0.	0.
!							

Finally, to read the experimental values and store the processed values, Excel[®] must be installed.

A.1 Program for HTC data reduction

```

% -----
% DATA REDUCTION PROGRAM for TWO PHASE FLOW CONDENSATION of
% R32 and R1234ze(E) BINARY ZEOTROPIC MIXTURES
% -----

clear
clc

format long
warning('off', 'all');

disp ' '
disp 'DATA REDUCTION PROGRAM FOR TWO-PHASE CONDENSATION TESTS'
disp 'RAN WITH R32 AND R1234ze(E) ZEOTROPIC MIXTURES'
disp ' '
disp '-----WARNING-----'
disp 'The excel file with mixture data must be saved in the same '
disp 'program folder as: "R32%mass_ratio_"R1234ze%mass_ratio" '
disp 'and worksheets must be named as "G###" where "###" is the '
disp 'mass velocity value in kg m-2 s-1 '
disp '-----'

%% ----- DATA READING

extension = ('.xlsx');
G = ('G');
US = ('_');

mixture = menu('Choose the R32-R1234ze(E) mixture concentrations',...
    '23%-77%', '46%-54%', '76%-24%');
if mixture == 1
    mf_R32 = 23;
    co_Q_ms = ('B5');
    co_HTC_corr = ('C5');
    co_HTC_Cavallini = ('D5');
    co_HTC_Moser = ('E5');
    co_HTC_Shah = ('F5');
    co_PF = ('X5');
    co_U_M = ('Y5');
    co_u_m_water = ('AE5');
    co_u_g = ('AA5');
    co_u_P = ('AD5');
    co_u_t_sat = ('AB5');
    co_u_t_wall = ('AC5');
    co_cont_m_w = ('AG5');
    co_cont_g = ('AH5');
    co_cont_t_sat = ('AI5');
    co_cont_t_wall = ('AJ5');
    co_cont_P = ('AK5');
    co_lint_03_exp = ('C17');
    co_lint_05_exp = ('C18');
    co_lint_06_exp = ('C19');
    co_lint_07_exp = ('C20');
    co_lint_03_Cav = ('D17');
    co_lint_05_Cav = ('D18');
    co_lint_06_Cav = ('D19');
    co_lint_07_Cav = ('D20');
    co_G_PF5 = ('A10');
    co_PF_G_PF5 = ('C5');
    co_HTC_PF5 = ('D5');
    co_U_Q = ('AA5');
    co_U_Q_G400 = ('AM5');

```

```
elseif mixture == 2
    mf_R32 = 46;
    co_Q_ms = ('B25');
    co_HTC_corr = ('C25');
    co_HTC_Cavallini = ('D25');
    co_HTC_Moser = ('E25');
    co_HTC_Shah = ('F25');
    co_PF = ('X25');
    co_U_M = ('Y25');
    co_u_m_water = ('AE25');
    co_u_g = ('AA25');
    co_u_P = ('AD25');
    co_u_t_sat = ('AB25');
    co_u_t_wall = ('AC25');
    co_cont_m_w = ('AG25');
    co_cont_g = ('AH25');
    co_cont_t_sat = ('AI25');
    co_cont_t_wall = ('AJ25');
    co_cont_P = ('AK25');
    co_lint_03_exp = ('C37');
    co_lint_05_exp = ('C38');
    co_lint_06_exp = ('C39');
    co_lint_07_exp = ('C40');
    co_lint_03_Cav = ('D37');
    co_lint_05_Cav = ('D38');
    co_lint_06_Cav = ('D39');
    co_lint_07_Cav = ('D40');
    co_G_PF5 = ('A30');
    co_PF_G_PF5 = ('C25');
    co_HTC_PF5 = ('D25');
    co_U_Q = ('AA25');
    co_U_Q_G400 = ('AM25');

elseif mixture == 3
    mf_R32 = 76;
    co_Q_ms = ('B45');
    co_HTC_corr = ('C45');
    co_HTC_Cavallini = ('D45');
    co_HTC_Moser = ('E45');
    co_HTC_Shah = ('F45');
    co_PF = ('X45');
    co_U_M = ('Y45');
    co_u_m_water = ('AE45');
    co_u_g = ('AA45');
    co_u_P = ('AD45');
    co_u_t_sat = ('AB45');
    co_u_t_wall = ('AC45');
    co_cont_m_w = ('AG45');
    co_cont_g = ('AH45');
    co_cont_t_sat = ('AI45');
    co_cont_t_wall = ('AJ45');
    co_cont_P = ('AK45');
    co_lint_03_exp = ('C57');
    co_lint_05_exp = ('C58');
    co_lint_06_exp = ('C59');
    co_lint_07_exp = ('C60');
    co_lint_03_Cav = ('D57');
    co_lint_05_Cav = ('D58');
    co_lint_06_Cav = ('D59');
    co_lint_07_Cav = ('D60');
    co_G_PF5 = ('A50');
    co_PF_G_PF5 = ('C45');
    co_HTC_PF5 = ('D45');
    co_U_Q = ('AA45');
    co_U_Q_G400 = ('AM45');

end
```

```

flow = menu('Choose the specific flow rate [kg/(h·m2)]',...
           '800', '600', '400', '300', '200', '150');
if flow == 1
    G_ref = 800;
elseif flow == 2
    G_ref = 600;
elseif flow == 3
    G_ref = 400;
elseif flow == 4
    G_ref = 300;
elseif flow == 5
    G_ref = 200;
elseif flow == 6
    G_ref = 150;
end

choice_1 = menu('Choose the calculation modality',...
               'THERMODYNAMIC EQUILIBRIUM', 'SAME BULK COMPOSITION');
choice_2 = ...
         menu('Consider the Silver, Bell & Ghaly correction for zeotropic mixtures?',...
             'YES', 'NO');

mf_R1234ze = 100-mf_R32;
mf_R32 = num2str (mf_R32);
mf_R1234ze = num2str (mf_R1234ze);
file = [mf_R32 US mf_R1234ze extension];

sheet = num2str(G_ref);
sheet = [G sheet];

mf_R32 = str2double(mf_R32)/100;
mf_R1234ze = 1-mf_R32;

aux = xlsread (file, sheet, 'B2:BC5');

%% ----- VECTORS DEFINITION

t_water = aux(3,2:16);
z_water = aux(1,2:16);

t_water(5:3:11) = [];
z_water(5:3:11) = [];
t_wall = aux(3,17:27);
z_wall = aux(1,17:27);

%% ----- POLYNOMIAL INTERPOLATIONS

pol_water = polyfit(z_water, t_water, 2);
t_water_pol = polyval(pol_water, z_water);           % [°C]
der_pol_water = polyder(pol_water);
der_t_water = polyval(der_pol_water, z_wall);       % [°C mm-1]
t_water_z_wall = polyval(pol_water, z_wall);        % [°C]

pol_t_wall = polyfit (z_wall, t_wall, 2);
der_t_wall = polyder(pol_t_wall);
der2_t_wall = polyder(der_t_wall);

t_water_mean = mean(t_water);
ess = 0;
tss = 0;

for k=1:length(t_water)
    ess = ess+(t_water_pol(k)-t_water_mean)^2;

```

```

    tss = tss+(t_water(k)-t_water_mean)^2;
end

r2_water = ess/tss;
err = 1-r2_water;

%% ----- CONSTANTS

syms DI_COND I_LG Q_OLD Q_NEW CP_L CP_V GLIDE

p_ips = aux(3,32)+1.01325;          % [bar]
p_ims = aux(3,33)+1.01325;          % [bar]
p_oms = p_ims-(aux(3,34));          % [bar]

t_amb = aux(3,51);                  % [°C]
t_water_ips = aux(3,49);            % [°C]
dt_water_ps = aux(4,40);
t_water_ops = aux(3,49)+aux(3,40); % [°C]
t_ips = aux(3,43);                  % [°C]

d_i = 0.00096;                      % [m]
d_e = 0.0028;                       % [m]
Ra = 1.3*10^(-6);                   % [m]

cp_w = refpropm('C','T',(t_water_ops+t_water_ips)/2+273.15,...
    'P',101.325,'water');            % [J/kgK]
m_ref = aux(3,29)/3600;              % [kg/s]
m_water_ps = aux(3,30)/3600;        % [kg/s]

l_ps = 50;                           % [mm]
l_ms = 227.5;                         % [mm]
lambda_cu = 350;                      % [W m^-1 K^-1]
A_cs = pi*(d_e^2-d_i^2)/4;          % [m^2]

%% ----- DE-SUPERHEATER PARAMETERS

t_mean_water_ps = (t_water_ips+t_water_ops)/2;          % [°C]
q_diss_ps = 0.1611*(t_amb-t_mean_water_ps)-0.0765;      % [W]

q_water_ps = m_water_ps*cp_w*(t_water_ops-t_water_ips)-q_diss_ps; % [W]
h_ips = refpropm('H','T',t_ips+273.15,'P',p_ips*100,...
    'R32','R1234ze',[mf_R32 mf_R1234ze]);              % [J/kg]

%% ----- MEASURING SECTION PARAMETERS

m_water_ms = aux(3,31)/3600;          % [kg/s]
t_mean_water_ms = (aux(3,46)+aux(3,46)+aux(3,38))/2;    % [°C]
q_diss_tot = 0.1772*(t_amb-t_mean_water_ms)+0.1253;     % [W]

z_p_ms = [-23 253.5];                 % [mm]
p_ms = [p_ims p_oms];                 % [bar]
pol_p_ms = polyfit(z_p_ms,p_ms,1);
p_sat_ms = polyval(pol_p_ms,z_wall);  % [bar]

%-----> Measuring section inlet vapor qualities

z_p_ps = [0 81];                      % [mm]
p_ps = [p_ips p_ims];                 % [bar]
pol_p_ps = polyfit(z_p_ps,p_ps,1);

h_dew_ims = refpropm('H','P',p_ims*100,'Q',1,...
    'R32','R1234ze',[mf_R32 mf_R1234ze]);              % [J/kg]

q_desurr_ps = m_ref*(h_ips-h_dew_ims); % [W]

```

```

q_tp_ps = q_water_ps - q_desurr_ps;           % [W]
dh_tp_ps = q_tp_ps / m_ref;                  % [J/kg]

z_Q1 = (l_ps * q_tp_ps) / (q_desurr_ps + q_tp_ps); % [mm]
z_Q1 = l_ps - z_Q1;                          % [mm]
p_Q1 = polyval(pol_p_ps, z_Q1);              % [bar]

t_dew_Q1 = refpropm('T', 'P', p_Q1 * 100, 'Q', 1, ...
    'R32', 'R1234ze', [mf_R32 mf_R1234ze]); % [K]
t_bub_Q1 = refpropm('T', 'P', p_Q1 * 100, 'Q', 0, ...
    'R32', 'R1234ze', [mf_R32 mf_R1234ze]); % [K]
glide_Q1 = t_dew_Q1 - t_bub_Q1;             % [K]

[liq vap] = refpropm('X', 'P', p_Q1 * 100, 'Q', 1, ...
    'R32', 'R1234ze', [mf_R32 mf_R1234ze]);
h_liq_Q1 = refpropm('H', 'P', p_Q1 * 100, 'Q', 0, 'R32', 'R1234ze', liq); % [J/kg]
h_vap_Q1 = refpropm('H', 'P', p_Q1 * 100, 'Q', 1, 'R32', 'R1234ze', vap); % [J/kg]
i_lg_Q1 = h_vap_Q1 - h_liq_Q1;             % [J/kg]

cp_l = refpropm('C', 'P', p_Q1 * 100, 'Q', 0, 'R32', 'R1234ze', liq); % [J/kgK]
cp_v = refpropm('C', 'P', p_Q1 * 100, 'Q', 1, 'R32', 'R1234ze', vap); % [J/kgK]

solution = solve(DI_COND - (I_LG * (Q_OLD - Q_NEW) ...
    + (1 - Q_NEW) * CP_L * GLIDE * (Q_OLD - Q_NEW) ...
    + Q_NEW * CP_V * GLIDE * (Q_OLD - Q_NEW)), Q_NEW);

sol = subs(solution ...
    , {DI_COND, I_LG, Q_OLD, CP_L, CP_V, GLIDE} ...
    , {dh_tp_ps, i_lg_Q1, 1, cp_l, cp_v, glide_Q1});

check = sol > 0 & sol < 1;
Q_ims = sol(check);

Q_ims_Koyama = refpropm('Q', 'P', p_ims * 100, 'H', h_ips - q_water_ps / m_ref, ...
    'R32', 'R1234ze', [mf_R32 mf_R1234ze]);

h_ims = refpropm('H', 'P', p_ims * 100, 'Q', Q_ims_Koyama, ...
    'R32', 'R1234ze', [mf_R32 mf_R1234ze]);

%-----> First measuring section vapor quality

t_dew_ims = refpropm('T', 'P', p_ims * 100, 'Q', 1, ...
    'R32', 'R1234ze', [mf_R32 mf_R1234ze]); % [J/kg]
t_bub_ims = refpropm('T', 'P', p_ims * 100, 'Q', 0, ...
    'R32', 'R1234ze', [mf_R32 mf_R1234ze]); % [J/kg]
glide_ims = t_dew_ims - t_bub_ims;

[liq vap] = refpropm('X', 'H', h_ims, 'P', p_ims * 100, ...
    'R32', 'R1234ze', [mf_R32 mf_R1234ze]);
cp_l = refpropm('C', 'P', p_ims * 100, 'Q', 0, 'R32', 'R1234ze', liq); % [J/kgK]
cp_v = refpropm('C', 'P', p_ims * 100, 'Q', 1, 'R32', 'R1234ze', vap); % [J/kgK]
h_liq = refpropm('H', 'P', p_ims * 100, 'Q', 0, 'R32', 'R1234ze', liq); % [J/kg]
h_vap = refpropm('H', 'P', p_ims * 100, 'Q', 1, 'R32', 'R1234ze', vap); % [J/kg]
i_lg_ims = h_vap - h_liq; % [J/kg]

t_water_ms = polyval(pol_water, z_wall); % [°C]
t_water_oms = polyval(pol_water, 3.75); % [°C]
cp_w = refpropm('C', 'T', (t_water_oms + t_water_ms(1)) / 2 + 273.15, ...
    'P', 101.325, 'water'); % [J/kgK]

sol = subs(solution, {DI_COND, I_LG, Q_OLD, CP_L, CP_V, GLIDE}, ...
    {m_water_ms * cp_w * (t_water_oms - t_water_ms(1)) / m_ref, ...
    i_lg_ims, Q_ims, cp_l, cp_v, glide_ims});

check = sol > 0 & sol < 1;

```



```

Q1_ms = sol(check);

h1_Koyama = h_ips-q_water_ps/m_ref-(m_water_ms/m_ref)*cp_w*...
            (t_water_oms-t_water_ms(1));                % [J/kg]

Q1_ms_Koyama = refpropm('Q','P', polyval(pol_p_ms,11.25)*100,...
            'H',h1_Koyama,'R32','R1234ze',[mf_R32 mf_R1234ze]);

%-----> Vapor qualities and HTCs calculation

t_dew_ms = zeros(size(t_wall));
glide_ms = zeros(size(t_wall));
t_sat_ms = zeros(size(t_wall));
Q_ms = zeros(size(t_wall));
Q_ms(1) = Q1_ms;
t_sat_ms_Koyama = zeros(size(t_wall));
Q_ms_Koyama = zeros(size(t_wall));
Q_ms_Koyama(1) = Q1_ms_Koyama;
h_Koyama = zeros(size(t_wall));
h_Koyama(1) = h1_Koyama;
HTC_Koyama = zeros(size(t_wall));
i_lg = zeros(size(t_wall));
q_ms = zeros(size(t_wall));
HTC = zeros(size(t_wall));
HTC_ASME = zeros(size(t_wall));
delta_t_wall = zeros(size(t_wall));
q_diss_Q = zeros(size(t_wall));
q_diss_ms = zeros(size(t_wall));

rho_liq_ms = zeros(size(t_wall));
rho_vap_ms = zeros(size(t_wall));

t_pipe = [aux(3,53) t_wall aux(3,end)];
z_pipe = [aux(1,53) z_wall aux(1,end)];
q_ax = zeros(size(t_pipe));

for i=1:length(t_pipe)

    if i==length(t_pipe)
        break
    end
    q_ax(i) = lambda_cu*(t_pipe(i)-t_pipe(i+1))*...
            A_cs/((z_pipe(i)-z_pipe(i+1))/1000);
end
q_ax(end) = [];

delta_q_ax = zeros(size(q_ax));

for j=1:length(q_ax)

    if j==length(q_ax)
        break
    end
    delta_q_ax(j) = q_ax(j)-q_ax(j+1);
end
delta_q_ax(end) = [];

for k=1:length(t_wall)

    cp_w = refpropm('C','T',t_water_ms(k)+273.15,'P',101.325,'water'); % [J/kgK]
    t_sat_ms_Koyama(k) = refpropm('T','P',p_sat_ms(k)*100,'H',h_Koyama(k),...
            'R32','R1234ze',[mf_R32 mf_R1234ze])-273.15;

    t_dew_ms(k) = refpropm('T','P',p_sat_ms(k)*100,'Q',1,...
            'R32','R1234ze',[mf_R32 mf_R1234ze]);                % [K]

```

```

t_bubble = refpropm('T','P',p_sat_ms(k)*100,'Q',0,...           % [K]
    'R32','R1234ze',[mf_R32 mf_R1234ze]);
glide_ms(k) = t_dew_ms(k)-t_bubble;                               % [K]

t_sat_ms(k) = t_dew_ms(k)-(glide_ms(k)*(1-Q_ms(k)));             % [K]

[liq vap] = refpropm('X','T',t_sat_ms(k),'P',p_sat_ms(k)*100,...
    'R32','R1234ze',[mf_R32 mf_R1234ze]);
cp_l = refpropm('C','P',p_sat_ms(k)*100,'Q',0,'R32','R1234ze',liq); % [J/kgK]
cp_v = refpropm('C','P',p_sat_ms(k)*100,'Q',1,'R32','R1234ze',vap); % [J/kgK]
rho_liq_ms(k) = refpropm('D','T',t_sat_ms(k),'Q',0,'R32','R1234ze',liq);
rho_vap_ms(k) = refpropm('D','T',t_sat_ms(k),'Q',1,'R32','R1234ze',vap);

h_liq = refpropm('H','T',t_sat_ms(k),'Q',0,'R32','R1234ze',liq); % [J/kg]
h_vap = refpropm('H','T',t_sat_ms(k),'Q',1,'R32','R1234ze',vap); % [J/kg]
i_lg(k) = h_vap-h_liq;                                           % [J/kg]

t_sat_ms(k) = t_sat_ms(k)-273.15;                                 % [°C]
q_ms(k) = -m_water_ms*cp_w*der_t_water(k)*1000;                 % [W m^-1]
HTC(k) = q_ms(k)/(pi*d_i*(t_sat_ms(k)-t_wall(k)));                % [W m^-2 K^-1]

delta_t_wall(k) = (q_ms(k)/pi)*log((d_i/2+0.0005)/(d_i/2))/(2*lambda_cu);
q_diss_ms(k) = q_diss_tot*(t_water_z_wall(k)-t_amb)/((1/3)...
    *pol_water(1)*z_wall(k)^3+0.5*pol_water(2)*z_wall(k)^2+pol_water(3)...
    *z_wall(k)-t_amb*z_wall(k));                                  % [W m^-1]

HTC_ASME(k) = (q_ms(k)+2*lambda_cu*A_cs*der2_t_wall+q_diss_ms(k))...
    /(pi*d_i*(t_sat_ms(k)-(t_wall(k)+delta_t_wall(k))));         % [W/(m^2K)]

HTC_Koyama(k) = (q_ms(k)+2*lambda_cu*A_cs*der2_t_wall+q_diss_ms(k))...
    /(pi*d_i*(t_sat_ms_Koyama(k)-(t_wall(k)+delta_t_wall(k)))); % [W/(m^2K)]

if k==length(t_wall)
    break
end

h_Koyama(k+1) = h_Koyama(k)-(1/m_ref)*(m_water_ms*cp_w*(t_water_ms(k)-...
    t_water_ms(k+1))+(delta_q_ax(k)*(z_wall(k+1)-z_wall(k))/1000)-...
    (q_diss_tot/11));                                             % [J kg^-1]

Q_ms_Koyama(k+1) = refpropm('Q','P',p_sat_ms(k+1)*100,'H',h_Koyama(k+1),...
    'R32','R1234ze',[mf_R32 mf_R1234ze]);

sol = subs(solution,{DI_COND,I_LG,Q_OLD,CP_L,CP_V,GLIDE},...
    {(m_water_ms*cp_w*(t_water_ms(k)-t_water_ms(k+1))+...
    delta_q_ax(k)-(q_diss_tot/11))/m_ref,...
    i_lg(k),Q_ms(k),cp_l,cp_v,glide_ms(k)});

check = sol > 0 & sol < 1;
Q_ms(k+1) = sol(check);

end

%% ----- HEAT TRANSFER COEFFICIENT MODELS CALLS

% Cavallini 2006
HTC_Cav = HTC_Cavallini(p_sat_ms,t_sat_ms_Koyama,t_wall,Q_ms_Koyama,...
    glide_ms,'R32','R1234ze',mf_R32,mf_R1234ze,...
    G_ref,d_i,choice_1,choice_2); % [W m^-2 K^-1]

% Moser 1998
HTC_Moser = HTC_Moser(p_sat_ms,t_sat_ms_Koyama,Q_ms_Koyama,glide_ms,...
    'R32','R1234ze',mf_R32,mf_R1234ze,...
    G_ref,d_i,choice_1,choice_2); % [W m^-2 K^-1]

% Shah 2009
HTC_Shah = HTC_Shah(p_sat_ms,t_sat_ms_Koyama,Q_ms_Koyama,glide_ms,...

```

```

'R32','R1234ze',mf_R32,mf_R1234ze,...
G_ref,d_i,choice_1,choice_2); % [W m^-2 K^-1]

%% ----- PRESSURE DROP MODEL CALL

% Cavallini 2009
dp_dz_Cavallini = PD_Cavallini(p_sat_ms,Q_ms_Koyama,'R32','R1234ze',...
mf_R32,mf_R1234ze,G_ref,d_i,Ra,choice_1); % [Pa m^-1]

%% ----- PENALTY FACTOR

t_pure = [40 40 40 40 40 40 40 40 40];
t_wall_pure = [30 30 30 30 30 30 30 30 30];
Q_pure = [0.1 0.2 0.3 0.4 0.5 0.6 0.7 0.8 0.9];
glide_pure = zeros(1,9);

%-----> Pure R32

rho_liq_pure = refpropm('D','T',40+273.15,'Q',0,'R32');
rho_vap_pure = refpropm('D','T',40+273.15,'Q',1,'R32');
p_R32 = refpropm('P','T',40+273.15,'Q',0.5,'R32')/100;
p_R32 = [p_R32 p_R32 p_R32 p_R32 p_R32 p_R32 p_R32 p_R32 p_R32];

HTC_R32 = HTC_Cavallini(p_R32,t_pure,t_wall_pure,Q_pure,glide_pure,...
'R32','R1234ze',1,0,G_ref,d_i,choice_1,2); % [W m^-2 K^-1]

dp_dz_R32 = PD_Cavallini(p_R32,Q_pure,'R32','R1234ze',...
1,0,G_ref,d_i,Ra,choice_1);

PF_R32 = (G_ref*d_i*(t_pure+273.15)/(4*HTC_R32)).*...
(1/rho_liq_pure-1/rho_vap_pure).*(-dp_dz_R32); % [K^2]

% mass velocity at PF = 5 K^2 for Q = 0.5 and T_sat = 40°C

G_PF5_R32 = 1500;
toll = 1;
cont = 1;
PF_toll = 10;

while toll > 0.001
    if cont~=1
        if PF_toll>5
            G_PF5_R32 = G_PF5_R32-(G_PF5_R32/cont);
        else
            G_PF5_R32 = G_PF5_R32+(G_PF5_R32/cont);
        end
        cont = 1;
    end

    HTC_toll = HTC_Cavallini(p_R32,t_pure,t_wall_pure,Q_pure,glide_pure,...
'R32','R1234ze',1,0,G_PF5_R32,d_i,choice_1,2); % [W m^-2 K^-1]

    dp_dz_toll = PD_Cavallini(p_R32,Q_pure,'R32','R1234ze',...
1,0,G_PF5_R32,d_i,Ra,choice_1);

    PF_toll = (G_PF5_R32*d_i*(t_pure(5)+273.15)/(4*HTC_toll(5)).*...
(1/rho_liq_pure-1/rho_vap_pure).*(-dp_dz_toll(5)));

    toll = abs(5-PF_toll);
    cont = cont+1;
end

PF_R32_G_PF5 = (G_PF5_R32*d_i*(t_pure+273.15)/(4*HTC_toll)).*...
(1/rho_liq_pure-1/rho_vap_pure).*(-dp_dz_toll); % [K^2]

HTC_PF5_R32 = HTC_Cavallini(p_R32,t_pure,t_wall_pure,Q_pure,glide_pure,...

```

```

'R32','R1234ze',1,0,G_Pf5_R32,d_i,choice_1,2); % [W m^-2 K^-1]

%-----> Pure R1234ze(E)
rho_liq_pure = refpropm('D','T',40+273.15,'Q',0,'R1234ze');
rho_vap_pure = refpropm('D','T',40+273.15,'Q',1,'R1234ze');
p_R1234ze = refpropm('P','T',40+273.15,'Q',0.5,'R1234ze')/100;
p_R1234ze = [p_R1234ze p_R1234ze p_R1234ze p_R1234ze p_R1234ze p_R1234ze...
p_R1234ze p_R1234ze p_R1234ze];

HTC_R1234ze = HTC_Cavallini(p_R1234ze,t_pure,t_wall_pure,Q_pure,glide_pure,...
'R1234ze','R32',1,0,G_ref,d_i,choice_1,2); % [W m^-2 K^-1]

dp_dz_R1234ze = PD_Cavallini(p_R1234ze,Q_pure,'R1234ze','R32',...
1,0,G_ref,d_i,Ra,choice_1);

PF_R1234ze = (G_ref*d_i*(t_pure+273.15)./(4*HTC_R1234ze)).*...
(1/rho_liq_pure-1/rho_vap_pure).*(-dp_dz_R1234ze); % [K^2]

% mass velocity at PF = 5 K^2 for Q = 0.5 and T_sat = 40rC
G_Pf5_R1234ze = 500;
toll = 1;
cont = 1;
PF_toll = 10;

while toll > 0.001
    if cont~=1
        if PF_toll>5
            G_Pf5_R1234ze = G_Pf5_R1234ze-(G_Pf5_R1234ze/cont);
        else
            G_Pf5_R1234ze = G_Pf5_R1234ze+(G_Pf5_R1234ze/cont);
        end
    end
    end

    HTC_toll = HTC_Cavallini(p_R1234ze,t_pure,t_wall_pure,Q_pure,glide_pure,...
'R1234ze','R32',1,0,G_Pf5_R1234ze,d_i,choice_1,2); % [W m^-2 K^-1]

    dp_dz_toll = PD_Cavallini(p_R1234ze,Q_pure,'R1234ze','R32',...
1,0,G_Pf5_R1234ze,d_i,Ra,choice_1);

    PF_toll = (G_Pf5_R1234ze*d_i*(t_pure(5)+273.15)./(4*HTC_toll(5))).*...
(1/rho_liq_pure-1/rho_vap_pure).*(-dp_dz_toll(5));

    toll = abs(5-PF_toll);
    cont = cont+1;
end

PF_R1234ze_G_Pf5 = (G_Pf5_R1234ze*d_i*(t_pure+273.15)./(4*HTC_toll)).*...
(1/rho_liq_pure-1/rho_vap_pure).*(-dp_dz_toll); % [K^2]

HTC_Pf5_R1234ze = HTC_Cavallini(p_R1234ze,t_pure,t_wall_pure,Q_pure,glide_pure,...
'R1234ze','R32',1,0,G_Pf5_R1234ze,d_i,choice_1,2); % [W m^-2 K^-1]

%-----> Mixtures
p_mix = refpropm('P','T',40+273.15,'Q',0.5,...
'R32','R1234ze',[mf_R32 mf_R1234ze])/100;
T_dew = refpropm('T','P',p_mix*100,'Q',1,...
'R32','R1234ze',[mf_R32 mf_R1234ze]);
T_bub = refpropm('T','P',p_mix*100,'Q',0,...
'R32','R1234ze',[mf_R32 mf_R1234ze]);
rho_liq_PF = refpropm('D','P',p_mix*100,'Q',0,...

```

```

'R32','R1234ze',[mf_R32 mf_R1234ze]);
rho_vap_PF = refpropm('D','P',p_mix*100,'Q',1,...
'R32','R1234ze',[mf_R32 mf_R1234ze]);

t_mix_PF = zeros(size(Q_pure));
t_wall_PF = zeros(size(Q_pure));

for i = 1:length(Q_pure)
    t_mix_PF(i) = refpropm('T','P',p_mix*100,'Q',Q_pure(i),...
'R32','R1234ze',[mf_R32 mf_R1234ze])-273.15;
    t_wall_PF(i) = t_mix_PF(i)-10;
end
glide_mix = T_dew-T_bub;
glide_mix = [glide_mix glide_mix glide_mix glide_mix glide_mix...
    glide_mix glide_mix glide_mix glide_mix ];
p_mix = [p_mix p_mix p_mix p_mix p_mix p_mix p_mix p_mix p_mix];

HTC_PF = HTC_Cavallini(p_mix,t_mix_PF,t_wall_PF,Q_pure,...
    glide_mix,'R32','R1234ze',mf_R32,mf_R1234ze,...
    G_ref,d_i,choice_1,choice_2); % [W m^-2 K^-1]

dp_dz_PF = PD_Cavallini(p_mix,Q_pure,'R32','R1234ze',...
    mf_R32,mf_R1234ze,G_ref,d_i,Ra,choice_1);

PF_th = (G_ref*d_i*(t_mix_PF+273.15)./(4*HTC_PF)).*...
    (1./rho_liq_PF-1./rho_vap_PF).*(-dp_dz_PF); % [K^2]

% mass velocity at PF = 5 K^2 for Q = 0.5 and T_sat = 40°C

G_PF5 = 1000;
toll = 1;
cont = 1;
PF_toll = 10;

while toll > 0.001
    if cont~=1
        if PF_toll>5
            G_PF5 = G_PF5-(G_PF5/cont);
        else
            G_PF5 = G_PF5+(G_PF5/cont);
        end
    end
    HTC_toll = HTC_Cavallini(p_mix,t_mix_PF,t_wall_PF,Q_pure,glide_mix,...
'R32','R1234ze',mf_R32,mf_R1234ze,G_PF5,d_i,choice_1,2); % [W m^-2 K^-1]

    dp_dz_toll = PD_Cavallini(p_mix,Q_pure,'R32','R1234ze',...
mf_R32,mf_R1234ze,G_PF5,d_i,Ra,choice_1);

    PF_toll = (G_PF5*d_i*(t_mix_PF(5)+273.15)./(4*HTC_toll(5))).*...
    (1./rho_liq_PF-1./rho_vap_PF).*(-dp_dz_toll(5));

    toll = abs(5-PF_toll);
    cont = cont+1;
end

PF_G_PF5 = (G_PF5*d_i*(t_mix_PF+273.15)./(4*HTC_toll)).*...
    (1./rho_liq_PF-1./rho_vap_PF).*(-dp_dz_toll); % [K^2]

HTC_PF5 = HTC_Cavallini(p_mix,t_mix_PF,t_wall_PF,Q_pure,glide_mix,...
'R32','R1234ze',mf_R32,mf_R1234ze,G_PF5,d_i,choice_1,2); % [W m^-2 K^-1]

%% ----- UNCERTAINTY CALL

std_m_water = aux(4,31)/3600; % [kg s^-1]

```

```

std_m_water_ps = aux(4,30)/3600;    % [kg s-1]
std_m_ref = aux(4,29)/3600;       % [kg s-1]
std_t_water_ips = aux(4,49);      % [°C]
std_t_water_ops = aux(4,50);      % [°C]
std_dt_water_ps = aux(4,40);

std_t_water = aux(4,2:16);        % [°C]
std_t_water(5:3:11) = [];
std_t_wall = aux(4,17:27);       % [°C]
std_p_ims = aux(4,33);           % [bar]
dp = aux(3,34);                  % [bar]
std_dp = aux(4,34);              % [bar]

[u_HTC,U_HTC_M,u_m_water,u_g,u_P,u_t_sat,u_t_wall,cont_m_w,cont_g,cont_t_sat,...
 cont_t_wall,cont_P,U_Q_ms] = HTC_Uncertainty(m_water_ms,t_water,std_m_water,...
 std_t_water,t_wall,std_t_wall,t_sat_ms_Koyama,z_water,z_wall,p_ims,...
 std_p_ims,dp,std_dp,d_i,h_Koyama(1),h_Koyama(end),...
 m_water_ps,std_m_water_ps,m_ref,std_m_ref,t_water_ips,...
 dt_water_ps,std_dt_water_ps,z_p_ms,p_sat_ms,h_Koyama,...
 t_water_ms,mf_R32,mf_R1234ze);

%% ----- RESULTS WRITING

disp '#####|'
disp '#####|'
disp '#####|'
disp '#####V'
disp '#####REDUCTION PERFORMED'

file = ('HTC_mixtures.xlsx');

statusQ_ms = xlswrite(file,Q_ms_Koyama',sheet,co_Q_ms);
statusHTC_corr = xlswrite(file,HTC_Koyama',sheet,co_HTC_corr);
statusHTC_Cavallini = xlswrite(file,HTC_Cav',sheet,co_HTC_Cavallini);
statusHTC_Moser = xlswrite(file,HTC_Moser',sheet,co_HTC_Moser);
statusHTC_Shah = xlswrite(file,HTC_Shah',sheet,co_HTC_Shah);

statusPF = xlswrite(file,PF_th',sheet,co_PF);
statusU_M = xlswrite(file,U_HTC_M',sheet,co_U_M);
if G_ref == 400
    statusU_Q = xlswrite(file,U_Q_ms',sheet,co_U_Q_G400);
else
    statusU_Q = xlswrite(file,U_Q_ms',sheet,co_U_Q);
end

statusG_PF5_R32 = xlswrite(file,G_PF5_R32,'PureFluids','B103');
statusPF_R32_G_PF5 = xlswrite(file,PF_R32_G_PF5', 'PureFluids','C103');
statusG_PF5_R1234ze = xlswrite(file,G_PF5_R1234ze,'PureFluids','K103');
statusPF_R1234ze_G_PF5 = xlswrite(file,PF_R1234ze_G_PF5', 'PureFluids','L103');
statusHTC_PF5_R32 = xlswrite(file,HTC_PF5_R32', 'PureFluids','D103');
statusHTC_PF5_R1234ze = xlswrite(file,HTC_PF5_R1234ze', 'PureFluids','M103');

statusG_PF5 = xlswrite(file,G_PF5,'PenaltyFactor',co_G_PF5);
statusPF_G_PF5 = xlswrite(file,PF_G_PF5', 'PenaltyFactor',co_PF_G_PF5);
statusHTC_PF5 = xlswrite(file,HTC_PF5', 'PenaltyFactor',co_HTC_PF5);

switch G_ref
case {800,400,200}
    HTC_lint_03_exp = 0;
    HTC_lint_03_Cav = 0;

```

```

HTC_lint_05_exp = 0;
HTC_lint_05_Cav = 0;
HTC_lint_06_exp = 0;
HTC_lint_06_Cav = 0;
HTC_lint_07_exp = 0;
HTC_lint_07_Cav = 0;

for i=1:(length(Q_ms_Koyama)-1)
    if Q_ms_Koyama(i) > 0.7 && Q_ms_Koyama(i+1) < 0.7
        HTC_lint_07_exp = HTC_Koyama(i+1)+(0.7-Q_ms_Koyama(i+1))*...
            (HTC_Koyama(i)-HTC_Koyama(i+1))/(Q_ms_Koyama(i)-Q_ms_Koyama(i+1));
        HTC_lint_07_Cav = HTC_Cav(i+1)+(0.7-Q_ms_Koyama(i+1))*...
            (HTC_Cav(i)-HTC_Cav(i+1))/(Q_ms_Koyama(i)-Q_ms_Koyama(i+1));
    end
    if Q_ms_Koyama(i) > 0.6 && Q_ms_Koyama(i+1) < 0.6
        HTC_lint_06_exp = HTC_Koyama(i+1)+(0.6-Q_ms_Koyama(i+1))*...
            (HTC_Koyama(i)-HTC_Koyama(i+1))/(Q_ms_Koyama(i)-Q_ms_Koyama(i+1));
        HTC_lint_06_Cav = HTC_Cav(i+1)+(0.6-Q_ms_Koyama(i+1))*...
            (HTC_Cav(i)-HTC_Cav(i+1))/(Q_ms_Koyama(i)-Q_ms_Koyama(i+1));
    end
    if Q_ms_Koyama(i) > 0.5 && Q_ms_Koyama(i+1) < 0.5
        HTC_lint_05_exp = HTC_Koyama(i+1)+(0.5-Q_ms_Koyama(i+1))*...
            (HTC_Koyama(i)-HTC_Koyama(i+1))/(Q_ms_Koyama(i)-Q_ms_Koyama(i+1));
        HTC_lint_05_Cav = HTC_Cav(i+1)+(0.5-Q_ms_Koyama(i+1))*...
            (HTC_Cav(i)-HTC_Cav(i+1))/(Q_ms_Koyama(i)-Q_ms_Koyama(i+1));
    end
    if Q_ms_Koyama(i) > 0.3 && Q_ms_Koyama(i+1) < 0.3
        HTC_lint_03_exp = HTC_Koyama(i+1)+(0.3-Q_ms_Koyama(i+1))*...
            (HTC_Koyama(i)-HTC_Koyama(i+1))/(Q_ms_Koyama(i)-Q_ms_Koyama(i+1));
        HTC_lint_03_Cav = HTC_Cav(i+1)+(0.3-Q_ms_Koyama(i+1))*...
            (HTC_Cav(i)-HTC_Cav(i+1))/(Q_ms_Koyama(i)-Q_ms_Koyama(i+1));
    end
end
statusHTC_lint_03_exp = xlswrite(file,HTC_lint_03_exp,sheet,co_lint_03_exp);
statusHTC_lint_03_Cav = xlswrite(file,HTC_lint_03_Cav,sheet,co_lint_03_Cav);
statusHTC_lint_05_exp = xlswrite(file,HTC_lint_05_exp,sheet,co_lint_05_exp);
statusHTC_lint_05_Cav = xlswrite(file,HTC_lint_05_Cav,sheet,co_lint_05_Cav);
statusHTC_lint_06_exp = xlswrite(file,HTC_lint_06_exp,sheet,co_lint_06_exp);
statusHTC_lint_06_Cav = xlswrite(file,HTC_lint_06_Cav,sheet,co_lint_06_Cav);
statusHTC_lint_07_exp = xlswrite(file,HTC_lint_07_exp,sheet,co_lint_07_exp);
statusHTC_lint_07_Cav = xlswrite(file,HTC_lint_07_Cav,sheet,co_lint_07_Cav);

end

if G_ref == 400

    statusu_m_water = xlswrite(file,100*(u_m_water/m_water_ms),sheet,co_u_m_water);
    statusu_g = xlswrite(file,100*abs((u_g/1000)./der_t_water)',sheet,co_u_g);
    statusu_P = xlswrite(file,100*(u_P/(pi*d_i)'),sheet,co_u_P);
    statusu_t_sat = xlswrite(file,100*(u_t_sat./t_sat_ms_Koyama)',sheet,co_u_t_sat);
    statusu_t_wall = xlswrite(file,100*(u_t_wall./t_wall)',sheet,co_u_t_wall);

    statuscont_m_w = xlswrite(file,100*(2*cont_m_w./HTC_Koyama)',sheet,co_cont_m_w);
    statuscont_g = xlswrite(file,100*(2*cont_g./HTC_Koyama)',sheet,co_cont_g);
    statuscont_t_sat = xlswrite(file,100*(2*cont_t_sat./HTC_Koyama)',...
        sheet,co_cont_t_sat);
    statuscont_t_wall = xlswrite(file,100*(2*cont_t_wall./HTC_Koyama)',...
        sheet,co_cont_t_wall);
    statuscont_P = xlswrite(file,100*(2*cont_P./HTC_Koyama)',sheet,co_cont_P);
end

if G_ref == 400 && mixture == 2

    statust_water = xlswrite(file,t_water',sheet,'BA25');
    statust_water_pol = xlswrite(file,t_water_pol',sheet,'BB25');

```

```

statusz_water = xlswrite(file,z_water',sheet,'BC25');
status_t_wall = xlswrite(file,t_wall',sheet,'BD25');
status_t_sat_ms_Koyama = xlswrite(file,t_sat_ms_Koyama',sheet,'BE25');
statusz_wall = xlswrite(file,z_wall',sheet,'BF25');
end

%% ----- RESULTS PLOTTING

pol_t_sat_ms = polyfit(z_wall,t_sat_ms,2);
t_sat_ms_pol = polyval(pol_t_sat_ms,z_wall);    % [°C]

mf_R32 = num2str (mf_R32*100);
mf_R1234ze = num2str (mf_R1234ze*100);
barra = ('/');
chart = ('R32/R1234ze(E)mixture');
chart = [sheet chart mf_R32 barra mf_R1234ze];

subplot(1,3,1)
plot(z_water,t_water,'b.'...
     ,z_water,t_water_pol,'b-'...
     ,z_wall,t_wall,'r.'...
     ,z_wall,t_sat_ms,'go'...
     ,z_wall,t_sat_ms_pol,'g-'...
     ,z_wall,t_sat_ms_Koyama,'m+')
title(chart)
legend('Measured Water',...
      'Polynomial Water',...
      'Measured Wall',...
      'Calculated Saturation (ASME)',...
      'Polynomial Saturation (ASME)',...
      'Calculated Saturation (Koyama)')
xlabel('Axial position [mm]')
ylabel('Temperature [°C]')
grid on

subplot(1,3,2)
plot(Q_ms,HTC_ASME,'oc-'...
     ,Q_ms_Koyama,HTC_Koyama,'or-'...
     ,Q_ms_Koyama,HTC_Cav,'sb-'...
     ,Q_ms_Koyama,HTC_Moser,'.g-'...
     ,Q_ms_Koyama,HTC_Shah,'+m-')
title(chart)
legend('Experimental HTC (ASME)',...
      'Experimental HTC (Koyama)',...
      'Predicted HTC (Cavallini)',...
      'Predicted HTC (Moser)',...
      'Predicted HTC (Shah)',...
      'Predicted HTC (Dobson & Chato)',4)
xlabel('Vapor Quality [\ ]')
xlim([0 1])
ylabel('Heat Transfer Coefficient [W m^{-2} K^{-1}]')
grid on

subplot(1,3,3)
plot(Q_pure,PF_R32,'ob-',Q_pure,PF_R1234ze,'og-',Q_pure,PF_th,'ok-')
title(chart)
legend('R32','R1234ze','Mixture',4)
xlabel('Vapor Quality [\ ]')
xlim([0 1])
ylabel('Penalty Factor [K^2]')
grid on

```


A.2 Program for PD data reduction

```

% -----
% PRESSURE DROP MEASURING SECTION INLET VAPOUR QUALITY CALCULATION
% -----

clear all;
clc;
format long;
warning ('off','all');

%% ----- DATA READING

file = ('PD_mixtures.xlsx');
sheet = ('Elaborated_Mean_Values');
aux = xlsread (file,sheet,'C26:T125');
[m,n] = size(aux);
parts = 30;
choice_1 = menu('Choose the calculation modality',...
    'THERMODYNAMIC_EQUILIBRIUM','SAME_BULK_COMPOSITION');

%% ----- MEASURING SECTION INLET VAPOR QUALITY CALCULATION

t_water_in = zeros(1,m);
t_water_out = zeros(1,m);
t_ips = zeros(1,m);

Q_ims = zeros(1,m);
Q_ims_REFPROP = zeros(1,m);
h_ips = zeros(1,m);
h_dew_ips = zeros(1,m);
h_bub_ips = zeros(1,m);
ilg = zeros(1,m);
h_ims = zeros(1,m);
t_ims = zeros(1,m);
h_oms = zeros(1,m);
t_oms = zeros(1,m);
Q_oms = zeros(1,m);
Q_oms_REFPROP = zeros(1,m);
Q_ps = zeros(1,parts+1);
Q_tot = zeros(1,parts+1);
t_ims_REFPROP = zeros(1,m);
t_oms_REFPROP = zeros(1,m);
final = zeros(1,parts+1);
dp_dz_Cavallini = zeros(1,m);

delta = zeros(1,m);

syms DI_COND DI_VAP I_LG Q_OLD Q_NEW CP_L CP_V GLIDE

D = 0.00096;    % [m]
Ra = 1.3e-6;    % [m]

for k=1:m

    mf_R32 = aux(k,1)/100;
    mf_R1234ze = 1-mf_R32;
    m_ref = aux(k,4)/3600;           % [kg s^-1]
    G = 4*m_ref/(pi*D^2);           % [kg m^-2 s^-1]

    m_water = aux(k,11)/3600;       % [kg s^-1]
    t_water_out(k) = aux(k,12);     % [°C]
    t_water_in(k) = aux(k,12)+aux(k,13); % [°C]
    t_water = t_water_in(k)+aux(k,12)/2; % [°C]

```

```

cp_w = refpropm('C','T',t_water+273.15,...
    'P',101.325,'water'); % [J kg^-1 K^-1]
q_water_ps = m_water*cp_w*(abs(aux(k,13))); % [W]

t_ips(k) = aux(k,6); % [°C]
p_ips = aux(k,5); % [bar]
p_ims = aux(k,7); % [bar]

if aux(k,9) <= 0.01
    p_oms = aux(k,7)-aux(k,10); % [bar]
else
    p_oms = aux(k,7)-aux(k,9); % [bar]
end

%-----> inlet vapor quality

z_p_ps = [0 55]; % [mm]
p_ps = [p_ips p_ims]; % [bar]
pol_p_ps = polyfit(z_p_ps,p_ps,1);

z_p_tot = [0 220]; % [mm]
p_tot = [p_ips p_oms]; % [bar]
pol_p_tot = polyfit(z_p_tot,p_tot,1);

h_ips(k) = refpropm('H','T',t_ips(k)+273.15,'P',p_ips*100,...
    'R32','R1234ze',[mf_R32 mf_R1234ze]); % [J kg^-1]
h_dew_ips(k) = refpropm('H','P',p_ips*100,'Q',1,...
    'R32','R1234ze',[mf_R32 mf_R1234ze]); % [J kg^-1]
h_bub_ips(k) = refpropm('H','P',p_ips*100,'Q',0,...
    'R32','R1234ze',[mf_R32 mf_R1234ze]); % [J kg^-1]
ilg(k) = h_dew_ips(k)-h_bub_ips(k); % [J kg^-1]

if h_ips(k) > h_dew_ips(k)

%----- TEST WITH CONDENSATION INSIDE THE PRE-SECTION

Q_ps(1) = 1;
final(1) = 1;
Q_tot(1) = 1;

%----- KOYAMA -----

h_ims_REFPROP = h_ips(k)-(q_water_ps/m_ref); % [J kg^-1]
Q_ims_REFPROP(k) = refpropm('Q','P',p_ims*100,...
    'H',h_ims_REFPROP,'R32','R1234ze',[mf_R32 mf_R1234ze]); % [J kg^-1]
Q_oms_REFPROP(k) = refpropm('Q','P',p_oms*100,...
    'H',h_ims_REFPROP,'R32','R1234ze',[mf_R32 mf_R1234ze]); % [J kg^-1]
t_ims_REFPROP(k) = refpropm('T','P',p_ims*100,...
    'H',h_ims_REFPROP,'R32','R1234ze',[mf_R32 mf_R1234ze])-273.15; % [°C]
t_oms_REFPROP(k) = refpropm('T','P',p_oms*100,...
    'H',h_ims_REFPROP,'R32','R1234ze',[mf_R32 mf_R1234ze])-273.15; % [°C]

%----- ASME -----

q_desurr = m_ref*(h_ips(k)-h_dew_ips(k)); % [W]
q_cond = q_water_ps-q_desurr; % [W]
q_part = q_cond/parts; % [W]

for i=1:parts

    z = (i)*(z_p_ps(end)/parts);
    p = polyval(pol_p_ps,z);

    t_dew = refpropm('T','P',p*100,'Q',1,...

```

```

    'R32','R1234ze',[mf_R32 mf_R1234ze]);          % [K]
t_bubble = refpropm('T','P',p*100,'Q',0,...
    'R32','R1234ze',[mf_R32 mf_R1234ze]);          % [K]
glide = t_dew-t_bubble;

if i == parts
    glide_ims = glide;
end

if choice_1 == 1

    % ---> equilibrium

    [liq vap] = refpropm('X','P',p*100,'Q',Q_ps(i),...
        'R32','R1234ze',[mf_R32 mf_R1234ze]);
    cp_l = refpropm('C','P',p*100,'Q',0,'R32','R1234ze',liq); % [J kg^-1 K^-1]
    cp_v = refpropm('C','P',p*100,'Q',1,'R32','R1234ze',vap); % [J kg^-1 K^-1]
    h_liq = refpropm('H','P',p*100,'Q',0,'R32','R1234ze',liq); % [J kg^-1]
    h_vap = refpropm('H','P',p*100,'Q',1,'R32','R1234ze',vap); % [J kg^-1]
    i_lg = h_vap-h_liq; % [J/kg]
else

    % ---> same composition

    cp_l = refpropm('C','P',p*100,'Q',0,...
        'R32','R1234ze',[mf_R32 mf_R1234ze]);
    cp_v = refpropm('C','P',p*100,'Q',1,...
        'R32','R1234ze',[mf_R32 mf_R1234ze]);
    h_liq = refpropm('H','P',p*100,'Q',0,...
        'R32','R1234ze',[mf_R32 mf_R1234ze]);
    h_vap = refpropm('H','P',p*100,'Q',1,...
        'R32','R1234ze',[mf_R32 mf_R1234ze]);
    i_lg = h_vap-h_liq;
end

solution = solve(DI_COND-(I_LG*(Q_OLD-Q_NEW)...
    +(1-Q_NEW)*CP_L*GLIDE*(Q_OLD-Q_NEW)...
    +Q_NEW*CP_V*GLIDE*(Q_OLD-Q_NEW)),Q_NEW);

sol = subs(solution...
    ,{DI_COND,I_LG,Q_OLD,CP_L,CP_V,GLIDE}...
    ,{q_part/m_ref,i_lg,Q_ps(i),cp_l,cp_v,glide});

check = sol > 0 & sol < 1;
Q_ps(i+1) = sol(check);

% ---> Outler vapor quality

z = (i)*(z_p_tot(end)/parts);
p = polyval(pol_p_tot,z);

t_dew = refpropm('T','P',p*100,'Q',1,...
    'R32','R1234ze',[mf_R32 mf_R1234ze]);          % [K]
t_bubble = refpropm('T','P',p*100,'Q',0,...
    'R32','R1234ze',[mf_R32 mf_R1234ze]);          % [K]
glide = t_dew-t_bubble;          % [K]

if choice_1 == 1

    % ---> equilibrium

    [liq vap] = refpropm('X','P',p*100,'Q',Q_tot(i),...
        'R32','R1234ze',[mf_R32 mf_R1234ze]);
    cp_l = refpropm('C','P',p*100,'Q',0,'R32','R1234ze',liq); % [J kg^-1 K^-1]
    cp_v = refpropm('C','P',p*100,'Q',1,'R32','R1234ze',vap); % [J kg^-1 K^-1]
    h_liq = refpropm('H','P',p*100,'Q',0,'R32','R1234ze',liq); % [J kg^-1]

```

```

h_vap = refpropm('H','P',p*100,'Q',1,'R32','R1234ze',vap); % [J kg-1]
i_lg = h_vap-h_liq; % [J kg-1]
else

    % ----> same composition

    cp_l = refpropm('C','P',p*100,'Q',0,...
        'R32','R1234ze',[mf_R32 mf_R1234ze]);
    cp_v = refpropm('C','P',p*100,'Q',1,...
        'R32','R1234ze',[mf_R32 mf_R1234ze]);
    h_liq = refpropm('H','P',p*100,'Q',0,...
        'R32','R1234ze',[mf_R32 mf_R1234ze]);
    h_vap = refpropm('H','P',p*100,'Q',1,...
        'R32','R1234ze',[mf_R32 mf_R1234ze]);
    i_lg = h_vap-h_liq;
end

    solution = solve(DI_COND-(I_LG*(Q_OLD-Q_NEW)...
        +(1-Q_NEW)*CP_L*GLIDE*(Q_OLD-Q_NEW)...
        +Q_NEW*CP_V*GLIDE*(Q_OLD-Q_NEW)),Q_NEW);

    sol = subs(solution...
        ,{DI_COND,I_LG,Q_OLD,CP_L,CP_V,GLIDE}...
        ,{q_part/m_ref,i_lg,Q_tot(i),cp_l,cp_v,glide});

    check = sol >0 & sol < 1;
    Q_tot(i+1) = sol(check);

end

else

%----- TEST WITH EVAPORATION INSIDE THE PRE-SECTION

Q_ps(1) = 0;
Q_tot(1) = 0;

    q_boil = m_ref*(h_bub_ips(k)-h_ips(k));
    q_vap = q_water_ps-q_boil;
    q_part = q_vap/parts;

%----- KOYAMA -----

    h_ims_REFPROP = h_ips(k)+(q_water_ps/m_ref); % [J kg-1]
    Q_ims_REFPROP(k) = refpropm('Q','P',p_ims*100,'H',h_ims_REFPROP,...
        'R32','R1234ze',[mf_R32 mf_R1234ze]);
    Q_oms_REFPROP(k) = refpropm('Q','P',p_oms*100,'H',h_ims_REFPROP,...
        'R32','R1234ze',[mf_R32 mf_R1234ze]);
    t_ims_REFPROP(k) = refpropm('T','P',p_ims*100,'H',h_ims_REFPROP,...
        'R32','R1234ze',[mf_R32 mf_R1234ze])-273.15; % [°C]
    t_oms_REFPROP(k) = refpropm('T','P',p_oms*100,'H',h_ims_REFPROP,...
        'R32','R1234ze',[mf_R32 mf_R1234ze])-273.15; % [°C]

%----- ASME -----

for i=1:parts

    z = (i)*(z_p_ps(end)/parts);
    p = polyval(pol_p_ps,z);

    t_dew = refpropm('T','P',p*100,'Q',1,...
        'R32','R1234ze',[mf_R32 mf_R1234ze]); % [°C]
    t_bubble = refpropm('T','P',p*100,'Q',0,...
        'R32','R1234ze',[mf_R32 mf_R1234ze]); % [°C]
    glide = t_dew-t_bubble;

```

```

if i == parts
    glide_ims = glide;
end

if choice_1 == 1

    % ---> equilibrium

    [liq vap] = refpropm('X','P',p*100,'Q',Q_ps(i),...
        'R32','R1234ze',[mf_R32 mf_R1234ze]);
    cp_l = refpropm('C','P',p*100,'Q',0,'R32','R1234ze',liq); % [J kg^-1 K^-1]
    cp_v = refpropm('C','P',p*100,'Q',1,'R32','R1234ze',vap); % [J kg^-1 K^-1]
    h_liq = refpropm('H','P',p*100,'Q',0,'R32','R1234ze',liq); % [J kg^-1]
    h_vap = refpropm('H','P',p*100,'Q',1,'R32','R1234ze',vap); % [J kg^-1]
    i_lg = h_vap-h_liq; % [J kg^-1]
else

    % ---> same composition

    cp_l = refpropm('C','P',p*100,'Q',0,...
        'R32','R1234ze',[mf_R32 mf_R1234ze]);
    cp_v = refpropm('C','P',p*100,'Q',1,...
        'R32','R1234ze',[mf_R32 mf_R1234ze]);
    h_liq = refpropm('H','P',p*100,'Q',0,...
        'R32','R1234ze',[mf_R32 mf_R1234ze]);
    h_vap = refpropm('H','P',p*100,'Q',1,...
        'R32','R1234ze',[mf_R32 mf_R1234ze]);
    i_lg = h_vap-h_liq; % [J kg^-1]
end

solution = solve(DI_VAP-(I_LG*(Q_NEW-Q_OLD)...
    +(1-Q_NEW)*CP_L*GLIDE*(Q_NEW-Q_OLD)...
    +Q_NEW*CP_V*GLIDE*(Q_NEW-Q_OLD)),Q_NEW);

sol = subs(solution...
    ,{DI_VAP,I_LG,Q_OLD,CP_L,CP_V,GLIDE}...
    ,{q_part/m_ref,i_lg,Q_ps(i),cp_l,cp_v,glide});

check = sol > 0 & sol < 1;
Q_ps(i+1) = sol(check);

% ---> Outlet vapor quality

z = (i)*(z_p_tot(end)/parts); % [mm]
p = polyval(pol_p_tot,z); % [bar]

t_dew = refpropm('T','P',p*100,'Q',1,...
    'R32','R1234ze',[mf_R32 mf_R1234ze]); % [K]
t_bubble = refpropm('T','P',p*100,'Q',0,...
    'R32','R1234ze',[mf_R32 mf_R1234ze]); % [K]
glide = t_dew-t_bubble; % [K]

if choice_1 == 1

    % ---> equilibrium

    [liq vap] = refpropm('X','P',p*100,'Q',Q_tot(i),...
        'R32','R1234ze',[mf_R32 mf_R1234ze]);
    cp_l = refpropm('C','P',p*100,'Q',0,'R32','R1234ze',liq); % [J kg^-1 K^-1]
    cp_v = refpropm('C','P',p*100,'Q',1,'R32','R1234ze',vap); % [J kg^-1 K^-1]
    h_liq = refpropm('H','P',p*100,'Q',0,'R32','R1234ze',liq); % [J kg^-1]
    h_vap = refpropm('H','P',p*100,'Q',1,'R32','R1234ze',vap); % [J kg^-1]
    i_lg = h_vap-h_liq; % [J kg^-1]
else

```

```

% ---> same composition

cp_l = refpropm('C','P',p*100,'Q',0,...
'R32','R1234ze',[mf_R32 mf_R1234ze]);
cp_v = refpropm('C','P',p*100,'Q',1,...
'R32','R1234ze',[mf_R32 mf_R1234ze]);
h_liq = refpropm('H','P',p*100,'Q',0,...
'R32','R1234ze',[mf_R32 mf_R1234ze]);
h_vap = refpropm('H','P',p*100,'Q',1,...
'R32','R1234ze',[mf_R32 mf_R1234ze]);
i_lg = h_vap-h_liq;
end

solution = solve(DI_VAP-(I_LG*(Q_NEW-Q_OLD)...
+(1-Q_NEW)*CP_L*GLIDE*(Q_NEW-Q_OLD)...
+Q_NEW*CP_V*GLIDE*(Q_NEW-Q_OLD)),Q_NEW);

sol = subs(solution...
,{DI_VAP,I_LG,Q_OLD,CP_L,CP_V,GLIDE}...
,{q_part/m_ref,i_lg,Q_tot(i),cp_l,cp_v,glide});

check = sol > 0 & sol < 1;
Q_tot(i+1) = sol(check);

end
end

Q_ims(k) = Q_ps(end);
Q_oms(k) = Q_tot(end);

t_dew_ims = refpropm('T','P',p_ims*100,'Q',1,'R32','R1234ze',...
[mf_R32 mf_R1234ze])-273.15; % [°C]
h_ims(k) = refpropm('H','P',p_ims*100,'Q',Q_ims(k),'R32','R1234ze',...
[mf_R32 mf_R1234ze]); % [J kg-1]
t_ims(k) = t_dew_ims-glide_ims*(1-Q_ims(k)); % [°C]
t_oms(k) = refpropm('T','H',h_ims(k),'P',p_oms*100,'R32','R1234ze',...
[mf_R32 mf_R1234ze])-273.15; % [°C]

% Pressure drop model call (Del Col 2009)
dp_dz_Cavallini(k) = PD_Cavallini(p_ims,Q_ims_REFPROP(k),'R32','R1234ze',...
mf_R32,mf_R1234ze,G,D,Ra,choice_1)/1000; % [kPa m-1]

end

delta1 = zeros(1,m);
delta2 = zeros(1,m);
deltaT = zeros(1,m);

for j = 1:m
    if j==1 Q_ims(j) > 0.4 && Q_ims(j+1) > 0.5

        delta = [0.5-Q_ims(j) Q_ims(j+1)-0.5];
        [x, i] = min(delta);
        t_water_in_05 = t_water_in(j-1+i);
        t_water_out_05 = t_water_out(j-1+i);
        t_ips_05 = t_ips(j-1+i);
        t_ims_05 = t_ims(j-1+i);

        delta1(j) = abs(t_ips_05 - t_water_out_05);
        delta2(j) = abs(t_ims_05 - t_water_in_05);
        deltaT(j) = (delta1(j)+delta2(j))/2;
    end
end

```

```

        delta1(j) = abs(t_ips(j)-t_water_out(j));
        delta2(j) = abs(t_ims(j)-t_water_in(j));
        deltaT(j) = (delta1(j)+delta2(j))/2;
        break
    end
end

check1 = delta1 > 0;
check2 = delta2 > 0;
checkT = deltaT > 0;

delta1 = delta1(check1);
delta2 = delta2(check2);
deltaT = deltaT(checkT);

Q_mean_ms = (Q_ims+Q_oms)/2;

%% ----- UNCERTAINTY CALCULATION

p_max_dp = 20.7;      % differential transducer max pressure [bar]
p_fs_dp = 1;         % differential transducer full scale pressure [bar]
p_max = 275.8;      % transducer max pressure [bar]
p_fs = 50;          % transducer full scale pressure [bar]

uB_dp = (0.015+0.005*(p_max_dp/p_fs_dp))*(p_fs_dp/100)/sqrt(3); % [bar]
u_L = 0.00002/sqrt(3); % [m]
z_p_ms = [-23 253.5]; % [mm]
aux_2 = xlsread (file, 'Elaborated_Mean_Deviation', 'C26:T125');
U_dp_dz = zeros(1,m);
U_Q1_ms = zeros(1,m);

for k = 1:m
    std_dp = aux_2(k,9); % [bar]
    uA_dp = std_dp/sqrt(50); % [bar]
    u_dp = 100*sqrt(uA_dp^2+uB_dp^2); % [kPa]
    U_dp_dz(k) = 2*sqrt((1/0.22)^2*u_dp^2+(100*aux(k,9)/...
        0.22^2)^2*u_L^2); % [kPa m^-1]

    t_water_ops = aux(k,12);
    dt_water_ps = aux(k,13);
    cp_w = refpropm('C','T',(2*t_water_ops+dt_water_ps)/2+273.15,...
        'P',101.325,'water');

    uA_m_water_ps = aux_2(k,11)/(3600*sqrt(50)); % [kg s^-1]
    uB_m_water = (0.001+0.004/(3600*m_water))*m_water/sqrt(3); % [kg s^-1]
    u_m_water_ps = sqrt(uA_m_water_ps^2+uB_m_water^2); % [kg s^-1]

    uA_dt_water_ps = aux_2(k,13)/sqrt(50); % [K]
    uB_dt_water_ps = 0.03/sqrt(3); % [K]
    u_dt_water_ps = sqrt(uA_dt_water_ps^2+uB_dt_water_ps^2); % [K]

    uA_m_ref = aux_2(k,4)/(3600*sqrt(50)); % [kg s^-1]
    uB_m_ref = (0.0015+0.001/(3600*m_ref))*m_ref/sqrt(3); % [kg s^-1]
    u_m_ref = sqrt(uA_m_ref^2+uB_m_ref^2); % [kg s^-1]

    cont_m_water_ps = (-cp_w*dt_water_ps/m_ref)^2*u_m_water_ps^2;
    cont_dt_water_ps = (-cp_w*m_water/m_ref)^2*u_dt_water_ps^2;
    cont_m_ref = (m_water*cp_w*dt_water_ps/m_ref^2)^2*u_m_ref^2;

    u_h1_ms = sqrt(cont_m_water_ps+cont_dt_water_ps+cont_m_ref); % [J kg^-1]

    uA_p_in = aux_2(k,5)/sqrt(50); % [bar]
    uB_p_atm = 0.001/sqrt(3); % [bar]

```

```

uB_p = (0.015+0.005*(p_max/p_fs))*(p_fs/100)/sqrt(3);           % [bar]
uB_p_in = sqrt(uB_p^2+uB_p_atm^2);                               % [bar]
u_p_in = sqrt(uA_p_in^2+uB_p_in^2);                               % [bar]

Q_h1_ms = refpropm('Q','P',p_ims*100,'H',h_ims_REFPROP,...
'R32','R1234ze',[mf_R32 mf_R1234ze]);
Q_h1_ms_unc = refpropm('Q','P',(p_ims+u_p_in)*100,'H',h_ims_REFPROP+u_h1_ms,...
'R32','R1234ze',[mf_R32 mf_R1234ze]);

U_Q1_ms(k) = abs(2*(Q_h1_ms-Q_h1_ms_unc));

end

%% ----- RESULTS WRITING

index = aux(1,end);
index = num2str(index);

co_Q_ims = ['P' index];
co_Q_oms = ['Q' index];
co_h_ips = ['V' index];
co_h_dew_ips = ['W' index];
co_ilg = ['X' index];
co_Q_ims_REFPROP = ['AA' index];
co_Q_oms_REFPROP = ['AB' index];
co_t_ims_REFPROP = ['AH' index];
co_t_oms_REFPROP = ['AI' index];
co_dp_dz_Cavallini = ['AO' index];
co_U_dp_dz = ['AX' index];
co_U_Q1_ms = ['AW' index];

statusQ_ims = xlswrite (file,Q_ims',sheet,co_Q_ims);
statusQ_oms = xlswrite (file,Q_oms',sheet,co_Q_oms);
statush_ips = xlswrite (file,h_ips',sheet,co_h_ips);
statush_dew_ips = xlswrite (file,h_dew_ips',sheet,co_h_dew_ips);
statusilg = xlswrite (file,ilg',sheet,co_ilg);

statusQ_ims_REFPROP = xlswrite (file,Q_ims_REFPROP',sheet,co_Q_ims_REFPROP);
statusQ_oms_REFPROP = xlswrite (file,Q_oms_REFPROP',sheet,co_Q_oms_REFPROP);
status_t_ims_REFPROP = xlswrite (file,t_ims_REFPROP',sheet,co_t_ims_REFPROP);
status_t_oms_REFPROP = xlswrite (file,t_oms_REFPROP',sheet,co_t_oms_REFPROP);
statusdp_dz_Cavallini = xlswrite (file,dp_dz_Cavallini',sheet,co_dp_dz_Cavallini);

statusU_Q1_ms = xlswrite (file,U_Q1_ms',sheet,co_U_Q1_ms);
statusU_dp_dz = xlswrite (file,U_dp_dz',sheet,co_U_dp_dz);

statusdelta1 = xlswrite (file,delta1,sheet,['AK' index]);
statusdelta2 = xlswrite (file,delta2,sheet,['AL' index]);
statusdeltaT = xlswrite (file,deltaT,sheet,['AM' index]);

```


A.3 Subroutines for HTC prediction

A.3.1 Cavallini et al. Model [5]

```

% -----
% IMPLEMENTATION of the CAVALLINI MODEL(2006) for the CALCULATION of
% HEAT TRANSFER COEFFICIENT for PURE FLUIDS CONDENSATION.
% The MODEL HERE IMPLEMENTED TAKE INTO ACCOUNT the POSSIBIITY to
% OPERATE with a BINARY MIXTURE.
% -----

% p_sat: mixture saturation pressure [abs bar]
% t_sat: mixture saturation temperature [K]
% t_wall: channel wall temperature [K]
% Q: vapor quality
% delta_t_glide: temperature glide [K]
% FluidA: first mixture fluid
% FluidB: second mixture fluid
% mf_FluidA: percent mass fraction of FluidA in the mixture
% mf_FluidB: percent mass fraction of FluidB in the mixture
% G: mass velocity [kg s-1 m-2]
% D: inner tube diameter [m]

% choose_1 == 1 for calculation at thermodynamic equilibrium,
%       else the program calculate properties
%       at the same composition of the mixture

% choice_2 == 1 for taking account of the Bell & Ghaly correction
%       for zeotropic mixtures. Otherwise any other value ignore
%       the correction

function [HTC] = Cavallini_Model_Function(p_sat,t_sat,t_wall,...
    Q,delta_t_glide,FluidA,FluidB,mf_FluidA,mf_FluidB...
    ,G,D,choice_1,choice_2)

C_T = 2.6;
g = 9.806;           % standard gravity acceleration [m s-2]
HTC = zeros(size(p_sat));

for i=1:length(p_sat)

    p = p_sat(i);
    x = Q(i);
    delta_t = t_sat(i)-t_wall(i);
    glide = delta_t_glide(i);

%----- REFPROP CALLS

if choice_1 == 1     % ----> equilibrium

    [liq vap] = refpropm('X','T',t_sat(i),'P',p*100,...
        FluidA,FluidB,[mf_FluidA mf_FluidB]);

    rho_L = refpropm('D','P',p*100,'Q',0,FluidA,FluidB,liq);   % [kg m-3]
    rho_G = refpropm('D','P',p*100,'Q',1,FluidA,FluidB,vap);   % [kg m-3]

    mu_L = refpropm('V','P',p*100,'Q',0,FluidA,FluidB,liq);   % [kg m-1 s-1]
    mu_G = refpropm('V','P',p*100,'Q',1,FluidA,FluidB,vap);   % [kg m-1 s-1]

    lambda_L = refpropm('L','P',p*100,'Q',0,FluidA,FluidB,liq); % [W m-1 K-1]
    lambda_G = refpropm('L','P',p*100,'Q',1,FluidA,FluidB,vap); % [W m-1 K-1]
    cp_L = refpropm('C','P',p*100,'Q',0,FluidA,FluidB,liq);   % [J kg-1 K-1]
    cp_G = refpropm('C','P',p*100,'Q',0,FluidA,FluidB,vap);   % [J kg-1 K-1]

```

```

h_BUBBLE = refpropm('H','P',p*100,'Q',0,FluidA,FluidB,liq); % [J kg^-1]
h_DEW = refpropm('H','P',p*100,'Q',1,FluidA,FluidB,vap); % [J kg^-1]
h_LG = h_DEW-h_BUBBLE; % [J kg^-1]

else % ----> same composition

rho_L = refpropm('D','P',p*100,'Q',0,FluidA,FluidB,[mf_FluidA mf_FluidB]);
rho_G = refpropm('D','P',p*100,'Q',1,FluidA,FluidB,[mf_FluidA mf_FluidB]);

mu_L = refpropm('V','P',p*100,'Q',0,FluidA,FluidB,[mf_FluidA mf_FluidB]);
mu_G = refpropm('V','P',p*100,'Q',1,FluidA,FluidB,[mf_FluidA mf_FluidB]);

lambda_L = refpropm('L','P',p*100,'Q',0,FluidA,FluidB,[mf_FluidA mf_FluidB]);
lambda_G = refpropm('L','P',p*100,'Q',1,FluidA,FluidB,[mf_FluidA mf_FluidB]);
cp_L = refpropm('C','P',p*100,'Q',0,FluidA,FluidB,[mf_FluidA mf_FluidB]);
cp_G = refpropm('C','P',p*100,'Q',1,FluidA,FluidB,[mf_FluidA mf_FluidB]);

h_BUBBLE = refpropm('H','P',p*100,'Q',0,FluidA,FluidB,[mf_FluidA mf_FluidB]);
h_DEW = refpropm('H','P',p*100,'Q',1,FluidA,FluidB,[mf_FluidA mf_FluidB]);
h_LG = h_DEW-h_BUBBLE;

end

%----- CAVALLINI MODEL(2006) IMPLEMENTATION

Pr_L = mu_L*cp_L/lambda_L;
Re_LO = G*D/mu_L;

X_tt = (mu_L/mu_G)^0.1*(rho_G/rho_L)^0.5*((1-x)/x)^0.9;
J_GT = ((7.5/(4.3*X_tt^1.111+1))^-3)+C_T^(-3))^(-1/3);
J_G = x*G/(g*D*rho_G*(rho_L-rho_G))^0.5;

alpha_LO = 0.023*Re_LO^0.8*Pr_L^0.4*lambda_L/D;
alpha_STRAT = 0.725*(1+0.741*((1-x)/x)^0.3321)^(-1)*...
(lambda_L^3*rho_L*(rho_L-rho_G)*g*h_LG/(mu_L*D*delta_t))^0.25...
+(1-x^0.087)*alpha_LO;

alpha_A = alpha_LO*(1+1.128*x^0.8170*(rho_L/rho_G)^0.3685...
*(mu_L/mu_G)^0.2363*(1-mu_G/mu_L)^2.144*Pr_L^(-0.1));
alpha_D = (alpha_A*(J_GT/J_G)^0.8-alpha_STRAT)*(J_G/J_GT)+alpha_STRAT;

if J_G <= J_GT %-----> delta_t dependent regime
    alpha = alpha_D;
else %-----> delta_t independent regime
    alpha = alpha_A;
end

%----- SILVER, BELL & GHALY COORECTION FOR ZEOTROPIC MIXTURES

if choice_2 == 1

Re_G = x*G*D/mu_G;
Pr_G = mu_G*cp_G/lambda_G;
alpha_G = (lambda_G/D)*0.023*Re_G^0.8*Pr_G^0.33;
correction = x*cp_G*(glide/h_LG)*(1/alpha_G);

R_T = (1/alpha)+correction;
HTC(i) = (R_T)^(-1);

else

HTC(i) = alpha; % [W m^-2 K^-1]
end
end
end

```

A.3.2 Moser et al. Model [11]

```

% -----
% IMPLEMENTATION of the MOSER MODEL(1998) for the CALCULATION of
% HEAT TRANSFER COEFFICIENT for PURE FLUIDS.
% The MODEL HERE IMPLEMENTED TAKE INTO ACCOUNT the POSSIBILITY to
% OPERATE with a BINARY MIXTURE and APPLIED the ZHANG & WEBB CORRECTION
% FOR MINICHANNEL FLOW
% -----

% p_sat: mixture saturation pressure [abs bar]
% t_sat: mixture saturation temperature [K]
% Q: vapor quality
% delta_t_glide: temperature glide [K]
% FluidA: first mixture fluid
% FluidB: second mixture fluid
% mf_FluidA: percent mass fraction of FluidA in the mixture
% mf_FluidB: percent mass fraction of FluidB in the mixture
% G: mass velocity [kg s-1 m-2]
% D: inner tube diameter [m]

% choice_1 == 1 for calculation at thermodynamic equilibrium,
%     else the program calculate properties
%     at the same composition of the mixture

% choice_2 == 1 for taking account of the Bell & Ghaly correction
%     for zeotropic mixtures. Otherwise any other value ignore
%     the correction

function [HTC] = Moser_Model_Function(p_sat,t_sat,Q,delta_t_glide,...
    FluidA,FluidB,mf_FluidA,mf_FluidB,G,D,choice_1,choice_2)

HTC = zeros(size(p_sat));
p_c = (refpropm('P','C',0,'',0,FluidA,FluidB,...
    [mf_FluidA mf_FluidB]))/100; % [bar]

for i=1:length(p_sat)

    x = Q(i);
    p = p_sat(i);
    glide = delta_t_glide(i);

%----- REFPROP CALLS

if choice_1 == 1 % ---> equilibrium

    [liq vap] = refpropm('X','T',t_sat(i),'P',p*100,...
        FluidA,FluidB,[mf_FluidA mf_FluidB]);

    mu_L = refpropm('V','P',p*100,'Q',0,FluidA,FluidB,liq); % [kg m-1 s-1]
    mu_V = refpropm('V','P',p*100,'Q',1,FluidA,FluidB,vap); % [kg m-1 s-1]

    k_L = refpropm('L','P',p*100,'Q',0,FluidA,FluidB,liq); % [W m-1 K-1]
    k_V = refpropm('L','P',p*100,'Q',1,FluidA,FluidB,vap); % [W m-1 K-1]
    cp_L = refpropm('C','P',p*100,'Q',0,FluidA,FluidB,liq); % [J kg-1 K-1]
    cp_V = refpropm('C','P',p*100,'Q',1,FluidA,FluidB,vap); % [J kg-1 K-1]

    h_BUBBLE = refpropm('H','P',p*100,'Q',0,FluidA,FluidB,liq); % [J kg-1]
    h_DEW = refpropm('H','P',p*100,'Q',1,FluidA,FluidB,vap); % [J kg-1]
    h_LG = h_DEW-h_BUBBLE; % [J kg-1]

else % ---> same composition

    mu_L = refpropm('V','P',p*100,'Q',0,FluidA,FluidB,[mf_FluidA mf_FluidB]);
    mu_V = refpropm('V','P',p*100,'Q',1,FluidA,FluidB,[mf_FluidA mf_FluidB]);

```

```

k_L = refpropm('L','P',p*100,'Q',0,FluidA,FluidB,[mf_FluidA mf_FluidB]);
k_V = refpropm('L','P',p*100,'Q',1,FluidA,FluidB,[mf_FluidA mf_FluidB]);
cp_L = refpropm('C','P',p*100,'Q',0,FluidA,FluidB,[mf_FluidA mf_FluidB]);
cp_V = refpropm('C','P',p*100,'Q',1,FluidA,FluidB,[mf_FluidA mf_FluidB]);

h_BUBBLE = refpropm('H','P',p*100,'Q',0,FluidA,FluidB,[mf_FluidA mf_FluidB]);
h_DEW = refpropm('H','P',p*100,'Q',1,FluidA,FluidB,[mf_FluidA mf_FluidB]);
h_LG = h_DEW-h_BUBBLE;

end

%----- MOSER MODEL(1998) IMPLEMENTATION

Pr_L = mu_L*cp_L/k_L;
Re_L = G*(1-x)*D/mu_L;
Re_LO = G*D/mu_L;

C_1 = 0.126*Pr_L^(-0.448);
C_2 = -0.113*Pr_L^(-0.563);

PHI_LO = ((1-x)^2+2.87*x^2*(p/p_c)^(-1)+1.68*x^0.8...
          *(1-x)^0.25*(p/p_c)^(-1.64))^(1/2);

Re_eq = PHI_LO^(8/7)*Re_LO;

Nu = (0.0994^C_1*Re_L^C_2*Re_eq^(1+0.875*C_1)*Pr_L^0.815)...
      /((1.58*log(Re_eq)-3.28)*(2.58*log(Re_eq)+13.7*Pr_L^(2/3)-19.1));

alpha = Nu*k_L/D;

%----- SILVER, BELL & GHALY COORECTION FOR ZEOTROPIC MIXTURES

if choice_2 == 1

    Re_G = x*G*D/mu_V;
    Pr_G = mu_V*cp_V/k_V;
    alpha_G = (k_V/D)*0.023*Re_G^0.8*Pr_G^0.33;
    correction = x*cp_V*(glide/h_LG)*(1/alpha_G);

    R_T = (1/alpha)+correction;
    HTC(i) = (R_T)^(-1);

else
    HTC(i) = alpha;    % [W m^-2 K^-1]
end
end
end

```

A.3.3 Shah Model [16]

```

% -----
% IMPLEMENTATION of the SHAH MODEL(2009) for the CALCULATION of
% HEAT TRANSFER COEFFICIENT for PURE FLUIDS CONDENSATION.
% The MODEL HERE IMPLEMENTED TAKE INTO ACCOUNT the POSSIBILITY to
% OPERATE with a BINARY MIXTURE.
% -----

% p_sat: mixture saturation pressure [abs bar]
% t_sat: mixture saturation temperature [K]
% Q: vapor qualities
% delta_t_glide: temperature glide [K]
% FluidA: first mixture fluid
% FluidB: second mixture fluid
% mf_FluidA: percent mass fraction of FluidA in the mixture
% mf_FluidB: percent mass fraction of FluidB in the mixture
% G: mass velocity [kg s-1 m-2]
% D: inner tube diameter [m]

% choice_1 == 1 for calculation at thermodynamic equilibrium,
%       else the program calculate properties at the same
%       bulk composition of the mixture

% choice_2 == 1 for taking account of the Bell & Ghaly correction
%       for zeotropic mixtures. Otherwise any other value ignore
%       the correction

function [HTC] = Shah_Model_Function(p_sat,t_sat,Q,delta_t_glide,...
    FluidA,FluidB,mf_FluidA,mf_FluidB,G,D,choice_1,choice_2)

HTC = zeros(size(p_sat));
p_c = (refpropm('P','C',0,'',0,FluidA,FluidB,[mf_FluidA mf_FluidB]))/100;
g = 9.806; % standard gravity acceleration [m s-2]

for i=1:length(p_sat)

    x = Q(i);
    p = p_sat(i);
    glide = delta_t_glide(i);

%----- REFPROP CALLS

if choice_1 == 1 % ---> equilibrium

    [liq vap] = refpropm('X','T',t_sat(i),'P',p*100,...
        FluidA,FluidB,[mf_FluidA mf_FluidB]);

    rho_L = refpropm('D','P',p*100,'Q',0,FluidA,FluidB,liq); % [kg m-3]
    rho_G = refpropm('D','P',p*100,'Q',1,FluidA,FluidB,vap); % [kg m-3]

    mu_L = refpropm('V','P',p*100,'Q',0,FluidA,FluidB,liq); % [kg m-1 s-1]
    mu_G = refpropm('V','P',p*100,'Q',1,FluidA,FluidB,vap); % [kg m-1 s-1]

    lambda_L = refpropm('L','P',p*100,'Q',0,FluidA,FluidB,liq); % [W m-1 K-1]
    lambda_G = refpropm('L','P',p*100,'Q',1,FluidA,FluidB,vap); % [W m-1 K-1]

    cp_L = refpropm('C','P',p*100,'Q',0,FluidA,FluidB,liq); % [J kg-1 K-1]
    cp_G = refpropm('C','P',p*100,'Q',0,FluidA,FluidB,vap); % [J kg-1 K-1]

    h_BUBBLE = refpropm('H','P',p*100,'Q',0,FluidA,FluidB,liq); % [J kg-1]
    h_DEW = refpropm('H','P',p*100,'Q',1,FluidA,FluidB,vap); % [J kg-1]
    h_LG = h_DEW-h_BUBBLE; % [J kg-1]

else % ---> same composition

```

```

rho_L = refpropm('D','P',p*100,'Q',0,FluidA,FluidB,[mf_FluidA mf_FluidB]);
rho_G = refpropm('D','P',p*100,'Q',1,FluidA,FluidB,[mf_FluidA mf_FluidB]);

mu_L = refpropm('V','P',p*100,'Q',0,FluidA,FluidB,[mf_FluidA mf_FluidB]);
mu_G = refpropm('V','P',p*100,'Q',1,FluidA,FluidB,[mf_FluidA mf_FluidB]);

lambda_L = refpropm('L','P',p*100,'Q',0,FluidA,FluidB,[mf_FluidA mf_FluidB]);
lambda_G = refpropm('L','P',p*100,'Q',1,FluidA,FluidB,[mf_FluidA mf_FluidB]);

cp_L = refpropm('C','P',p*100,'Q',0,FluidA,FluidB,[mf_FluidA mf_FluidB]);
cp_G = refpropm('C','P',p*100,'Q',1,FluidA,FluidB,[mf_FluidA mf_FluidB]);

h_BUBBLE = refpropm('H','P',p*100,'Q',0,FluidA,FluidB,[mf_FluidA mf_FluidB]);
h_DEW = refpropm('H','P',p*100,'Q',1,FluidA,FluidB,[mf_FluidA mf_FluidB]);
h_LG = h_DEW-h_BUBBLE;

end

%----- SHAH MODEL (2009) IMPLEMENTATION

p_r = p/p_c;
Z = (1/x-1)^0.8*p_r^0.4;

Pr_L = mu_L*cp_L/lambda_L;
Re_LO = G*D/mu_L;

h_LT = 0.023*Re_LO^0.8*Pr_L^0.4*lambda_L/D;
n = 0.0058+0.557*p_r;

alpha = h_LT*(mu_L/(14*mu_G))^n*((1-x)^0.8...
+((3.8*x^0.76*(1-x)^0.04)/p_r^0.38));

J_g = x*G/(g*D*rho_G*(rho_L-rho_G))^0.5;
J_boundary = 0.98*(Z+0.263)^(-0.62);

if J_g < J_boundary
    Re_L = G*(1-x)*D/mu_L;
    h_Nu = 1.32*Re_L^(-1/3)*((rho_L*(rho_L-rho_G)...
    *lambda_L^3)/(mu_L^2))^(-1/3);
    alpha = alpha+h_Nu;
end

%----- SILVER, BELL & GHALY COORECTION FOR ZEOTROPIC MIXTURE

if choice_2 == 1
    Re_G = x*G*D/mu_G;
    Pr_G = mu_G*cp_G/lambda_G;
    alpha_G = (lambda_G/D)*0.023*Re_G^0.8*Pr_G^0.33;
    correction = x*cp_G*(glide/h_LG)*(1/alpha_G);

    R_T = (1/alpha)+correction;
    HTC(i) = (R_T)^(-1);

else
    HTC(i) = alpha;    % [W m^-2 K^-1]

end
end
end

```

A.4 Subroutine for PD prediction

A.4.1 Del Col et al. Model [8]

```

% -----
% IMPLEMENTATION of the DEL COL MODEL(2009) for the CALCULATION of
% PRESSURE DROP VALUE for PURE FLUID CONDENSATION
% INSIDE CIRCULAR or SQUARE CHANNELS with HYDRAULIC DIAMETER
% RANGING FROM 0.96 TO 2 mm.
% The MODEL HERE IMPLEMENTED TAKE INTO ACCOUNT the POSSIBILITY to
% OPERATE with a BINARY MIXTURE.
% -----

% p_sat: mixture saturation pressure [abs bar]
% Q: vapor quality
% FluidA: first mixture fluid
% FluidB: second mixture fluid
% mf_FluidA: percent mass fraction of FluidA in the mixture
% mf_FluidB: percent mass fraction of FluidB in the mixture
% G: mass velocity [kg s-1 m-2]
% D: hydraulic tube diameter [m]
% Ra: arithmetical mean deviation of the assessed profile
%     dubbed roughness (according to ISO 4287:1997) [m]

% choice == 1 for calculation at thermodynamic equilibrium,
%     any other value let the program calculate properties
%     at the same mixture composition

function [dp_dz] = PD_Cavallini(p_sat,Q,FluidA,FluidB,mf_FluidA,...
    mf_FluidB,G,D,Ra,choice)

dp_dz = zeros(size(p_sat));
g = 9.806;      % [m s-2]
C = 16;        % circular cross section, C=14.3 for square cross section
toll = 0.0005; % loop exit value for the E parameter calculation
p_crit = refpropm('P','C',0,'',0,...
    FluidA,FluidB,[mf_FluidA mf_FluidB])/100; % [bar]

for i=1:length(p_sat)

    p = p_sat(i);
    x = Q(i);

%----- REFPROP CALLS

    if choice == 1      % ---> equilibrium

        [liq vap] = refpropm('X','P',p*100,'Q',x,...
            FluidA,FluidB,[mf_FluidA mf_FluidB]);

        sigma = refpropm('I','P',p*100,'Q',0.5,FluidA,FluidB,liq); % [kg s-2]
        rho_L = refpropm('D','P',p*100,'Q',0,FluidA,FluidB,liq); % [kg m-3]
        rho_V = refpropm('D','P',p*100,'Q',1,FluidA,FluidB,vap); % [kg m-3]
        mu_L = refpropm('V','P',p*100,'Q',0,FluidA,FluidB,liq); % [kg m-1 s-1]
        mu_V = refpropm('V','P',p*100,'Q',1,FluidA,FluidB,vap); % [kg m-1 s-1]

    else                % ---> same composition

        sigma = refpropm('I','P',p*100,'Q',0.5,FluidA,FluidB,[mf_FluidA mf_FluidB]);
        rho_L = refpropm('D','P',p*100,'Q',0,FluidA,FluidB,[mf_FluidA mf_FluidB]);
        rho_V = refpropm('D','P',p*100,'Q',1,FluidA,FluidB,[mf_FluidA mf_FluidB]);
        mu_L = refpropm('V','P',p*100,'Q',0,FluidA,FluidB,[mf_FluidA mf_FluidB]);
        mu_V = refpropm('V','P',p*100,'Q',1,FluidA,FluidB,[mf_FluidA mf_FluidB]);
    end
end

```

```

end

%----- CAVALLINI MODEL (2009) IMPLEMENTATION

J_G = x*G/(g*D*rho_V*(rho_L-rho_V))^0.5;
j_G = x*G/rho_V;      % [m s^-1]
p_R = p/p_crit;

Re_L0 = G*D/mu_L;
RR = 2*Ra/D;
A = 8.9938e-3;
Re_L0_plus = ((A+0.7*RR)/0.046)^(-5);

if Re_L0 <= Re_L0_plus
    X = 0;
elseif Re_L0 >= 3500
    X = 1;
else
    X = 1+(A-0.046*Re_L0^(-0.2))/(0.7*RR);
end

f_L0 = 0.046*Re_L0^(-0.2)+0.7*RR*X;
F = x^0.9525*(1-x)^0.414;
H = (rho_L/rho_V)^1.132*(mu_V/mu_L)^0.44*(1-mu_V/mu_L)^3.542;
Z = (1-x)^2+x^2*rho_L/rho_V*(mu_V/mu_L)^0.2;
W = 1.398*p_R;

E = 0.5;      % starting value
delta = 1;    % starting value
while delta > toll
    rho_GC = (x+(1-x)*E)/(x/rho_V+(1-x)*E/rho_L);
    E_new = 0.015+0.44*log10((rho_GC/rho_L)*(mu_L*j_G/sigma)^2*1e4);
    if E_new <= 0
        E_new = 0;
    elseif E_new >= 0.95
        E_new = 0.95;
    end
    delta = abs(E-E_new);
    E = E_new;
end

PHI_L0_2 = Z+3.595*F*H*(1-E)^W;
dp_dz_f = PHI_L0_2*2*f_L0*G^2/(D*rho_L);

dp_dz(i) = dp_dz_f;      % [Pa m^-1]

    % ---> for low vapor qualities and mass velocities

if J_G < 2.5
    if Re_L0 > 2000
        f_L0 = 0.046*Re_L0^(-0.2);
    else
        f_L0 = C/Re_L0;
    end
    dp_dz_f_L0 = 2*f_L0*G^2/(D*rho_L);

    if dp_dz_f_L0 > dp_dz_f
        dp_dz(i) = dp_dz_f_L0;    % [Pa m^-1]
    end
end
end
end
end

```


A.5 Subroutine for uncertainty calculation

A.5.1 HTC Uncertainty Function

```

% -----
% UNCERTAINTY CALCULATION for the EXPERIMENTAL HTC VALUES
% -----

% m_water: water flow rate inside the measuring section [kg s^-1]
% t_water: water temperatures vector [řC]
% std_m_water: water flow rate standard deviation [kg s^-1]
% std_t_water: water temperature standard deviation [řC]
% t_wall: wall temperatures vector[řC]
% std_t_wall: vector of wall temperature standard deviation [řC]
% t_sat: saturation temperatures vector [řC]
% z_water: water temperatures measuring positions [mm]
% z_wall: measuring positions along the measuring section [mm]
% p_in: inlet pressure in the measurement section [bar]
% std_p_in: inlet pressure standard deviation [bar]
% dp: pressure drop in the measurement section [bar]
% std_dp: pressure drop standard deviation [bar]
% d_i: inner tube diameter [m]
% h_in: measuring section inlet specific enthalpy [J kg^-1]
% h_out: measuring section outlet specific enthalpy [J kg^-1]
% m_water_ps: water flow rate inside the pre-section [kg s^-1]
% m_ref: refrigerant flow rate [kg s^-1]
% std_m_ref: refrigerant flow rate standard deviation [kg s^-1]
% t_water_ips: pre-section inlet water temperature [řC]
% dt_water_ps: pre-section water temperature drop [řC]
% std_dt_water_ps: pre-section water temperature drop standar deviation [řC]
% z_ps: pressure ports positions in the measuring section [mm]
% p_sat: saturation pressures inside the measuring section [bar]
% h: specific enthalpis in th measuring section [J kg^-1]
% t_water_ms: water temperatures in the measuring section [řC]

% mf_FluidA: percent mass fraction of Fluid A in the mixure
% mf_FluidB: percent mass fraction of Fluid B in the mixure

function [u_HTC,U_HTC_M,u_m_water,u_g,u_P,u_t_sat,u_t_wall,cont_m_w,...
    cont_g,cont_t_sat,cont_t_wall,cont_P,U_Q_ms] = HTC_Uncertainty(m_water,...
    t_water,std_m_water,std_t_water,t_wall,std_t_wall,t_sat,z_water,...
    z_wall,p_in,std_p_in,dp,std_dp,d_i,h_in_Koyama,h_out_Koyama,...
    m_water_ps,std_m_water_ps,m_ref,std_m_ref,t_water_ips,dt_water_ps,std_dt_water_ps,...
    z_p_ms,p_sat,h_Koyama,t_water_ms,...
    mf_FluidA,mf_FluidB)

%----- CONSTANT VALUES

n = 50; % number of readings
k = 2; % overall uncertainty coverage factor

p_max = 275.8; % transducer max pressure [bar]
p_fs = 50; % transducer full scale pressure [bar]
p_max_dp = 20.7; % differential transducer max pressure [bar]
p_fs_dp = 1; % differential transducer full scale pressure [bar]

l_ms = z_wall(end)-z_wall(1); % [mm]
p_out = p_in-dp; % [bar]

pol_w = polyfit(z_water,t_water,2); % a2*z^2+a1*z+a0
dpol_w = polyder(pol_w); % 2*a2*z+a1
g = 1000*polyval(dpol_w,z_wall); % [K m^-1]
t_water_z_wall = polyval(pol_w,z_wall); % [řC]

%----- A TYPE UNCERTAINTY

```

```

uA_m_water = std_m_water/sqrt(n);           % [kg s^-1]
uA_m_ref = std_m_ref/sqrt(n);               % [kg s^-1]
uA_m_water_ps = std_m_water_ps/sqrt(n);    % [kg s^-1]
uA_t_wall = std_t_wall/sqrt(n);            % [K]
uA_t_water = std_t_water/sqrt(n);          % [K]

uA_dt_water_ps = std_dt_water_ps/sqrt(n);  % [K]

uA_p_in = std_p_in/sqrt(n);                 % [bar]
uA_dp = std_dp/sqrt(n);                     % [bar]

%----- B TYPE UNCERTAINTY

uB_m_water = (0.001+0.004/(3600*m_water))*m_water/sqrt(3); % [kg s^-1]
uB_m_ref = (0.0015+0.001/(3600*m_ref))*m_ref/sqrt(3); % [kg s^-1]

uB_t_wall = 0.05/sqrt(3);                  % [K]
uB_t_water = 0.05/sqrt(3);                 % [K]
uB_dt_water_ps = 0.03/sqrt(3);             % [K]

uA_P = (pi*0.02/1000)/sqrt(3);             % internal perimeter uncertainty [m]
uB_p_atm = 0.001/sqrt(3);                  % [bar]
uB_p = (0.015+0.005*(p_max/p_fs))*(p_fs/100)/sqrt(3); % [bar]
uB_p_in = sqrt(uB_p^2+uB_p_atm^2);          % [bar]
uB_dp = (0.015+0.005*(p_max_dp/p_fs_dp))*(p_fs_dp/100)/sqrt(3); % [bar]

%----- COMBINED STANDARD UNCERTAINTY A+B

u_m_water = sqrt(uA_m_water^2+uB_m_water^2); % [kg s^-1]
u_m_water_ps = sqrt(uA_m_water_ps^2+uB_m_water^2); % [kg s^-1]
u_m_ref = sqrt(uA_m_ref^2+uB_m_ref^2); % [kg s^-1]

u_P = uA_P;                                % [m]
u_t_wall = sqrt(uA_t_wall.^2+uB_t_wall^2); % [K]
u_t_water = sqrt(uA_t_water.^2+uB_t_water^2); % [K]

u_dt_water_ps = sqrt(uA_dt_water_ps^2+uB_dt_water_ps^2); % [K]

u_p_in = sqrt(uA_p_in^2+uB_p_in^2);         % [bar]
u_dp = sqrt(uA_dp^2+uB_dp^2);              % [bar]
u_p_out = sqrt(u_p_in^2+u_dp^2);           % [bar]

% -----> saturation temperature uncertainties

t_sat_in = refpropm('T','P',p_in*100,'H',h_in_Koyama,...
'R32','R1234ze',[mf_FluidA mf_FluidB])-273.15;
t_sat_out = refpropm('T','P',p_out*100,'H',h_out_Koyama,...
'R32','R1234ze',[mf_FluidA mf_FluidB])-273.15;
t_sat_in_unc = refpropm('T','P',(p_in+u_p_in)*100,'H',h_in_Koyama,...
'R32','R1234ze',[mf_FluidA mf_FluidB])-273.15;
t_sat_out_unc = refpropm('T','P',(p_out-u_p_out)*100,'H',h_out_Koyama,...
'R32','R1234ze',[mf_FluidA mf_FluidB])-273.15;

u_t_sat_in = abs(t_sat_in-t_sat_in_unc);    % [°C]
u_t_sat_out = abs(t_sat_out-t_sat_out_unc); % [°C]

u_t_sat = sqrt((z_wall./l_ms+1).^2*u_t_sat_in^2+...
(z_wall./l_ms).^2*u_t_sat_out^2);          % [°C]

% -----> temperature gradient uncertainties

A_2 = zeros(numel(z_water),3);

```

```

for i = 1:numel(z_water)
    for j = 1:3
        A_2(i,j) = z_water(i)^(j-1)/u_t_water(i);
    end
end

C_2 = inv(A_2'*A_2);

u2_a0_2 = C_2(1,1);
u2_a1_2 = C_2(2,2);
u2_a2_2 = C_2(3,3);

cov_a0a1_2 = C_2(1,2);
cov_a1a2_2 = C_2(2,3);
cov_a0a2_2 = C_2(1,3);

% -----> pre-allocations

u_g = zeros(size(z_wall));
dHTC_dm_w = zeros(size(z_wall));
dHTC_dg = zeros(size(z_wall));
dHTC_dt_wall = zeros(size(z_wall));
dHTC_dt_sat = zeros(size(z_wall));
dHTC_dP = zeros(size(z_wall));
u_HTC = zeros(size(z_wall));
cont_m_w = zeros(size(z_wall));
cont_g = zeros(size(z_wall));
cont_t_sat = zeros(size(z_wall));
cont_t_wall = zeros(size(z_wall));
cont_P = zeros(size(z_wall));

% -----> HTC UNCERTAINTY CALCULATION

for i = 1:numel(z_wall)

    cp_w = refpropm('C','T',(t_water_z_wall(i))+273.15,...
        'P',101.325,'water'); % [J kg^-1 K^-1]
    u_g(i) = 1000*sqrt(u2_a1_2+(2*z_wall(i))^2*u2_a2_2+4*cov_a1a2_2*z_wall(i));

% -----> sensitivity coefficients

    dHTC_dm_w(i) = -cp_w*g(i)/(pi*d_i*(t_sat(i)-t_wall(i)));
    dHTC_dg(i) = -m_water*cp_w/(pi*d_i*(t_sat(i)-t_wall(i)));
    dHTC_dt_wall(i) = -m_water*cp_w*g(i)/(pi*d_i*(t_sat(i)-t_wall(i))^2);
    dHTC_dt_sat(i) = -dHTC_dt_wall(i);
    dHTC_dP(i) = m_water*cp_w*g(i)/(pi^2*d_i^2*(t_sat(i)-t_wall(i)));

% -----> HTC uncertainty

    cont_m_w(i) = sqrt(dHTC_dm_w(i)^2*u_m_water^2);
    cont_g(i) = sqrt(dHTC_dg(i)^2*u_g(i)^2);
    cont_t_sat(i) = sqrt(dHTC_dt_sat(i)^2*u_t_sat(i)^2);
    cont_t_wall(i) = sqrt(dHTC_dt_wall(i)^2*u_t_wall(i)^2);
    cont_P(i) = sqrt(dHTC_dP(i)^2*u_P^2);

    u_HTC(i) = sqrt(dHTC_dm_w(i)^2*u_m_water^2+...
        dHTC_dg(i)^2*u_g(i)^2+...
        dHTC_dt_sat(i)^2*u_t_sat(i)^2+...
        dHTC_dt_wall(i)^2*u_t_wall(i)^2+...
        dHTC_dP(i)^2*u_P^2);

end

U_HTC_M = k*u_HTC; % expandend uncertainty [W m^-2 K^-1]

```

```

% -----> VAPOR QUALITY UNCERTAINTY CALCULATION

cp_w = refpropm('C','T',(t_water_ips+dt_water_ps)/2+273.15,'P',101.325,'water');

cont_m_water_ps = (-cp_w*dt_water_ps/m_ref)^2*u_m_water_ps^2;
cont_dt_water_ps = (-cp_w*m_water_ps/m_ref)^2*u_dt_water_ps^2;
cont_m_ref = (m_water_ps*cp_w*dt_water_ps/m_ref^2)^2*u_m_ref^2;

u_h1_ms = sqrt(cont_m_water_ps+cont_dt_water_ps+cont_m_ref);

p_unc = [p_in-u_p_in p_in-dp-u_p_out];
pol_p_unc = polyfit(z_p_ms,p_unc,1);
p_sat_unc = polyval(pol_p_unc,z_wall);

Q_h1_ms = refpropm('Q','P',p_sat(1)*100,'H',h_in_Koyama,...
'R32','R1234ze',[mf_FluidA mf_FluidB]);
Q_h1_ms_unc = refpropm('Q','P',p_sat_unc(1)*100,'H',h_in_Koyama+u_h1_ms,...
'R32','R1234ze',[mf_FluidA mf_FluidB]);

U_Q1_ms = abs(k*(Q_h1_ms-Q_h1_ms_unc));

% -----> polynomial water uncertainty calculation

u_t_water_pol = sqrt(u2_a0_2+...
u2_a1_2*z_wall.^2+...
u2_a2_2*z_wall.^4+...
2*cov_a0a1_2*z_wall+...
2*cov_a1a2_2*z_wall.^3+...
2*cov_a0a2_2*z_wall.^2);

% -----> Vapor quality uncertainty

u_h_ms = zeros(size(z_wall));
u_h_ms(1) = u_h1_ms;
U_Q_ms = zeros(size(z_wall));
U_Q_ms(1) = U_Q1_ms;

for i = 1:numel(z_wall)

    if i == numel(z_wall)
        break
    end

    cp_w = refpropm('C','T',t_water(i+1)+273.15,'P',101.325,'water');

    u_h_ms(i+1) = sqrt(u_h_ms(i)^2+...
        (cp_w*(t_water_ms(i)-t_water_ms(i+1))/m_ref)^2*u_m_water^2+...
        (cp_w*m_water/m_ref)^2*u_t_water_pol(i)^2+...
        (cp_w*m_water/m_ref)^2*u_t_water_pol(i+1)^2+...
        (cp_w*m_water*(t_water_ms(i)-t_water_ms(i+1))/m_ref^2)^2*u_m_ref^2);

    Q = refpropm('Q','P',p_sat(i+1)*100,'H',h_Koyama(i+1),...
'R32','R1234ze',[mf_FluidA mf_FluidB]);
    Q_unc = refpropm('Q','P',p_sat_unc(i+1)*100,'H',h_Koyama(i+1)+u_h_ms(i+1),...
'R32','R1234ze',[mf_FluidA mf_FluidB]);

    U_Q_ms(i+1) = abs(k*(Q-Q_unc));

end
end

```

Acronyms

CFCs Chloro-Fluoro-Carbons

COP Coefficient of Performance

GWP Global Warming Potential

HCFCs Hydro-Chloro-Fluoro-Carbons

HFCs Hydro-Fluoro-Carbons

HFOs Hydro-Fluoro-Olefins

HTC Heat Transfer Coefficient

HVAC Heating, Ventilation and Air Conditioning

ODP Ozone Depleting Potential

PD Pressure Drop

PEC Performance Evaluation Criterion

PF Penalty Factor

PID Proportional, Integrative and Derivative

WLS Weighted Least Square

Index

Comparisons, 85

- Against Pure Fluids, 98
- Against Theoretical Models, 85

Conclusions, 105

Data

- Acquisition, 35
- Comparisons, 85
- Reduction (HTC test section), 38
- Reduction (PD test section), 44
- Reduction Codes, 115

Experimental

- Apparatus, 21
- Data Reduction Corrections, 43
- Results, 61
- Tests, 33
- Uncertainty, 47

HTC

- Comparisons, 85
- Experimental Results, 61
- Theoretical Models, 73
- Uncertainty, 48

Measuring Instruments, 29

- Uncertainty (Type B), 48

Mixtures, 13

- Definition, 15
- Preparation, 33

PD

- Comparisons, 92
- Experimental Results, 68
- Theoretical Model, 80
- Uncertainty, 54

Penalty Factor, 97

Preliminary Tests, 36

R1234ze(E), 11

R32, 11

Refrigerants, 7

- Environmental characteristics, 9
- Historical review, 8
- Properties, 7

Tests

- Condensation, 35
- Pressure Drop, 36

Test

- Rig, 21
- Section (HTC), 25
- Section (PD), 28

Theoretical

- Models, 73
- Models Correction, 79

Uncertainty

- Analysis, 55
- Expression, 47
- Overall, 52

Vapor Quality

- Uncertainty, 52

The limit of my knowledge is just my curiosity.

Yusef Karam

This thesis was written with L^AT_EX.

Rock'n'roll!